A TIME-DOMAIN FORMULATION OF INVERSE SOURCE PROBLEMS USING THE TRANSMISSION-LINE MATRIX METHOD

A TIME-DOMAIN FORMULATION OF INVERSE SOURCE PROBLEMS USING THE TRANSMISSION-LINE MATRIX METHOD

By

YU ZHANG, B. Sc. Eng.

A Thesis

Submitted to the School of Graduate Studies

in Partial Fulfillment of the Requirements

for the Degree

Master of Applied Science

McMaster University

MASTER OF APPLIED SCIENCE (2010) MCMASTER UNIVERSITY
(Electrical and Computer Engineering) Hamilton, Ontario

TITLE: **A Time Domain Formulation of Inverse Source Problems Using the Transmission-Line Matrix Method**

AUTHOR: Yu Zhang
B. Sc. in Electrical Engineering (University of Manitoba)

SUPERVISORS: Mohamed H. Bakr, Associate Professor
Department of Electrical and Computer Engineering
B. Sc., M. Sc. (Cairo University)
Ph. D. (McMaster University)
P. Eng. (Province of Ontario, Canada)

Natalia K. Nikolova, Professor
Department of Electrical and Computer Engineering
Dipl. Eng. (Technical University of Varna)
Ph. D. (University of Electro-Communication)
P. Eng. (Province of Ontario, Canada)

NUMBER OF PAGES: xi, 106

Abstract

The inverse source problem of electromagnetics for homogeneous background medium is investigated numerically using the Transmission-Line Matrix (TLM) method. By transforming all sources and fields into their equivalent link impulses inside a TLM computational domain, a discrete linear inversion formulation is developed. Our approach solves for the unknown source distribution inside a given source region using the near-field measurements on its boundary. Unlike the conventional frequency-domain treatments, both our source solution and the field measurements are obtained in the time domain. The non-uniqueness of the inverse source problem is addressed by additionally imposing a smoothness *prior* constraint. First-order time and spatial derivatives of the source distribution are minimized. The source reconstruction algorithm introduced in this thesis is illustrated through various two-dimensional numerical examples. It is also shown that our algorithm is robust against the noise from the boundary field measurements.

Acknowledgments

First and foremost, I wish to express my sincere appreciation to my supervisor Dr. Mohamed H. Bakr for his expert guidance, constant encouragement, and patience during the course of this work. I am grateful for all the great research experiences that I have gained while under his supervision. Special thanks go to my co-supervisor Dr. Natalia N. Nikolova for her being always available for support and providing me fruitful comments and discussion. During the past year, both my supervisors have contributed greatly to my personal growth in both technical and inter-personal skills. In fact, it was a great honor and pleasurable experience to work under their supervision.

Secondly, I wish to express my gratitude to my colleagues, Mohamed H. Negm, Osman S. Ahmed, Li Liu, and Yifan Zhang for sharing research experiences and friendship. In particular, I want to thank my former colleague Dr. Mohamed A. Swillam for his helpful discussion and support during the tough period in one of my graduate courses. Many thanks are also due to the technical and support staff members in the Department of Electrical and Computer Engineering at McMaster University, Cheryl Gies, Terry Greenlay, Cosmin Coroiu, and Steve Spencer for always

being available for support. Without their help, the completion of this work would not be possible.

Finally, I want to express my heartfelt gratitude to my parents, who raised me to the best of their ability, for consistently being there for me, for continuous encouragement and understanding. I am deeply indebted to them for their endless support—hoping they could share this moment with me.

Contents

Abstract iii

Acknowledgments iv

Contents vi

List of Figures ix

1 Introduction 1

1.1 Inverse Source Problems in the Time Domain 4

1.2 Outline of the Thesis 6

1.3 Contribution 8

2 Inverse Source Problems in Electromagnetics 12

2.1 The Ill-Posedness and the Non-Radiating Sources 15

2.1.1 Non-Uniqueness and the Invisible Object 16

2.1.2 Non-Radiating Sources 18

2.2 Prior Conditions and the Regularization Procedure 23

2.2.1 Prior Constraints for Inverse Source Problems 25

2.2.2 The Regularization Procedure 27

2.3 The Scalar Inverse Source Problem 28

2.3.1 The Approach of Porter-Bojarski Integral Equation 29

2.4 The Vector Inverse Source Problem 31

2.4.1 Minimum Energy Solution Using Multipole Expansion of the Far-Field data 32

2.5 Inverse Source Problems in the Time Domain 34

2.5.1 The Source Solution with Separable Space-Time Dependence 34

2.5.2 The Source Solution Using the Far-field Data 36

2.6 Conclusion 37

3 TLM Formulation of Inverse Source Problems for Thin Source Regions **43**

3.1 TLM Method and the Direct Problem 45

3.2 The Linear Inversion Formulation 47

3.3 The Reconstruction Algorithm 49

3.4 Numerical Results 52

3.4.1 A Two-Dimensional Thin Source Region Composed of Eight Source Cells 54

3.4.2 A Two-Dimensional Thin Source Region Composed of 400 Source Cells 54

3.4.3 A Two-Dimensional Thin Reentrant Source Region Composed of 12 Source Cells 56

3.4.4 A Three-Dimensional Thin Source Region Composed of 288 Source Cells 56

3.5 Effect of Noise 61

3.6 Conclusions 62

4 TLM Formulation of Inverse Source Problems with Smoothness Constraints **67**

4.1 TLM Formulation of the Direct Problem... 68

4.2 The Linear Inverse Formulation 72

4.3 The Solution with the Smoothness Constraint 77

4.4 Practical Implementation 80

4.5 Numerical Examples 82

4.5.1 A Rectangular Source Region 84

4.5.2 A Re-entrant Source Region 89

4.5.3 Effect of Noise 89

4.6 Conclusions 92

5 Conclusion **97**

List of Figures

2.1 Illustration of a direct problem whose inverse problem is ill-posed. 17

3.1 A discretized two-dimensional source region with arbitrary shape. 44

3.2 Examples of two-dimensional thin source regions inside a two-dimensional computational domain. 45

3.4 A discretized two-dimensional source region composed of 8 source cells with shape 2 by 4 grids. 52

3.3 Illustration of solving $(\boldsymbol{EA})\,\mathbf{v}_{k-1}^{s} = \mathbf{v}_{k}^{b} - \boldsymbol{E}\tilde{\mathbf{v}}_{k}$ at the kth time step using the time-reversal property of the TLM method. 53

3.5 The reconstructed excitation sources on six arbitrarily selected source cells inside the thin source region with shape 2 by 4 grids. 55

3.6 A discretized two-dimensional source region composed of 400 source cells with shape 2 by 200 grids. 56

3.7 The reconstructed excitation sources on six arbitrarily selected source cells inside the thin source region with shape 2 by 200 grids. . . . 57

3.8 A discretized two-dimensional thin reentrant source region composed of 12 source cells. 58

3.10 A three-dimensional source region with size $12 \times 12 \times 2$ cubes. 58

3.9 The reconstructed excitation sources on six arbitrarily selected source cells inside the thin reentrant source region. 59

3.11 The reconstructed excitation sources on six arbitrarily selected source cells inside the three-dimensional thin source region with shape 12 by 12 by 2 cubes. 60

3.12 The reconstructed excitation sources under noisy condition with noise level -26 dB for the two-dimensional thin source region with shape 2 by 200 grids. 63

3.13 The reconstructed excitation sources under noisy condition with noise level -20 dB for the two-dimensional thin source region with shape 2 by 200 grids. 64

3.14 The reconstructed excitation sources under noisy condition with noise level -16 dB for the two-dimensional thin source region with shape 2 by 200 grids. 65

4.1 Illustration of the scattering and connection TLM procedures in a two-dimensional computational domain. 70

4.2 A discretized two-dimensional source region in a rectangular shape. ... 73

4.3 A six-layer source region with size 12 by 16 grids. 85

4.4 The spatial distribution of the exact sources and the reconstructed sources at selected time steps for the rectangular source region of size 12 by 16 grids. 86

4.5 The reconstructed sources with respect to time at selected cell locations inside the rectangular source region of size 12 by 16 grids. ... 87

4.6 A four-layer reentrant source region composed of 172 source cells. 88

4.7 The spatial distribution of the exact sources and the reconstructed sources at selected time steps for the reentrant source region composed of 172 source cells. 90

4.8 The reconstructed sources with respect to time at selected cell locations inside the reentrant source region composed of 172 source cells. 91

4.9 The reconstructed excitation sources using the noisy field data with noise level -28 dB. 93

4.10 The reconstructed excitation sources using the noisy field data with noise level -5.6 dB. 94

4.11 The reconstructed excitation sources using the noisy field data with noise level 8.2 dB. 95

Chapter 1

Introduction

Today, inverse problems arise in many branches of applied sciences: medical diagnostics, atmospheric sounding, radar and sonar target estimation, seismology, radio astronomy, microscopy, etc. In the most general sense, an *inverse problem* may be broadly described as a problem of determining the internal structure or past state of a system from indirect external measurements [1], which corresponds to the reverse of the usual "cause-effect" sequence of events [1].

In the domain of electromagnetism and optics, inverse problems are usually divided into two broad classes: (1) *inverse scattering problems* (also known as inverse medium problems), that obtain the characteristics of a scattering object form its scattered wave due to external illumination, and (2) *inverse source problems*, that determine the constitution of a source from measured values of its emitted radiation.

Inverse scattering problems have been very successful in recent years, most signif-

icantly in medical imaging, due to the rapid development of Computed Tomography (CT) technology [2]. Other common applications include concealed weapon detection, non-destructive evaluation or testing, and remote sensing, see [3, 4, 5]. The inverse source problems, in contrast, have received little attention, partially because of the severe non-unique nature in the solutions. Despite this ill-posedness, inverse source problems still find direct applications in antenna design [6] and holographic imaging [7, 8].

Inverse scattering problems are in general nonlinear. They have been the objective of elegant mathematical investigations. However, it is well known that the electromagnetic parameters like permittivity and conductivity of a scattering object can be retrieved from its induced current sources—the equivalent sources producing the scattered waves. Therefore, in these cases, inverse scattering problems can sometimes be transformed into their equivalent inverse source problems. Solving an inverse source problems can be considered as an intermediate step in solving inverse scattering problems. In the literature, there are a series of inverse scattering papers [9, 10, 11, 12, 13] in which an inverse source problem is first solved. The work included in this thesis considers the vector inverse source problem for the Maxwell's system. Our work shall be applied for solving the correspondent inverse scattering problem in the future.

Inverse source problems are conventionally addressed by using frequency-domain approaches, in which a Fourier transform with respect to time is taken for all physical quantities and the resultant time-independent equations are studied for a fixed fre-

quency. Different aspects of the frequency-domain solutions have been investigated by many authors, for both deterministic and random sources. Ref. [6] discusses its application in antenna pattern design. Ref. [14, 15, 16] addresses the non-radiating (NR) sources in the solutions of the inverse source problems. Ref. [17, 18, 19, 20] examines the inverse source problem for partial coherent sources and random sources. And in Ref. [7, 8, 21, 22], the so-called Minimal Energy (ME) solutions of inverse source problems are studied.

In our work, the inverse source problem for the Maxwell's system is treated numerically by applying the Transmission-Line Matrix (TLM) method [23], a numerical technique for the field computation. Unlike the classic frequency domain approach, our solution is obtained in the time domain using the time-domain knowledge of discrete near-field measurements outside the source supporting region. The time-domain approach to the inverse source problems is complementary to that of the frequency-domain approach. While the frequency-domain approach relates the radiation pattern to the sources for a fixed frequency, the time-domain approach studies simultaneously a band of frequencies or a short pulse in the time domain.

This work aims at solving inverse scattering problems in the time domain using wideband (WB) short-pulse fields as the illuminating sources. Because of the wide band of these fields, solution techniques directly in the time domain, where the fields are localized, are preferable over the more conventional approach of transforming the frequency-domain solution into the time domain. This motivates us in seeking the solutions of inverse source problems in the time domain. A recent review of short

pulse systems, applications, and of analysis techniques can be found in [24].

1.1 Inverse Source Problems in the Time Domain

Our work considers the reconstruction of current source distribution $\boldsymbol{J}(\boldsymbol{r}, t)$ inside a closed spatial region D. The exterior of D is assumed to be source-free. The background medium is assumed to be homogeneous (free space) containing the vector electric field $\boldsymbol{E}(\boldsymbol{r}, t)$ and the vector magnetic field $\boldsymbol{H}(\boldsymbol{r}, t)$. The coupling between the two fields are governed by Maxwell's equations. Our time-domain inverse source problem can then be stated as that of reconstructing the excitation source $\boldsymbol{J}(\boldsymbol{r}, t)$ for $\forall \boldsymbol{r} \in D$ from discrete measurements of the radiated field $\boldsymbol{E}(\boldsymbol{r}, t)$ or $\boldsymbol{H}(\boldsymbol{r}, t)$ for $\mathbf{r} \notin D$, for all retarded time t. In our case, all the field observation points are located on boundary of D, and supply near-field radiation data. The time-dependent excitation source distribution $\boldsymbol{J}(\boldsymbol{r}, t)$ is assumed to satisfy the Sommerfeld radiation condition at infinity.

It has been known for a long time that solutions of the inverse source problems in general are affected by rather serious non-uniqueness. This phenomenon is primarily due to the so-called non-radiating (NR) sources, a distribution of sources that does not produce a radiation field, however, stores reactive field energy within the source region. Concerning the time-domain solutions of inverse source problems, it has been shown in [25] that in addition to the NR sources there is another class of source distributions that generate nulls in the time-domain radiation pattern only for certain

discrete and/or continuous sets of directions. Thus in our time-dependent inverse source problem with discrete measurements, the class of sources that do not radiate at all (NR sources) and the class of sources that are NR only with respect to certain observation points, together, contribute to the non-uniqueness of the solutions.

Our treatment of solving the inverse source problem is dealt with numerically by using the Transmission-Line Matrix method [23]. By transforming the sources and the field into the equivalent link voltages defined in the TLM methodology, a linear inversion formalism for the inverse source problem is developed. The non-uniqueness of its solution is resolved by the adoption of Tikhonov-like regularization approach [1] using the additionally provided smoothness *prior* condition. Solving inverse problems in electromagnetics using TLM method have appeared two times in the past. In [26] and [27], time-reversal property of TLM method is utilized for the localization of scattering object from external field measurement in the time domain. However, their proposed approach fails to determine the shape and the internal composition of the scattering object, and thus does not solve the inverse problem completely.

Inverse source problems in the time domain have been reported two times in the past. The earliest treatment appears to be in [28, 29][1], where inverse initial value problems for both the scalar wave equation and Maxwell's equations are considered. This work provides expressions for the field distribution at some initial time period (say $t = 0$) from the field distribution at a later time ($t > 0$) using the expansion in homogeneous plane waves. In [25][2], the inverse source problem in the time domain

1 Also discussed in Section 2.5.1.

for the scalar Helmholtz's equation is dealt with by processing the field data in the far zone by using a limited-view Radon inversion framework [30, 31]. Our work, to the author's knowledge, is the first time-domain treatment of the vector inverse source problem using near field measurements.

1.2 Outline of the Thesis

The main objective of this thesis is to introduce a numerical approach for solving the inverse source problem in the time domain. We start by investigating the inverse source problem inside a thin discretized source region whose enclosed mesh cells are all exposed to its exterior. For this special case, the source solution can be uniquely determined at every discrete time step. We then generalized our approach to a discretized source region with arbitrary shape. For this broader case, a unique solution can be obtained by imposing a smoothness *prior* constraint to refining the solution space.

Chapter 2 reviews the fundamental theory of inverse source problems as well as the generalized ill-posed inverse problems. The non-unique nature in inverse source problems is discussed with emphasis on the so-called non-radiating (NR) sources [14, 15, 16]. For the treatment of the non-uniqueness, regularization techniques and the use of *prior* conditions are also covered. This chapter also includes a review on past

2 Also discussed in Section 2.5.2

approaches of solving inverse source problems for both the scalar cases and the vector cases.

In Chapter 3, our TLM-based inversion approach for solving time-domain inverse source problems is applied to thin source regions for both two-dimensional and three-dimensional cases. Our algorithm requires three TLM iterations for reconstructing the source distribution at one single time step using the discrete field data on the boundary of the source region. Our approach is verified through reconstructing the sources inside a two-dimensional source region composed of 8 source cell, a two-dimensional source region composed of 400 source cells, and a three-dimensional source region composed of 288 source cells. In addition, we also evaluated our approach using noisy field data.

Chapter 4 generalizes our inversion approach to accommodate a two-dimensional source region with arbitrary geometry. Unlike the case for thin source regions, the resultant inversion formulation for a generalized source region appears to be a low-rank linear algebraic system. For overcoming the non-uniqueness, we additionally impose the smoothness constraint (*a priori*) on the solution space by minimizing the first-order time and spatial derivatives of the reconstructed sources. Our approach is illustrated through the reconstruction of sources inside a rectangular source region and a reentrant source region, for both noise-free case and noisy case.

The thesis conclude in Chapter 5, providing suggestions for further research. For convenience, a bibliography is given at the end of the thesis collecting all the references used.

1.3 Contribution

The author's original contributions presented in this thesis are:

(1) introducing a discrete linear inversion formulation for solving vector inverse source problem inside a thin discretized region;

(2) development and implementation of a source reconstruction algorithm for solving the inverse source problem inside a thin discretized region;

(3) introducing a discrete linear inversion formulation for solving vector inverse source problem inside a discretized region with arbitrary shape;

(4) development of a discrete regularization procedure for rendering the non-uniqueness of the inverse source problem;

(5) development and implementation of a source reconstruction algorithm for solving the inverse source problem inside a discretized region with arbitrary;

(6) contribution to the comprehensive review on the concept and theory of inverse source problems.

Reference

[1] M. Bertero and P. Boccacci, *Introduction to Inverse Problems in Imaging*, Philadelphia, PA: Institute of Physics Publishing, 1998.

[2] M. Bertero, "Linear inverse and ill-posed problems," *Advances in electronics and electron physics*, vol. 75, no. 1, pp. 1–120, 1989.

[3] H. M. Chen, S. Lee, R. M. Rao, M. A. Slamani, and P. K. Varshney, "Imaging for concealed weapon detection: a tutorial overview of development in imaging sensors and processing," *IEEE signal processing Magazine*, vol. 22, no. 2, pp. 52–61, 2005.

[4] J. H. Bungey, "Sub-surface radar testing of concrete: a review," *Construction and Building Materials*, vol. 18, no. 1, pp. 1–8, 2004.

[5] B. W. Schilling and G. C. Templeton, "Three-dimensional remote sensing by optical scanning holography," *Applied Optics*, vol. 40, no. 30, pp. 5474–5481, 2001.

[6] C. Müller, "Electromagnetic radiation patterns and sources," *IEEE Transactions on Antennas and Propagation*, vol. 4, no. 3, pp. 224–232, 1956.

[7] R. P. Porter and A. J. Devaney, "Holography and the inverse source problem," *Journal of the Optical Society of America*, vol. 72, no. 3, pp. 327–330, 1982a.

[8] A. J. Devaney and R. P. Porter, "Holography and the inverse source problem. Part II: Inhomogeneous media," *Journal of the Optical Society of America A*, vol. 2, no. 11, pp. 2006–2011, 1985.

[9] W. C. Chew, Y. M. Wang, G. Otto, D. Lesselier, and J. C. Bolomey, "On the inverse source method of solving inverse scattering problems," *Inverse Problems*, vol. 10, pp. 547, 1994.

[10] A. Abubakar and P. M. Berg, "The contrast source inversion method for location and shape reconstructions," *Inverse Problems*, vol. 18, pp. 495, 2002.

[11] M. M. Ney, A. M. Smith, and S. S. Stuchly, "A solution of electromagnetic imaging using pseudoinverse transformation," *IEEE Transactions on Medical Imaging*, vol. 3, pp. 155–162, 1984.

[12] S. Caorsi, G. L. Gragnani, and M. Pastorino, "Two-dimensional microwave imaging by a numerical inverse scattering solution," *IEEE Transactions on Microwave Theory and Techniques*, vol. 38, no. 8, 1990.

[13] W. Weiyan and Z. Shourong, "Unrelated illumination method for electromagnetic inverse scattering of inhomogeneous lossy dielectric bodies," *IEEE Transactions on Antennas and Propagation*, vol. 40, no. 11, pp. 1292–1296, 1992.

[14] A. J. Devaney and E. Wolf, "Radiating and nonradiating classical current distributions and the fields they generate," *Physical Review D*, vol. 8, no. 4, pp. 1044–1047, 1973.

[15] N. Bleistein and J. K. Cohen, "Nonuniqueness in the inverse source problem in acoustics and electromagnetics," *Journal of Mathematical Physics*, vol. 18, no. 2, pp. 194–201, 1977.

[16] A. J. Devaney, "Nonuniqueness in the inverse scattering problem," *Journal of Mathematical Physics*, vol. 19, pp. 1526–1535, 1978.

[17] A. J. Devaney, "The inverse problem for random sources," *Journal of Mathematical Physics*, vol. 20, no. 8, pp. 1687–1691, 1979.

[18] I. J. LaHaie, "Inverse source problem for three-dimensional partially coherent sources and fields," *Journal of the Optical Society of America A*, vol. 2, no. 1, pp. 35–45, 1985.

[19] I. J. LaHaie, "Uniqueness of the inverse source problem for quasi-homogeneous partially coherent sources," *Journal of the Optical Society of America A*, vol. 3, no. 7, pp. 1073–1079, 1986.

[20] W. H. Carter and E. Wolf, "Inverse problem with quasi-homogeneous sources," *Journal of the Optical Society of America A*, vol. 2, no. 11, pp. 1994–2000, 1985.

[21] E. A. Marengo and A. J. Devaney, "The inverse source problem of electromagnetics: linear inversion formulation and minimum energy solution," *IEEE Transactions on Antennas and Propagation*, vol. 47, no. 2, pp. 410–412, 1999.

[22] E. A. Marengo, A. J. Devaney, and R. W. Ziolkowski, "Inverse source problem and minimum-energy sources," *Journal of the Optical Society of America A*, vol. 17, no. 1, pp. 34–45, 2000.

[23] W. J. R. Hoefer, "The transmission-line matrix method–theory and applications," *IEEE Transactions on Microwave Theory and Techniques*, vol. 33, no. 10, pp. 882–893, 1985.

[24] *Proceedings of the Ninth International Conference on Ultrawideband Short Pulse Electromagnetics*, edited by F. Sabath, D. V. Giri, F. Rachidi, and A. Kaelin, Lausanne, Swizerland, 1998.

[25] E. A. Marengo, A. J. Devaney, and R. W. Ziolkowski, "New aspects of the inverse source problem with far-field data," *Journal of the Optical Society of America A*, vol. 16, no. 7, pp. 1612–1622, 1999.

[26] D. M. Hailu, N. K. Nikolova, and M. H. Bakr, "Sub-wavelength microwave radar imaging for detection of breast cancer tumors," in *International Symposium on Signals, Systems and Electronics*, 2007, pp. 107–110.

[27] Y. Kagawa and M. Analoui, "Application of TLM model to an inverse problem (identification of source and scatterer in time domain)," *Compel-International Journal for Computation and Math in Electrical and Electronic Engineering*, vol. 13, pp. 271–276, 1994.

[28] H. E. Moses, "Solution of Maxwell's equations in terms of a spinor notation: the direct and inverse problem," *Physical Review*, vol. 113, no. 6, pp. 1670–1679, 1959.

[29] H. E. Moses, "The time-dependent inverse source problem for the acoustic and electromagnetic equations in the one-and three-dimensional cases," *Journal of Mathematical Physics*, vol. 25, no. 6, pp. 1905–1923, 1984.

[30] P. R. Smith, T. M. Peters, and R. H. T. Bates, "Image reconstruction from finite numbers of projections," *Journal of Physics A: Mathematical, Nuclear and General*, vol. 6, pp. 361–382, 1973.

[31] A. K. Louis and A. Rieder, "Incomplete data problems in X-ray computerized tomography," *Numerische Mathematik*, vol. 56, no. 4, pp. 371–383, 1989.

Chapter 2

Inverse Source Problems in Electromagnetics

In the most general sense, the inverse source problem for a given partial differential operator (PDO) may be defined as deducing the "source", in a general coordinate space of interest (i.e. spatial or spatial-temporal), from the "field" it generates outside the support of the source [1]. In the literature of inverse source problems, particular descriptions are applicable to specific PDOs. Some commonly investigated PDOs include the Helmholtz operator [2, 3], the vector wave equation operator [4, 5], the D'Alembertian operator [6], the operator for the heat equation [7], and the operator for the diffusion equation [8].

In this review chapter, we restrict our attention to two fundamental PDOs in wave theory: (1) the scalar wave equation operator as defined by the inhomogeneous

Helmholtz equation; (2) the vector wave equation operator as defined by Maxwell's equations.

Within the context of the scalar wave equation, the inverse source problem consists of deducing a localized source $q(\boldsymbol{r}, t)$ inside a closed source region D. The scalar problem is described by the inhomogeneous Helmholtz wave equation:

$$(\nabla^2 + \frac{1}{c^2}\frac{\partial^2}{\partial t^2})u(\boldsymbol{r}, t) = -4\pi q(\boldsymbol{r}, t). \tag{2.1}$$

The radiated field $u(\boldsymbol{r}, t)$ is measured outside the source region. The exterior of D is assumed to be source-free.

Similarly for the electromagnetic case, the correspondent inverse source problem consists of deducing the electric current density $\boldsymbol{J}(\boldsymbol{r}, t)$ inside the source region. The fields are related to $\boldsymbol{J}(\boldsymbol{r}, t)$ through the vector Maxwell equations

$$\begin{aligned} \nabla \times \boldsymbol{H}(\boldsymbol{r}, t) &= \boldsymbol{J}(\boldsymbol{r}, t) + \frac{\partial \boldsymbol{D}}{\partial t} \\ \nabla \times \boldsymbol{E}(\boldsymbol{r}, t) &= -\frac{\partial \boldsymbol{B}}{\partial t} \\ \nabla \cdot \boldsymbol{D}(\boldsymbol{r}, t) &= 0 \\ \nabla \cdot \boldsymbol{B}(\boldsymbol{r}, t) &= 0. \end{aligned} \tag{2.2}$$

$\boldsymbol{J}(\boldsymbol{r}, t)$ is recovered using the knowledge of the fields $\boldsymbol{E}(\boldsymbol{r}, t)$ or $\boldsymbol{H}(\boldsymbol{r}, t)$ outside the source region.

Conventionally, the inverse source problems are addressed in the frequency domain, in which a Fourier transform with respect to time is taken for all physical

quantities. The resultant time-independent equations are studied for a fixed frequency. For example, let us consider the inhomogeneous Helmholtz equation given in (2.1) and write

$$q(\boldsymbol{r},t) = \frac{1}{\sqrt{2\pi}} \int_{-\infty}^{+\infty} q(\boldsymbol{r},\omega) e^{i\omega t} d\omega \tag{2.3}$$

$$u(\boldsymbol{r},t) = \frac{1}{\sqrt{2\pi}} \int_{-\infty}^{+\infty} u(\boldsymbol{r},\omega) e^{i\omega t} d\omega. \tag{2.4}$$

Then (2.1) becomes

$$(\nabla^2 + k^2) u(\boldsymbol{r},\omega) = -4\pi q(\boldsymbol{r},\omega), \tag{2.5}$$

where $k = \omega/c$ is the wave number at the frequency ω. $q(\boldsymbol{r},\omega)$ and $u(\boldsymbol{r},\omega)$ are the monochromatic sources and the resultant monochromatic field, respectively, at ω.

The frequency-domain approach simplifies the inverse source problems by studying the source solution at a single frequency. The time-domain approach to the inverse source problems, on the other hand, is more difficult to solve. In the literature, only two time-domain treatments [9, 6] are reported.

This chapter is organized as follows. Section 2.1 through Section 2.4 discuss the frequency-domain aspects of the inverse source problems. In Section 2.1, the non-uniqueness in the solutions of inverse source problems is discussed with emphasis on the so-called Non-Radiating (NR) sources. Subsequently in Section 2.2, we review the *prior* conditions that are used to overcome the non-uniqueness in the inverse source problems. In Section 2.3 and Section 2.4, treatments of the ISP for the scalar wave

equation and the vector wave equation are presented respectively. In Section 2.5, the prior work on the time-domain treatment of the ISP is reviewed. Finally, conclusions are drawn in Section 2.6.

2.1 The Ill-Posedness and the Non-Radiating Sources

In Chapter 1, we mention that inverse source problems, in general, are ill-posed due to the phenomenon of non-uniqueness in its solutions. In this section, we comment on these concepts from a general perspective. We then explore the nature of the so-called non-radiating sources in inverse source problems for the wave equations in both the scalar and vector cases.

Like many other inverse problems that have been investigated, inverse source problems are ill-posed in the sense of Hadamard [10]. In his formulation, a problem is said to be *ill-posed*, if its solution does not exist, or is not unique for arbitrary data, or does not depend continuously on the data. With reference to the inverse theory, the above three properties are termed as non-existence, non-uniqueness, and ill-conditioning, respectively.

To explain these concepts more precisely, let us consider a direct problem represented by an operator $\mathcal{A}$ acting on an "object", x. Then the produced "image" of the object, y, follows the equation:

$$\mathcal{A}(x) = y, \tag{2.6}$$

where the forward operator $\mathcal{A}$ defines a mapping between the object space, $\mathcal{X}$, and the image space, $\mathcal{Y}$. The inverse problem is characterized by the inverse operation $\mathcal{A}^{-1}$ acting upon the image y. As illustrated in Figure 2.1, if the inverse problem is ill-conditioned, a slight variation in the image y (due to noise, for instance), may result in a drastic change in the reconstructed object. If the inverse problem is non-unique, even a noise-free image cannot be used to determine the object, because multiple objects can produce the same image. If the solution of the inverse problem does not exist, there is no physical object that could produce the image. An excellent introduction to these concepts can also be found in [11]. In this section, we are only concerned with the non-uniqueness aspect of the inverse source problems.

2.1.1 Non-Uniqueness and the Invisible Object

Non-uniqueness is a phenomenon which, unfortunately, arises very often in many classes of inverse problems including inverse source problems. It occurs when an inverse problem defines a transition for a physical quantity with a certain information content to another quantity with a higher information content. Consider the same direct problem as defined in (2.6). We further introduce non-uniqueness to its inverse problem by imposing the condition that there exist two distinct objects in the object $\mathcal{X}$, say x_1 and x_2, that produce exactly the same image y in the image space $\mathcal{Y}$, or equivalently

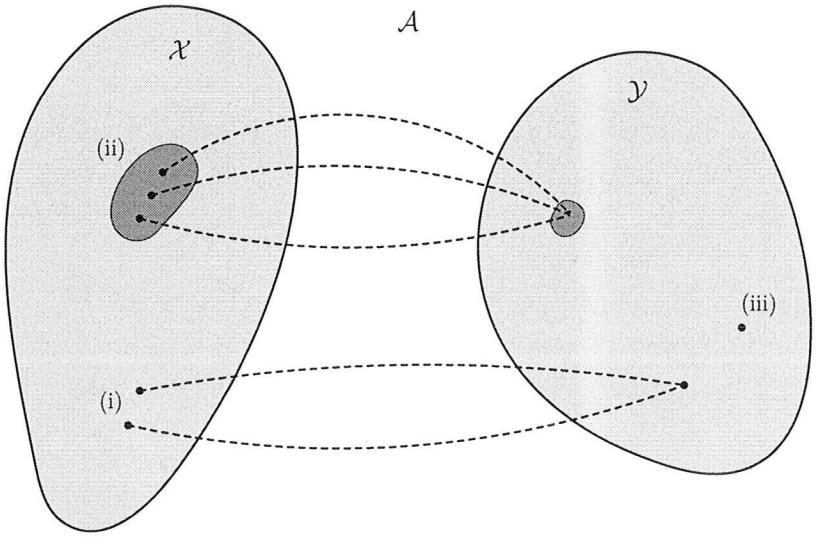

Figure 2.1 Illustration of a direct problem whose inverse problem is ill-posed, and the forward operator $\mathcal{A}$ defines the mapping from the object space $\mathcal{X}$ to the image space $\mathcal{Y}$. (i) Nonuniqueness corresponds to two different objects which map to the same image; (ii) ill-conditioning corresponds to two significantly different objects which produce nearly the same image, and the shaded subsets in $\mathcal{X}$ and $\mathcal{Y}$ illustrate the loss of information; (iii) non-existence corresponds to a image which cannot map to the object space.

$$\mathcal{A}(x_1) = y \qquad \text{and} \qquad \mathcal{A}(x_2) = y. \tag{2.7}$$

Furthermore, we assume that the forward operator $\mathcal{A}$ in (2.6) and (2.7) is a linear operator as for the case of many inverse source problems. Then by linearity, it follows that

$$\mathcal{A}(x_2 - x_1) = 0, \tag{2.8}$$

and a third object $x_3 = x_2 - x_1$ is constructed whose image is exactly zero. The object x_3 is known as *invisible object* [11], and contributes to the non-uniqueness of the inverse problem. When any object in space $\mathcal{X}$ is added to an invisible object, the new object would produce exactly the same image.

In the context of inverse source problems, the nature of the invisible objects are some certain source distribution, whose generated fields remain confined (are nonzero only) within the region of its localization. In the literature, this distribution of sources is commonly referred to as Non-Radiating (NR) [12, 13, 14][1]. The existence of NR sources simply implies that a source distribution cannot be uniquely determined from the field measurement outside the source supporting region.

2.1.2 Non-Radiating Sources

Non-Radiating (NR) sources, as defined in the previous section, have been of interest for a long time in connection with inverse source problems. Different aspects of NR

1 For a distinction, there also exists another type of invisible object called *non-scattering scatterer*. It often appears in the literature on inverse scattering problem. The non-scattering scatterer is not a primary radiation source, however it does not scatter incident plane waves for one or several directions of incidence.

sources have been investigated, and here we list some of the most notable works in the sequence of their appearance.

In 1973, an early work by Devaney and Wolf [15] investigated the NR current sources for full Maxwell's system by transforming all time-harmonic field vectors in the forms of multipole expansions. In 1977, Bleistein and Cohen [16] readdressed the NR sources for both scalar wave equations (Helmholtz model) and vector wave equations (Maxwell model) by formulating the correspondent inverse source problem as the Fredholm integral equation of the first kind. Their work also explicitly showed how the existence of NR sources implies the non-uniqueness of the inverse source problem. In the 1980s, work on this subject focused on the mathematical properties of such sources, and work includes Ref. [17] by Kim and Wolf in 1986 and Ref. [18] by Gamlliel *et al.* in 1989. And recently, much work has focused on the description of the "radiating" and "nonradiating" parts of a source, see [12],[13] and [14]. A very good review about NR sources can also be found in Ref. [19].

Now we focus on some of previously established fundamental characteristics or NR sources. We start by considering the scalar NR sources for the time-harmonic inhomogeneous Helmholtz equation given by (2.5).

In (2.5), if $q(\boldsymbol{r},\omega)$ does not radiates outside D, or equivalently, $u(\boldsymbol{r},\omega) = 0$ for $\forall \boldsymbol{r} \notin D$, then either one of the following three conditions must hold [17]:

(i) $\tilde{q}(k\boldsymbol{s},\omega) = 0$ for all real unit vectors $\boldsymbol{s}$ [16, *lemma 1*], and $\tilde{q}(\boldsymbol{K},\omega)$ denotes the spatial Fourier transform of $q(\boldsymbol{r},\omega)$ given by

$$\tilde{q}(\boldsymbol{K},\omega) = \int_D q(\boldsymbol{r}',\omega)\exp(-i\boldsymbol{K}\boldsymbol{r}')d^3\boldsymbol{r}'. \tag{2.9}$$

Equation (2.9), perhaps, is the most-often mentioned requirement that a scalar NR source must satisfy. It simply states that the three-dimensional Fourier transform of the source distribution must vanish on a sphere of radius equal to the wavenumber k of the incident radiation.

(ii) $q(\boldsymbol{r},\omega)$ is of the form

$$q(\boldsymbol{r},\omega) = -(1/4\pi)(\nabla^2 + k^2)f(\boldsymbol{r}), \tag{2.10}$$

where $f(\boldsymbol{r})$ is any function with continuous second partial derivatives that vanishes identically outside D [15, *theorem V*].

(iii) The following equation [16, *theorem 1*] holds for all points $\boldsymbol{r}$, whether inside or outside of the source volume D,

$$\int_D q(\boldsymbol{r}',\omega)j_0(k|\boldsymbol{r}-\boldsymbol{r}'|)d^3\boldsymbol{r}' = 0,$$

where $j_0(k\boldsymbol{r})$ is the spherical Bessel function of order zero.

Now, we consider the vector electromagnetic sources and field in the full Maxwell's system. From the Maxwell equations in free-space, it follows that the monochromatic fields $\boldsymbol{E}(\boldsymbol{r},\omega)$, $\boldsymbol{H}(\boldsymbol{r},\omega)$ and the monochromatic electric current source $\boldsymbol{J}(\boldsymbol{r},\omega)$ satisfy, respectively [20, ch. 1, eq. (55)]

$$
\begin{aligned}
(\nabla^2 + k^2)\boldsymbol{E}(\boldsymbol{r},\omega) &= -i\left[\omega\mu_0 \boldsymbol{J}(\boldsymbol{r},\omega) + \frac{\nabla\nabla\cdot\boldsymbol{J}(\boldsymbol{r},\omega)}{\omega\epsilon_0}\right] \\
(\nabla^2 + k^2)\boldsymbol{H}(\boldsymbol{r},\omega) &= -\nabla\times\boldsymbol{J}(\boldsymbol{r},\omega),
\end{aligned}
\tag{2.11}
$$

where $k = \omega\sqrt{\mu_0\epsilon_0}$ is the wavenumber of the field and ∇^2 is the vector Laplacian operator.

If there exists a time harmonic current source distribution $\boldsymbol{J}(\boldsymbol{r},\omega)$ confined within a region D, the resultant electric field $\boldsymbol{E}(R\boldsymbol{s},\omega)$ and the magnetic field $\boldsymbol{H}(R\boldsymbol{s},\omega)$ in a direction $\boldsymbol{s}$ and at a distance R in the far zone of the source are given by [21, eqs. (4.4), (4.5) and (4.19)]

$$
\boldsymbol{E}(R\boldsymbol{s},\omega) = -(2\pi)^3\frac{ik}{c}\left(\boldsymbol{s}\times[\boldsymbol{s}\times\tilde{\boldsymbol{J}}(k\boldsymbol{s},\omega)]\right)\frac{e^{ikR}}{R} \tag{2.11a}
$$

$$
\boldsymbol{H}(R\boldsymbol{s},\omega) = (2\pi)^3\frac{ik}{c}\times\tilde{\boldsymbol{J}}(k\boldsymbol{s},\omega)\frac{e^{ikR}}{R}, \tag{2.11b}
$$

where $\tilde{\boldsymbol{J}}(k\boldsymbol{s},\omega)$ is the three-dimensional spatial Fourier transform of the current density given by

$$
\tilde{\boldsymbol{J}}(k\boldsymbol{s},\omega) = \frac{1}{(2\pi)^3}\int_D \boldsymbol{J}(\mathbf{r}',\omega)e^{-ik\boldsymbol{s}\cdot\mathbf{r}'}d^3\mathbf{r}'. \tag{2.12}
$$

By (2.11), it is evident that the current distribution will not radiate if

$$
\tilde{\boldsymbol{J}}(k\boldsymbol{s},\omega) = 0 \qquad \text{for all unit direction } \boldsymbol{s}. \tag{2.13}
$$

This non-radiating condition is comparable to NR condition (i) for the scalar radiation source, and is first derived in [15, *theorem III*]. Similarly, condition (ii) and condiiton

(iii) may also apply to vector NR sources with little modification, and has been derived in [16, *lemma 2*] and [15, *theorem V*], respectively.

Due to the vectorial nature of electromagnetic fields, there is another class of sources which do not radiate power. For instance[2], consider a current density source of the form

$$\boldsymbol{J}(\mathbf{r},\omega) = \mathbf{r} f(r), \tag{2.14}$$

where $f(r), r = |\boldsymbol{r}|$ is a spherically symmetric, continuous function. The current is then purely radial, and the sphere might be described to be "pulsating" [19].

Substituting (2.14) into (2.12), and noting that

$$\boldsymbol{r} e^{-i\boldsymbol{s}\cdot\mathbf{r}} = i\nabla_K e^{-i\boldsymbol{K}\cdot\mathbf{r}}, \tag{2.15}$$

we may express the spatial Fourier transform of the current density as

$$\begin{aligned}\tilde{\boldsymbol{J}}(k\mathbf{r},\omega) &= \frac{i}{(2\pi)^3}\nabla_K \int_D f(r')e^{-i\boldsymbol{K}\cdot\mathbf{r}'}d^3\mathbf{r}' \\ &= i\nabla_k \tilde{f}(K),\end{aligned} \tag{2.16}$$

where $\tilde{f}(K)$ is the three-dimensional Fourier transform of $f(r)$. Therefore

$$\tilde{\boldsymbol{J}}(k\boldsymbol{s},\omega) = i\nabla_K \tilde{f}(K)|_{\boldsymbol{K}=k\boldsymbol{s}} = i\left(\frac{\partial}{\partial K}\tilde{f}(K)|_{K=k}\right)\boldsymbol{s}. \tag{2.17}$$

It can be seen that

2 This example follows from [19].

$$\boldsymbol{s} \times \tilde{\boldsymbol{J}}(k\boldsymbol{s}, \omega) = \boldsymbol{s} \times [\boldsymbol{s} \times \tilde{\boldsymbol{J}}(ks, \omega)] = 0, \tag{2.18}$$

which shows that the fields vanish in the far zone of the current density.

2.2 Prior Conditions and the Regularization Procedure

As discussed in the previous section, the ill-posedness to an inverse problem, in general, comes from three difficulties: *non-existence* of the solution, *non-uniqueness* in the solution, and large errors in the solution of the problem produced by small errors in the data (in which case the problem is said to be *ill-conditioned*). In particular, inverse source problems, suffer rather serious non-uniqueness in their solution. In this section, we review the general approach to curing the ill-posedness of the inverse source problems.

It is well known that a linear problem can be discretized to produce a linear algebraic system. Let's reconsider the direct problem given in (2.6), where the forward operator $\mathcal{A}$ is a linear operator defining the mapping from the object space $\mathcal{X}$ (the solution space) to the image space $\mathcal{Y}$ (the data space). For its discrete case, each image in $\mathcal{Y}$ is sampled at m discrete locations (or composed of m pixels), and is represented by the vector $\boldsymbol{y} \in \mathbb{R}^m$, in a new image space $\mathcal{Y}_m$, with finite dimension m. Similarly, we adopt the object space $\mathcal{X}$, discretized into n dimensions and denoted by $\mathcal{X}_n$. There, each object is represented by another vector $\boldsymbol{x} \in \mathbb{R}^n$. Then the forward operator $\mathcal{A}$ in (2.6) can be discretized according to the dimension of the new image

space $\mathcal{Y}_m$ and the new object space $\mathcal{X}_n$, leading to a discrete formulation of the direct problem:

$$\boldsymbol{A}\boldsymbol{x} = \boldsymbol{y}, \tag{2.19}$$

where the matrix $\boldsymbol{A} \in \mathbb{R}^{m \times n}$ is the discrete form of the operator $\mathcal{A}$.

Now, we consider the inverse of the direct problem as formulated in (2.6). If the inverse problem to (2.6) is well-posed and $\boldsymbol{y}$ is given, then a unique solution $\boldsymbol{x}$ can be obtained by solving the linear system given in (2.19). If there exists a $\boldsymbol{y}$ that is not in the range of $\boldsymbol{A}$ (as in the case of *non-existence*), only one least-square solution of $\boldsymbol{x}$ can be obtained. However, if the solution to the inverse problem is *non-unique*, then the resultant system matrix $\boldsymbol{A}$ in (2.19) would be low-ranked, and a unique solution of $\boldsymbol{x}$ cannot be obtained. Furthermore, if the inverse problem is *ill-conditioned* and even the solution is known to be unique, the noise on the image vector $\boldsymbol{y}$ can be augmented by a factor related to the condition number of $\boldsymbol{A}$, leading to oscillations in the reconstructed object vector $\boldsymbol{x}$, which would completely hide the physical solution corresponding to the noise-free image.

In all above cases for an ill-posed problem, a "regularizing" action is required, to overcome the uncertainties of the solution space and the problem model in response to the noise in the images. The general approach is to restrict the solution space $\mathcal{X}$ to a subspace $\mathcal{X}'$, characterized by additional information not considered in (2.6) or in its discrete counterpart (2.19). This information, which is also called *a priori*, is additional in the sense that it cannot be derived from the data (the image) or from the

properties of the mapping $\mathcal{A}$, but expresses some expected physical properties on the solution space (or the object space) to discriminate the solution of our interest from other spurious solutions produced by the nature of ill-posedness. In inverse theory, the process of using additional information to construct the approximate solution, is called *regularization* [11].

In the subsequent part of this section, we shall review the *prior* constraints that have appeared in the literature about inverse source problems and their implications. Then we shall discuss the general approach to regularizing an ill-posed problem.

2.2.1 Prior Constraints for Inverse Source Problems

In an early work [16] by Bleistein and Cohen, the non-uniqueness of the inverse source problem for the scalar wave equation is first demonstrated by using *a priori* knowledge of known multiplicative time dependence of the sources. Other constraints can also be considered for solving inverse source problems. Here we discuss the *prior* constraints that have appeared in the literature about inverse source problems and their implications.

The most simple and important form of additional information is that the energy of the source cannot be too large, which implies a constraint consisting of an upper bound on the energy. Most treatments of this type consider the requirement of minimizing the L_2 norm (the energy) of the source, where for a time-harmonic source distribution $q(\boldsymbol{r}, \omega)$ confined in a volume D, the term L_2 norm is given by

$$E = \left[\int_D d^3r \, |q(\mathbf{r}, \omega)|^2 \right]^{\frac{1}{2}}. \tag{2.20}$$

By minimizing the L^2 norm, the resulting particular solution, denoted as $q_{ME}(\mathbf{r}, \omega)$, is usually termed as the minimum-energy (ME) solution, or the normal solution as in linear inversion language. Literature utilizing this constraint is abundant, and we cite [2], [22], [3], [23] for scalar inverse source problems, and [4] for the vector case.

For the scalar-wave problem, the physical interpretations of these ME solutions have been given in papers by Devaney and Porter [2], [22] in the context of generalized holography. Their work first demonstrated that the ME solutions to the usual scalar inverse source problem are orthogonal to the class of NR sources or mathematically

$$q_{ME} \in [N(L)]^{\perp} \tag{2.21}$$

where the space $N(L)$ is the subspace of all NR sources. (2.21) implies that ME solutions possess no NR component and are the most efficient solutions to inverse source problems.

In addition to the energy minimization, another kind of additional constraint may be that the profile of the source is smooth, so that its derivatives must be smaller than a certain quantity. For example, [24] incorporates an additional smoothness constraint which requires the solution to be everywhere continuous with continuous derivatives up to a desired order. By imposing this latter constraint in addition to energy minimization, the NR components of the source that are not inherently available from the data can be recovered.

Consider the vector inverse source problem with the existence of the pulsating sources[1] which only produce fields in the near zone. One may also impose an additional constraint that the source has a prescribed reactive power (which can be zero), and such constraints are closely related to the problem of antenna synthesis. In the solution obtained in [25], a NR source component is optimally added (with minimum current level) whose reactive power cancels out the reactive power of its minimum energy counterpart, so to reduce the reactive power as much as desired at the expense of high NR components in the interior of the source.

2.2.2 The Regularization Procedure [26]

For ill-posed inverse problems, the accuracy of the solution is limited by the amount of available information, and by the "conditioning" of the problem. The process of using additional information explicitly, at the start, to construct the approximate solution, is called *regularization procedure* [11]. Here in this section, we consider the generalized regularizing method for the discrete version of a linear inverse problem.

The most popular regularized form of (2.19) can be stated as a minimization problem [26]:

$$\underset{\boldsymbol{x}}{\text{minimize}} \quad \|\boldsymbol{T}(\boldsymbol{A}\boldsymbol{x}-\boldsymbol{y})\|_2^2 + w^2 \|\boldsymbol{R}\boldsymbol{x}\|_2^2, \tag{2.22}$$

1 The pulsating sources are described in section 2.1.2.

where $\boldsymbol{T}$ is the preconditioning matrix for the system (2.19), frequently used to rank the system equations on the basis of their relevance and of their trustworthiness; $\boldsymbol{R}$ is the regularization matrix; and w is the regularization factor, defining the relative balance between the residual of (2.19) and the regularization term.

The formulation given in (2.22) recalls the well-known Tikhonov Regularization Method [11], which is based on a fundamental paper from Tikhonov in 1961. The associated minimization problem given in (2.22) can be then solved by means of the method of Lagrange multipliers.

The matrix $\boldsymbol{R}$ defines the chosen regularization. For instance, the choice of $\boldsymbol{R}$ of being the identity matrix drives the problem to yield minimal norm solutions, such as the case of inverse source problems when the elements of $\boldsymbol{x}$ are associated with energies. Generally, diagonal matrices are well suited to weigh vectors representing energy densities [26]. Another good choice of $\boldsymbol{R}$ may also drive the minimization problem towards solutions in which elements of $\boldsymbol{x}$ follow some assigned distribution [26]. In summary, the choice of the regularization parameter would influence the solution of the problem. More details about the Tikhonov Regularization approach can be found in [11].

2.3 The Scalar Inverse Source Problem

The inverse source problem of the scalar inhomogeneous Helmholtz equation given by (2.5) has been extensively investigated by many authors from homogeneous domain

[2, 3, 24, 27] to inhomogeneous lossy domain [22, 28, 23], from deterministic sources to random sources [29, 30, 31, 32]. The goal of the problem is to determine the source distribution $q(\boldsymbol{r})$ within the source volume D from knowledge of the radiated field

$$u(\boldsymbol{r},\omega) = \int_D d^3\boldsymbol{r}' q(\boldsymbol{r}',\omega)\frac{e^{ik|\boldsymbol{r}-\boldsymbol{r}'|}}{|\boldsymbol{r}-\boldsymbol{r}'|} \tag{2.23}$$

at all observation points $\boldsymbol{r} \notin D$ not contained in the source volume D.

In this section, we shall only discuss the treatment proposed by Porter and Devaney [2], which delivers a minimal energy solution.

2.3.1 The Approach of Porter-Bojarski Integral Equation [2]

In the work by Porter and Bojarski [2], they found that the inverse source problem as described above can be mathematically reduced to solving an integral equation first derived by Porter [33] and later derived independently in a different (but equivalent) form by Bojarski [16]. The integral equation in Porter's formulation is

$$\Gamma(\boldsymbol{r},k) = \frac{ik}{2\pi}\int_D d^3r' q^*(\boldsymbol{r}',\omega) j_0(k|\boldsymbol{r}-\boldsymbol{r}'|), \tag{2.24}$$

where the asterisk denotes a complex conjugate and $j_0(\cdot)$ is the spherical Bessel function of the first kind and zero order. The quantity $\Gamma(\boldsymbol{r},k)$ is determined from the value of the field and its normal derivative over any closed surface Σ completely surrounding the source volume D. In particular,

$$\Gamma(\boldsymbol{r},k)=\int_{\Sigma}ds'\left[u^{*}(\boldsymbol{r}',\omega)\frac{\partial}{\partial\boldsymbol{n}'}u^{*}(\boldsymbol{r}')G(|\boldsymbol{r}-\boldsymbol{r}'|)\right], \tag{2.25}$$

where

$$G(|\boldsymbol{r}-\boldsymbol{r}'|)=\frac{e^{ik|\boldsymbol{r}-\boldsymbol{r}'|}}{|\boldsymbol{r}-\boldsymbol{r}'|} \tag{2.26}$$

is the free-space Green function and $\partial/\partial\boldsymbol{n}'$ denotes differentiation along the outward normal to the surface Σ. The integral equation (2.25) holds at all points $\boldsymbol{r}$ lying within the region enclosed by the surface Σ.

Unfortunately, due the existence of NR sources, the integral equation (2.25) do not possess unique solutions. This is because the associated homogeneous integral equation (2.25) after setting $\Gamma(\boldsymbol{r},k)=0$ possess nontrivial solutions.

Porter and Devaney show that a unique solution to the Porter and Bojarski integral equations can be obtained by demanding that the solution minimize the source energy given by (2.20). The minimum energy solution $q_{ME}(\boldsymbol{r},\omega)$ to the inverse source problem is of interest because it can be shown to be orthogonal to all non-radiating sources and can be readily determined from the boundary field value on the surface Σ.

Consider the integral equation (2.25), and take D to be a sphere of radius R_0 centered at the origin of a spherical coordinate system (r,θ,ϕ). After some deviation, the resultant minimum energy solution is, for $r\leq R_0$

$$q^{*}_{ME}(\boldsymbol{r},\omega)=\sum_{l=0}^{\infty}\sum_{m=-l}^{l}q_{l}^{m^{*}}j_{l}(kr)Y_{l}^{m^{*}}(\theta,\phi), \tag{2.27}$$

with the expansion coeficients $q_l^{m^*}$ given by

$$q_l^{m^*} = -\frac{i}{2k\sigma_l^2} \int_{r' \leq R_0} \times d^3r' \Gamma(\mathbf{r}', k) j_l(kr') Y_l^m(\theta', \phi'). \tag{2.28}$$

In these equations $j_l(kr)$ is the spherical Bessel function of the first kind with order l, $Y_l^m(\theta, \phi)$ is the spherical harmonic of degree l and order m, and σ_l is given by

$$\sigma_l = \int_0^{R_0} r^2 j_l^2(kr) dr. \tag{2.29}$$

For a special case when the surface Σ is well removed from the source volume, the minimum energy solution can be determined from the real-image field generated by a point-reference hologram recorded over Σ.

2.4 The Vector Inverse Source Problem

The problem of determination of current source distributions from external measurements of the electromagnetic fields is commonly known as the inverse source problem of electromagnetics.

Due to the complexity of Maxwell's equation, additional assumptions like the scalar approximation of the quasi-static regime are usually imposed to derive a simplified model, see [34, 35, 36, 37]. However, the coupling bewteen the electric and the magnetic fields cannot, in general be neglected [38]. Thus treatment that using the full Maxwell's system is required.

In the literature, there are not many papers about inverse source problems for Maxwell equations. In this Section, we shall only review the work by Marengo and Devaney [4].

2.4.1 Minimum Energy Solution Using Multipole Expansion of the Far-Field data [4]

The work by Marengo and Devaney [4] considers the reconstruction of current sources $\boldsymbol{J}(\boldsymbol{r},\omega)$ inside a sphere for $|\boldsymbol{r}| < a$ and $\boldsymbol{J}(\boldsymbol{r},\omega)$ is zero for $|\boldsymbol{r}| > a$. Their treatment is based on the well-known multipole expansion of the electromagnetic field [21] and applies, in principle, to both near- and far-field data.

Using multipole expansion, for $r = |\boldsymbol{r}| > a$, the fields $\boldsymbol{E}(\boldsymbol{r},\omega)$ and $\boldsymbol{H}(\boldsymbol{r},\omega)$ can be represented as [39]

$$\begin{aligned}
\boldsymbol{E}(\boldsymbol{r},\omega) &= \sum_{l=1}^{\infty}\sum_{m=-l}^{l}\left[a_{l,m}\nabla\times\left[h_l^{(1)}(kr)\boldsymbol{Y}_{l,m}(\theta,\phi)\right] + ikb_{l,m}h_l^{(1)}(kr)\boldsymbol{Y}_{l,m}(\theta,\phi)\right] \\
\boldsymbol{H}(\boldsymbol{r},\omega) &= \frac{1}{\eta}\sum_{l=1}^{\infty}\sum_{m=-l}^{l}\left[b_{l,m}\nabla\times\left[h_l^{(1)}(kr)\boldsymbol{Y}_{l,m}(\theta,\phi)\right] - ika_{l,m}h_l^{(1)}(kr)\boldsymbol{Y}_{l,m}(\theta,\phi)\right],
\end{aligned} \tag{2.30}$$

where $\eta = \sqrt{\mu_0/\epsilon_0}$ is the wave impedance of the free space. $h^{(1)_l}(\cdot)$ is the spherical Hankel function of the first kind with order l. $\mathbf{Y}_{l,m}(\theta,\phi)$ is the vector spherical harmonic of degree l and order m as defined in [21, eqs. (4.7), (4.8)]. The multipole moments $a_{l,m}$ and $b_{l,m}$ are given in [4, eq. (3), (7) (4.8)].

Equation (2.30) yields, by using large argument expressions for $h^{(1)l}(kr)$, the far-field approximations

$$\begin{aligned} \boldsymbol{E}(\boldsymbol{r}) &\sim \frac{e^{ikr}}{r}\boldsymbol{f}(\boldsymbol{s}) \quad \text{as} \quad kr \to \infty \\ \boldsymbol{H}(\boldsymbol{r}) &\sim \frac{e^{ikr}}{\eta r} \times \boldsymbol{f}(s) \quad \text{as} \quad kr \to \infty \end{aligned} \tag{2.31}$$

with

$$\boldsymbol{f}(\boldsymbol{s}) = \sum_{l=1}^{\infty}\sum_{m=-l}^{l}(-i)^l\left[a_{l,m}\hat{\mathbf{r}} \times \mathbf{Y}_{l,m}(\theta,\phi) + b_{l,m}\,\mathbf{Y}_{l,m}(\theta,\phi)\right]. \tag{2.32}$$

In summary, the multipole moments $a_{l,m}$ and $b_{l,m}$ uniquely specify both the radiated field everywhere outside $r \leq a$ as well as the radiation pattern $\boldsymbol{f}(\boldsymbol{s})$. It follows that the inverse source problem can be formulated as being that of reconstructing $\boldsymbol{J}(\boldsymbol{s},\omega)$ from either the multipole moments or the radiation pattern $\boldsymbol{f}(\boldsymbol{s})$.

By minimizing the L^2 source energy, the obtained expression for the source solution is given by [4]

$$\boldsymbol{J}_{ME} = -\frac{1}{\eta}M(\mathbf{r})\sum_{l=1}^{\infty}\sum_{m=-l}^{l}\left[\frac{a_{l,m}}{\alpha_l^2}\nabla \times \left[j_l(kr)\,\mathbf{Y}_{l,m}(\theta,\phi)\right] + i\frac{b_{l,m}}{k\beta_l^2}j_l(kr)\,\mathbf{Y}_{l,m}(\theta,\phi)\right], \tag{2.33}$$

where $j_l(\cdot)$ is the spherical Bessel function of order l, and $M(\mathbf{r})$ is given by

$$M(\mathbf{r}) = \begin{cases} 1 & \text{if } r \leq a; \\ \\ 2 & \text{if } r > a. \end{cases} \tag{2.34}$$

The singular values α_l^2 and β_l^2 (see [4, eq.(17)]) in the reconstruction formula (2.33) decay exponentially for $l \leq ka$ and confirm the ill-posedness (see [40] for a detailed account of the properties of β_l^2).

Similar result to (2.33) is obtained in [25, eq.(14)] by using a simpler derivation based on Lagrangian optimization.

2.5 Inverse Source Problems in the Time Domain

All previous sections discuss the frequency-domain aspects of inverse source problems. The time-domain treatments of inverse source problems are reviewed in this section.

To our knowledge, only two papers about solving inverse source problems in the time domain have been reported in the past. The earliest work on this subject is due to Moses [9] in 1983, in which the inverse source problems for the time-dependent acoustic and electromagnetic equations in one and three dimensions are investigated. Then until recently in 2000, the work by Marengo *et al.* studies the inverse source problem for the scalar Helmholtz equation in the time domain using the time-domain knowledge of the far-field pattern. Here, these two investigations are briefly summarized.

2.5.1 The Source Solution with Separable Space-Time Dependence [9]

In the work by Moses [9], the inverse source problem to the Maxwell's equations given

by (2.2) is investigated in the time domain using the assumption that the sources are nonzero only for a finite interval of time (say $t_0 < t < t_1$).

In the direct problem, his work is concerned with the initial value problem in which the field is prescribed as a solution of the homogeneous Maxwell's equations before the sources are turned on. Then one could solve the equation for times after the sources are turned on, by using appropriate Riemann functions. After the sources are turned off, one again could obtain a solution of the homogeneous equation which is determined by the initial solution for $t < t_0$ and by the known time-dependent sources.

The inverse problem, as formulated by Moses, is as follows. Let us prescribe t_0 and t_1 and the solutions of the homogeneous Maxwell's equations for $t < t_0$ and $t > t_1$. We want to find the sources as functions of time and space which will lead us to the prescribed solution for $t > t_1$ from the initial solution for $t < t_0$.

Due to the non-unique nature of the inverse source problem, Moses' work also shows that there are actually an infinite number of sources which would satisfy the above condition. Therefore he gives additional condition (a *priori*) on the time dependence which leads to unique sources as far as the space dependence is concerned. This time-dependence of source was to impose the condition

$$\boldsymbol{J}(\boldsymbol{r}, t) = \boldsymbol{J}_e(\boldsymbol{r}) h_e(t) + \boldsymbol{J}_o(\boldsymbol{r}) h_o(t), \tag{2.35}$$

where $\boldsymbol{J}(\boldsymbol{r}, t)$ is the electric current density source as in (2.2). $h_e(t)$ is a real, essentially arbitrary, function of t which is symmetric about the midpoint of the interval $t_0 <$

$t < t_1$. $h_o(t)$ is a real odd function about the midpoint. The subscripts e and o stand for "even" and "odd", respectively. $\boldsymbol{J}_e(\boldsymbol{r})$ and $\boldsymbol{J}_o(\boldsymbol{r})$ are functions of space and are both time-independent.

In his work, Moses review the concept of eigenfunctions of the curl operator [41] as a means of treating electromagnetic theory, fluid dynamics, and other phenomena obeying vector field equations in the infinite domain. He applies this concept first to the direct source problem and then the inverse source problem to simplify drastically the radiation field and its currents from the longitudinal field and its sources. He proves explicitly in closed-form expressions that the $\boldsymbol{J}_e(\boldsymbol{r})$ and $\boldsymbol{J}_o(\boldsymbol{r})$ as in (2.35) can be uniquely determined for three-dimensional electromagnetic theory.

2.5.2 The Source Solution Using the Far-field Data [6]

In the work by Marengo *et al.* [6], the inverse source problem for the inhomogeneous scalar Helmholtz equation is considered in the time domain. The source solution $q(\boldsymbol{r}, t)$ as in (2.1) is deduced from knowledge of the radiated field [42]

$$u(\boldsymbol{r}, t) = \int_{\infty}^{\infty} dt' \int d^3\boldsymbol{r}' \frac{q(\boldsymbol{r}', t')\delta\left(t' + \frac{|\boldsymbol{r}-\boldsymbol{r}'|}{c} - t\right)}{|\boldsymbol{r} - \boldsymbol{r}'|} \tag{2.36}$$

for all $\boldsymbol{r} \notin D$, where $\delta(\cdot)$ is Dirac's delta function.

They define the time-domain far-field radiation pattern $f(\boldsymbol{s}, \tau)$ as

$$u(r\boldsymbol{s}, t) \sim \frac{1}{r} f(\boldsymbol{s}, \tau) \quad \text{as} \quad r \to \infty, \tag{2.37}$$

where $\boldsymbol{s}$ is a unit vector specifying the observation direction, $\tau = t - r/c$, and

$$f(\boldsymbol{s}, \tau) = \int_{\infty}^{\infty} dt' \int d^3\mathbf{r}' q(\mathbf{r}', t') \delta\left(t' - \mathbf{r}' \cdot \frac{\boldsymbol{s}}{c} - \tau\right). \tag{2.38}$$

Their work demonstrates two achievements: (a) that of synthesizing the minimum-energy source of specified spatial support that generates a prescribed far field, and (b) that of reconstructing an unknown source from field data gathered in the far-zone region of the source (i.e. a source/target interrogation application). In (a), the far field can be prescribed for all $\boldsymbol{s}$, while in (b) far-field data are available only for a discrete set of observation directions.

Their approach of reconstructing the sources in the time domain is through a limited-view Radon inversion framework. The time-dependent inverse source problem is transformed into a limited-view computed tomography (CT) reconstruction problem [43, 44]. The reconstructed minimal energy source is found to obey a homogeneous wave equation in the interior of the source region D. They also found that the NR sources in the time domain are analogous to the so-called ghost objects that arise in the formalism of the limited-view CT problem. An orthogonality relation for NR sources derived previously under time-harmonic conditions [17] was generalized to the time domain and used as the basis for a new definition of a NR source having a given spatial-temporal support.

2.6 Conclusion

To summarize of this chapter, the concept and theory of inverse source problems

are reviewed. The generalized ill-posed inverse problems is addressed. The non-uniqueness natural to the inverse source problems is discussed with emphasis on the so-called non-radiating (NR) sources [15, 16, 45]. The regularization techniques and the use of *prior* conditions are also discussed. Past approaches for solving inverse source problems are reviewed.

Reference

[1] E. A. Marengo and A. J. Devaney, "Nonradiating sources with connections to the adjoint problem," *Physical Review E*, vol. 70, no. 3, pp. 37601, 2004.

[2] R. P. Porter and A. J. Devaney, "Holography and the inverse source problem," *Journal of the Optical Society of America*, vol. 72, no. 3, pp. 327–330, 1982a.

[3] E. A. Marengo, A. J. Devaney, and R. W. Ziolkowski, "Inverse source problem and minimum-energy sources," *Journal of the Optical Society of America A*, vol. 17, no. 1, pp. 34–45, 2000.

[4] E. A. Marengo and A. J. Devaney, "The inverse source problem of electromagnetics: linear inversion formulation and minimum energy solution," *IEEE Transactions on Antennas and Propagation*, vol. 47, no. 2, pp. 410–412, 1999.

[5] E. A. Marengo, M. R. Khodja, and A. Boucherif, "Inverse source problem in non-homogeneous background media. Part II: Vector formulation and antenna substrate performance characterization," *SIAM Journal on Applied Mathematics*, vol. 69, no. 1, pp. 81–110, 2008.

[6] E. A. Marengo, A. J. Devaney, and R. W. Ziolkowski, "New aspects of the inverse source problem with far-field data," *Journal of the Optical Society of America A*, vol. 16, no. 7, pp. 1612–1622, 1999.

[7] M. Ikehata, "An inverse source problem for the heat equation and the enclosure method," *Inverse Problems*, vol. 23, pp. 183–202, 2007.

[8] V. Isakov, "Some inverse problems for the diffusion equation," *Inverse Problems*, vol. 15, pp. 3–10, 1999.

[9] H. E. Moses, "The time-dependent inverse source problem for the acoustic and electromagnetic equations in the one-and three-dimensional cases," *Journal of Mathematical Physics*, vol. 25, no. 6, pp. 1905–1923, 1984.

[10] J. Hadamard, *Lectures on Cauchy's Problem in Linear Partial Differential Equations*, Mineola, NY: Dover Pubns, 2003.

[11] M. Bertero and P. Boccacci, *Introduction to Inverse Problems in Imaging*, Philadelphia, PA: Institute of Physics Publishing, 1998.

[12] A. J. Devaney and E. A. Marengo, "A method for specifying non-radiating, monochromatic, scalar sources and their fields," *Pure and Applied Optics: Journal of the European Optical Society Part A*, vol. 7, pp. 1213–1220, 1998.

[13] B.J. Hoenders and H.A. Ferwerda, "The non-radiating component of the field generated by a finite monochromatic scalar source distribution," *Pure and Applied Optics: Journal of the European Optical Society Part A*, vol. 7, pp. 1201–1211, 1998.

[14] E. A. Marengo and R. W. Ziolkowski, "On the radiating and nonradiating components of scalar, electromagnetic, and weak gravitational sources," *Physical review letters*, vol. 83, no. 17, pp. 3345–3349, 1999.

[15] A. J. Devaney and E. Wolf, "Radiating and nonradiating classical current distributions and the fields they generate," *Physical Review D*, vol. 8, no. 4, pp. 1044–1047, 1973.

[16] N. Bleistein and J. K. Cohen, "Nonuniqueness in the inverse source problem in acoustics and electromagnetics," *Journal of Mathematical Physics*, vol. 18, no. 2, pp. 194–201, 1977.

[17] K. Kim and E. Wolf, "Non-radiating monochromatic sources and their fields," *Optics Communications*, vol. 59, no. 1, pp. 1–6, 1986.

[18] A. Gamliel, K. Kim, AI Nachman, and E. Wolf, "A new method for specifying nonradiating, monochromatic, scalar sources and their fields," *Journal of the Optical Society of America A*, vol. 6, no. 9, pp. 1388–1393, 1989.

[19] G. Gbur and E. Wolf, "Nonradiating sources and other 'invisible' objects," *Progress in Optics*, vol. 45, pp. 273–316, 2003.

[20] R. E. Collin, *Field Theory of Guided Waves*, McGraw-Hill New York, 1960.

[21] A. J. Devaney and E. Wolf, "Multipole expansions and plane wave representations of the electromagnetic field," *Journal of Mathematical Physics*, vol. 15, pp. 234, 1974.

[22] A. J. Devaney and R. P. Porter, "Holography and the inverse source problem. Part II: Inhomogeneous media," *Journal of the Optical Society of America A*, vol. 2, no. 11, pp. 2006–2011, 1985.

[23] A. J. Devaney, E. A. Marengo, and M. Li, "Inverse source problem in nonhomogeneous background media," *SIAM Journal on Applied Mathematics*, vol. 67, no. 5, pp. 1353–1378, 2007.

[24] E. A. Marengo and R. W. Ziolkowski, "Inverse source problem with regularity constraints: normal solution and nonradiating source components," *Journal of Optics A: Pure and Applied Optics*, vol. 2, pp. 179–187, 2000a.

[25] E. A. Marengo, A. J. Devaney, and F. K. Gruber, "Inverse source problem with reactive power constraint," *IEEE Transactions on Antennas and Propagation*, vol. 52, no. 6, pp. 1586–1595, 2004.

[26] A. Formisano, "Regularization of inverse magnetostatic problems: possibilities and pitfalls," *COMPEL: The International Journal for Computation and Mathematics in Electrical and Electronic Engineering*, vol. 24, 2005.

[27] J. C. E. Sten and E. A. Marengo, "Inverse source problem in an oblate spheroidal geometry," *IEEE Transactions on Antennas and Propagation*, vol. 54, no. 11, pp. 3418–3428, 2006.

[28] L. Tsang, A. Ishimaru, R. P. Porter, and D. Rouseff, "Holography and the inverse source problem. III. Inhomogeneous attenuative media," *Journal of the Optical Society of America A*, vol. 4, no. 9, pp. 1783–1787, 1987.

[29] A. J. Devaney, "The inverse problem for random sources," *Journal of Mathematical Physics*, vol. 20, no. 8, pp. 1687–1691, 1979.

[30] I. J. LaHaie, "Inverse source problem for three-dimensional partially coherent sources and fields," *Journal of the Optical Society of America A*, vol. 2, no. 1, pp. 35–45, 1985.

[31] I. J. LaHaie, "Uniqueness of the inverse source problem for quasi-homogeneous partially coherent sources," *Journal of the Optical Society of America A*, vol. 3, no. 7, pp. 1073–1079, 1986.

[32] W. H. Carter and E. Wolf, "Inverse problem with quasi-homogeneous sources," *Journal of the Optical Society of America A*, vol. 2, no. 11, pp. 1994–2000, 1985.

[33] R. P. Porter, "Diffraction-limited, scalar image formation with holograms of arbitrary shape," *Journal of the Optical Society of America*, vol. 60, no. 8, pp. 1051–1059, 1970.

[34] H. Ammari, G. Bao, and J. L. Fleming, "An inverse source problem for Maxwell's equations in magnetoencephalography," *SIAM Journal on Applied Mathematics*, vol. 62, no. 4, pp. 1369–1382, 2002.

[35] T. M. Habashy, R. W. Groom, and B. R. Spies, "Beyond the Born and Rytov approximations: a nonlinear approach to electromagnetic scattering," *Journal of Geophysical Research*, vol. 98, no. B2, pp. 1759–1775, 1993.

[36] S. He and V. G. Romanov, "Identification of dipole sources in a bounded domain for Maxwell's equations," *Wave Motion*, vol. 28, no. 1, pp. 25–40, 1998.

[37] R. Kress, L. K "uhn, and R. Potthast, "Reconstruction of a current distribution from its magnetic field," *Inverse Problems*, vol. 18, pp. 1127–1146, 2002.

[38] A. E. Bulyshev, A. E. Souvorov, S. Y. Semenov, V. G. Posukh, and Y. E. Sizov, "Three-dimensional vector microwave tomography: theory and computational experiments," *Inverse Problems*, vol. 20, pp. 1239–1259, 2004.

[39] E. Heyman and A. J. Devaney, "Time-dependent multipoles and their application for radiation from volume source distributions," *Journal of Mathematical Physics*, vol. 37, no. 2, pp. 682–692, 1996.

[40] R. P. Porter and A. J. Devaney, "Generalized holography and computational solutions to inverse source problems," *Journal of the Optical Society of America*, vol. 72, no. 12, pp. 1707–1713, 1982b.

[41] H. E. Moses, "Eigenfunctions of the curl operator, rotationally invariant Helmholtz theorem, and applications to electromagnetic theory and fluid mechanics," *SIAM Journal on Applied Mathematics*, vol. 21, no. 1, pp. 114–144, 1971.

[42] J. D. Jackson and R. F. Fox, "Classical electrodynamics," *American Journal of Physics*, vol. 67, pp. 841, 1999.

[43] P. R. Smith, T. M. Peters, and R. H. T. Bates, "Image reconstruction from finite numbers of projections," *Journal of Physics A: Mathematical, Nuclear and General*, vol. 6, pp. 361–382, 1973.

[44] A. K. Louis and A. Rieder, "Incomplete data problems in X-ray computerized tomography," *Numerische Mathematik*, vol. 56, no. 4, pp. 371–383, 1989.

[45] A. J. Devaney, "Nonuniqueness in the inverse scattering problem," *Journal of Mathematical Physics*, vol. 19, pp. 1526–1535, 1978.

Chapter 3

TLM Formulation of Inverse Source Problems for Thin Source Regions

The Transmission-Line Matrix (TLM) method is a numerical technique for the field computation in the time domain (referring to [1] for more details). We consider a homogeneous air-filled computational domain. Given the excitation sources, the TLM method computes the field distribution everywhere inside the computational domain for every time step. In this chapter, we restrict our attention to a closed subregion inside this domain, which encloses all the excitation sources. We call this subregion as *source region*, and its enclosed mesh cells as *source cells*. Using the knowledge of the excitation sources within the source cells, the forward TLM iteration finds the link impulses emitted from the boundary of source region. For its reverse process, our proposed algorithm reconstructs the excitation sources inside the source region

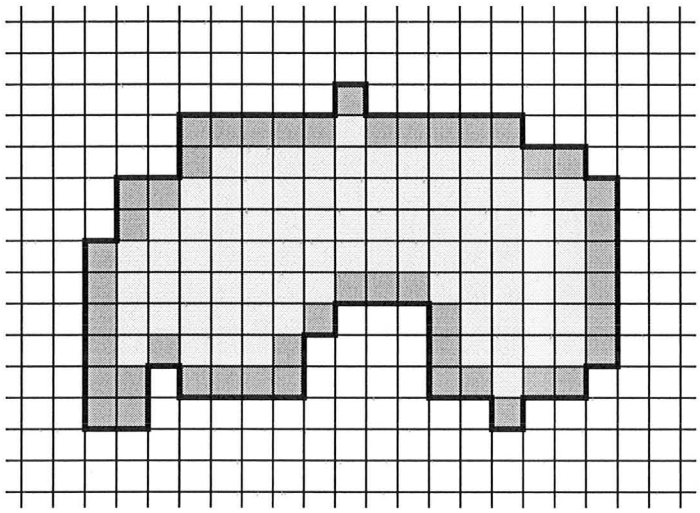

Figure 3.1 A discretized two-dimensional source region with arbitrary shape. Boundary cells are shown by dark squares.

using the time-domain knowledge of produced fields on its boundary. In this chapter, we only limit our approach applying to thin source regions, a special class of source regions whose enclosed source cells are all exposed to the exterior of their belonging source region.

For a better description, consider the discretized two-dimensional source region shown in Figure 3.1. We refer to mesh cells with one or more edges exposed to the exterior of the source region as *boundary cells* (shown by dark squares in Figure 3.1), while the remaining mesh cells which are enclosed by the boundary cells are referred to as *interior cells*. For our case, thin source regions, as suggested by its name, are closed regions whose enclosed mesh cells are all *boundary cells*. Typical examples of two-dimensional source regions are shown in Figure 3.2.

In this chapter, we formulate the source reconstruction problem inside thin regions

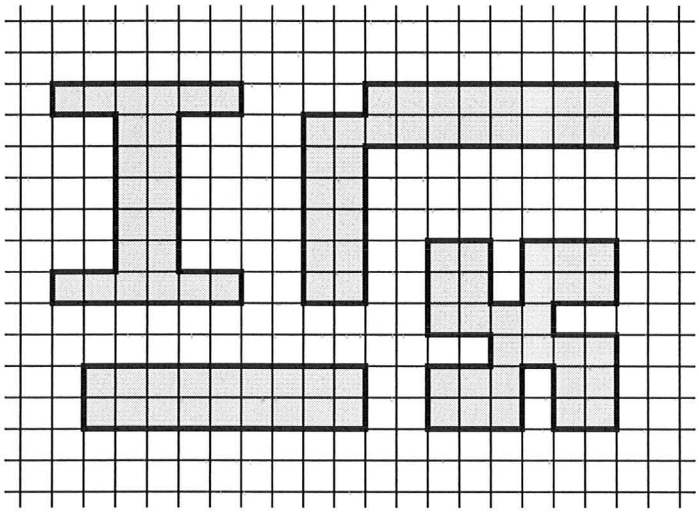

Figure 3.2 Examples of two-dimensional thin source regions inside a two-dimensional computational domain.

using the TLM method. The time-domain solution of the sources is obtained by applying the time-reversal property of the TLM method [2]. For the outline of this chapter, Section 3.1 discusses the formulation of the direct problem. Our inversion formulation and our reconstruction algorithm are each presented in Section 3.2 and 3.3, respectively. Numerical examples are given in Section 3.4. Finally, Section 3.5 investigates the noise performance of our algorithm.

3.1 TLM Method and the Direct Problem

TLM method carries out a sequence of scattering and connection procedures modelling the propagation of waves [1]. For a homogeneous lossless domain composed of Q

number of mesh cells, it follows that a single TLM time step can be mathematically expressed as [3]:

$$\boldsymbol{v}_k = \boldsymbol{CS}\boldsymbol{v}_{k-1} + \boldsymbol{v}_k^s = \boldsymbol{A}\boldsymbol{v}_{k-1} + \boldsymbol{v}_k^s, \tag{3.1}$$

where $\boldsymbol{v}_k \in \mathbb{R}^{Q_L \times 1}$ is the vector of link impulses for all mesh links at the kth time step, and $Q_L = 4Q$ (for a two-dimensional domain) or $Q_L = 12Q$ (for a three-dimensional domain) is the total number of mesh links associated with the Q mesh cells. $\boldsymbol{v}_k^s \in \mathbb{R}^{Q_L \times 1}$ is the excitation at the kth time step on all mesh links. $\boldsymbol{S} \in \mathbb{R}^{Q_L \times Q_L}$ and $\boldsymbol{C} \in \mathbb{R}^{Q_L \times Q_L}$ are the scattering matrix and connection matrix for the whole domain respectively. The matrix $\boldsymbol{A} \in \mathbb{R}^{Q_L \times Q_L}$ is the matrix product of $\boldsymbol{C}$ and $\boldsymbol{S}$.

By substituting $\boldsymbol{v}_{k-1}$ with $\boldsymbol{v}_{k-1} = \boldsymbol{A}\boldsymbol{v}_{k-2} + \boldsymbol{v}_{k-1}^s$, (3.1) can be written as

$$\begin{aligned} \boldsymbol{v}_k &= \boldsymbol{A}\left(\boldsymbol{A}\boldsymbol{v}_{k-2} + \boldsymbol{v}_{k-1}^s\right) + \boldsymbol{v}_k^s \\ &= \boldsymbol{A}^2\boldsymbol{v}_{k-2} + \boldsymbol{A}\boldsymbol{v}_{k-1}^s + \boldsymbol{v}_k^s. \end{aligned} \tag{3.2}$$

Following the same procedure, by substituting for $\boldsymbol{v}_{k-2}$ in (3.2) and then repeating for $\boldsymbol{v}_{k-3}$, $\boldsymbol{v}_{k-4}$, ..., up to $\boldsymbol{v}_1$, the vector of link impulses at the kth time step $\boldsymbol{v}_k$ can then be expressed as a linear combination of the excitations at all previous time steps. The resultant expression is given by

$$\begin{aligned} \boldsymbol{v}_k &= \boldsymbol{A}^k\boldsymbol{v}_0 + \boldsymbol{A}^k\boldsymbol{v}_0^s + \boldsymbol{A}^{k-1}\boldsymbol{v}_1^s + \cdots + \boldsymbol{v}_k^s \\ &= \boldsymbol{A}^k\boldsymbol{v}_0^s + \boldsymbol{A}^{k-1}\boldsymbol{v}_1^s + \cdots + \boldsymbol{v}_k^s. \end{aligned} \tag{3.3}$$

In (3.3), we drop the term $\boldsymbol{A}^k \boldsymbol{v}_0$ by assuming that the field is zero everywhere inside the computational domain at the 0th time step.

3.2 The Linear Inversion Formulation

Now, we focus our attention to the source region composed of N source cells. At the kth time step, each of its enclosed source cells is excited by an unknown source value given by the vector $\boldsymbol{v}_k^s$. Here, the elements inside the vector $\boldsymbol{v}_k^s$ are non-zero only for those elements with their correspondent mesh links located inside the source region. The link impulses emitted from boundary at the kth time step are given in the vector $\boldsymbol{v}_k^b \in \mathbb{R}^{M\times 1}$.

Considering only the 1st forward time step, (3.1) can be written as

$$\boldsymbol{v}_1 = \boldsymbol{A}\boldsymbol{v}_0 + \boldsymbol{v}_1^s. \tag{3.4}$$

Extract $\boldsymbol{v}_1^b$ from $\boldsymbol{v}_1$ by multiplying both side of (3.4) by a selecting matrix $\boldsymbol{E}$, then it follows that

$$\boldsymbol{E}\boldsymbol{v}_1 = \boldsymbol{E}\boldsymbol{A}\boldsymbol{v}_0^s + \boldsymbol{E}\boldsymbol{v}_1^s, \tag{3.5}$$

which yields

$$\boldsymbol{v}_1^b = \boldsymbol{E}\boldsymbol{A}\boldsymbol{v}_0^s, \tag{3.6}$$

where $\boldsymbol{E} \in \mathbb{R}^{M\times Q_L}$ is given by

$$E_{ij} = \begin{cases} E_{ij} = 1 & \text{if the } j\text{th element in } \boldsymbol{v}_k \text{ and the } i\text{th element} \\ & \text{in } \mathbf{v}_k^b \text{ are referring to a same mesh link.} \\ 0 & \text{otherwise.} \end{cases}$$

Note that the term $\boldsymbol{E}\boldsymbol{v}_1^s$ on the right-hand side of (3.5) can be removed, because it does not affect the boundary link impulses.

The linear system described in (3.6) contains N number of unknowns in $\mathbf{v}_0^s$ and M number of equations. Therefore, $\mathbf{v}_0^s$ can then be retrieved by solving (3.6).

For the 2nd time step, we have

$$\boldsymbol{v}_2 = \mathbf{A}^2\mathbf{v}_0^s + \mathbf{A}\mathbf{v}_1^s + \mathbf{v}_2^s. \tag{3.7}$$

Following the same procedure by eliminating the last term in the right hand side of (3.7), (3.7) can then be rewritten as

$$\boldsymbol{v}_2^b - \boldsymbol{E}\boldsymbol{A}^2\mathbf{v}_0^s = \boldsymbol{E}\boldsymbol{A}\mathbf{v}_1^s. \tag{3.8}$$

In (3.8), $\mathbf{v}_0^s$ is determined at the previous time step, and thus $\mathbf{v}_1^s$ can then be solved by evaluating (3.8).

Similarly for the 3rd time step, it follows that

$$\mathbf{v}_3^b - \boldsymbol{E}\left(\boldsymbol{A}^3\mathbf{v}_0^s + \boldsymbol{A}^2\mathbf{v}_1^s\right) = \boldsymbol{E}\boldsymbol{A}\mathbf{v}_2^s, \tag{3.9}$$

where $\mathbf{v}_0^s$ and $\mathbf{v}_1^s$ are determined in the previous two time steps, and $\mathbf{v}_2^s$ can be solved by evaluating (3.9).

We may extend this procedure to the kth time step, then $\boldsymbol{v}_{k-1}^s$ can be solved by evaluating

$$(\boldsymbol{EA})\, \boldsymbol{v}_{k-1}^s = \boldsymbol{v}_k^b - \boldsymbol{E}\tilde{\boldsymbol{v}}_k, \tag{3.10}$$

where $\tilde{\boldsymbol{v}}_k$ is given by

$$\tilde{\boldsymbol{v}}_k = \boldsymbol{A}^k \boldsymbol{v}_0^s + \boldsymbol{A}^{k-1} \boldsymbol{v}_1^s + \cdots + \boldsymbol{A}^2 \boldsymbol{v}_{k-2}^s, \tag{3.11}$$

and $\boldsymbol{v}_i^s$ $(i = 0, 1, \ldots, k-2)$ can each be determined in all previous time steps.

3.3 The Reconstruction Algorithm

Using the linear formulation given in (3.11), at the kth time step our algorithm determines the excitation at the $(k-1)th$ time step, $\boldsymbol{v}_{k-1}^s$, using the following two sequences:

I. obtain $\tilde{\boldsymbol{v}}_k$ given by (3.11);

II. solve for $\boldsymbol{v}_{k-1}^s$ by evaluating (3.10).

Considering only the first sequence, one may note that it is computationally impractical to obtain $\tilde{\boldsymbol{v}}_k$ by applying (3.11) directly, which would require $(k+2)(k-$

1)/2 number of TLM iterations[1] for the computation at the kth time step. The number of TLM iterations for computing $\tilde{\boldsymbol{v}}_k$ also grows as k increases, thus applying (3.11) requires huge computational resources.

As an improved alternative, we rewrite (3.11) using the previous result of $\tilde{\boldsymbol{v}}_k$, $\tilde{\boldsymbol{v}}_{k-1}$. Now, the resultant expression for $\tilde{\boldsymbol{v}}_k$ at the kth time step is given by

$$\tilde{\boldsymbol{v}}_k = \boldsymbol{A}\left(\tilde{\boldsymbol{v}}_{k-1} + \boldsymbol{A}\boldsymbol{v}_{k-2}^s\right), \tag{3.12}$$

where the vector $\tilde{\boldsymbol{v}}_{k-1}$ is the previous result of $\tilde{\boldsymbol{v}}_k$ computed at the $(k-1)$th time step. The vector $\boldsymbol{v}_{k-2}^s$ is the reconstructed sources for the $(k-2)$th time step. Using (3.12), $\tilde{\boldsymbol{v}}_k$ can be updated from $\tilde{\boldsymbol{v}}_{k-1}$ using only two TLM iterations. At the start of the source reconstruction process (i.e. 0th time step), elements in $\tilde{\boldsymbol{v}}_0$ and $\boldsymbol{v}_{-1}^s$ are initialized to zeros. For the kth time step, the computation of $\tilde{\boldsymbol{v}}_k$ can be summarized into the following steps:

Step 1. Compute the vector term $\boldsymbol{A}\boldsymbol{v}_{k-2}^s$ in one computational domain (say, domain I);

Step 2. Add the resultant vector term $\boldsymbol{A}\boldsymbol{v}_{k-2}^s$ to $\tilde{\boldsymbol{v}}_{k-1}$ in another computational domain (say, domain II). Here, $\tilde{\boldsymbol{v}}_{k-1}$ is computed at the $(k-1)$th time step;

---

1 The operation of matrix-vector product with matrix $\boldsymbol{A}$ is referred to as one single TLM iteration. It consists of one scattering procedure and one connection procedure.

Step 3. Then $\tilde{\mathbf{v}}_k$ can be obtained by performing another TLM iteration on the vector $\left(\tilde{\mathbf{v}}_{k-1} + \boldsymbol{A}\mathbf{v}^s_{k-2}\right)$ on the computational domain II.

Now, we consider the procedure (sequence II) of obtaining $\mathbf{v}^s_{k-1}$ using (3.10). The matrix $\boldsymbol{A}$ in (3.10) is rather a huge sparse matrix. For a two-dimensional computational domain consisting of Q mesh cells, the size of $\boldsymbol{A}$ is $4Q$ by $4Q$. Solving such a huge linear sparse system is computationally inefficient.

Instead of solving the linear system given by (3.10), our treatment of computing $\mathbf{v}^s_{k-1}$ is by applying the time-reversal property of TLM method (see [2] for detail). The time-reversal property states that if a TLM network is excited by only a single link impulses at the 0th time step, and if after k computational steps the link impulses on all mesh links have been computed and stored, one can return to the initial state at the 0th time step by reversing the direction of all the link impulses and iterating k time steps [2]. For the case of multiple excitation sources inside a thin source region, we can still reconstruct the sources from the emitted link impulses by applying this time-reversal technique with little modification. The detailed procedures are illustrated in Figure 3.3, and can also be summarized into the following three steps:

Step 1. Back-propagate the resultant vector on the right-hand-side of (3.10), $\mathbf{v}^b_k - \boldsymbol{E}\tilde{\mathbf{v}}_k$, into the source region. This corresponds to the inversion of the connection TLM procedure, see Figure 3.3(b);

Step 2. Balance the link impulses inside each source cells by inserting compensa-

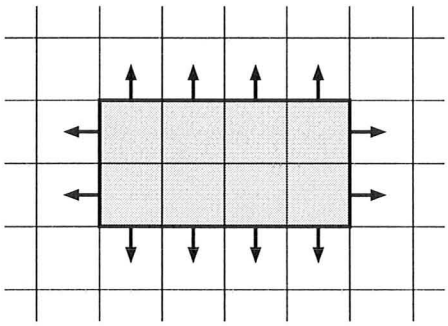

Figure 3.4 A discretized two-dimensional source region composed of 8 source cells with shape 2 by 4 grids. Observed link impulses are shown by arrows.

tion link impulses such that all link impulses inside a single source cell are equal in magnitude see Figure 3.3(c);

Step 3. The source solution $\boldsymbol{v}_{k-1}^{s}$ can then be obtained by carrying a scattering TLM procedure[2], see Figure 3.3(d). All above steps are performed in a single computational domain (say, domain III).

3.4 Numerical Results

In this section, we illustrate our approach through reconstructing the excitation sources inside various thin source regions. For each of our examples, all source cells are imposed with isotropic sources, and the link impulses emitted from the source region are stored. By using our algorithm, we reconstruct the original excitation

2 The inverse of the scattering matrix $\boldsymbol{S}$ is itself.

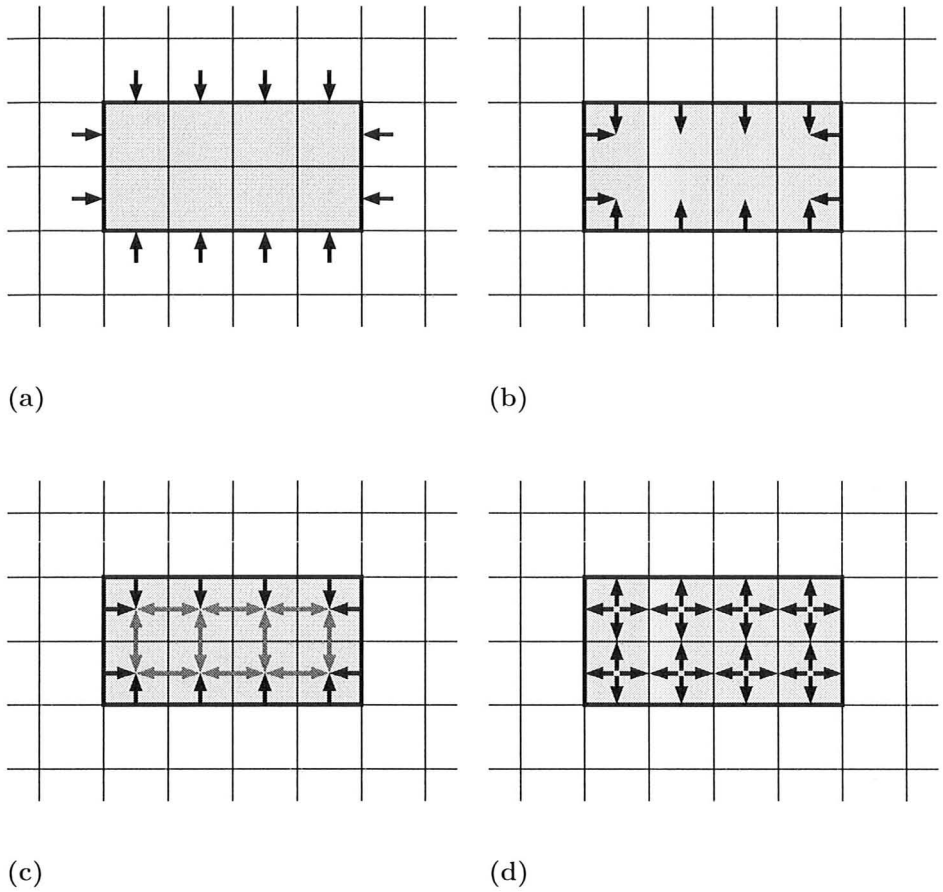

Figure 3.3 Illustration of solving $(\boldsymbol{EA})\,\boldsymbol{v}_{k-1}^{s} = \boldsymbol{v}_{k}^{b} - \boldsymbol{E}\tilde{\boldsymbol{v}}_{k}$ at the kth time step using the time-reversal property of the TLM method. (a) Initial state, and arrows represent the link impulses emitted from the source region; (b) Back-propagate $\boldsymbol{v}_{k}^{b} - \boldsymbol{E}\tilde{\boldsymbol{v}}_{k}$ into the source region; (c) insert compensation link impulses $\boldsymbol{v}_{k}^{b}$ (shown by light arrows) inside each source cells; (d) compute $\boldsymbol{v}_{k-1}^{s}$ by carrying a scattering TLM procedure.

sources on all source cells using the knowledge of the stored link impulses. These reconstructed excitation signals are then compared with their correspondent exacted signals. Our results are presented here.

3.4.1 A Two-Dimensional Thin Source Region Composed of Eight Source Cells

This testing source region is composed of 8 source cells in a rectangular shape as shown in Figure 3.4. It occupies the center of a computational domain with size 60×20 grids bounded by zero-reflection absorbing boundaries.

Each source cell is isotropically excited by a modulated Gaussian signal for different modulation frequencies. The link impulses emitted from the source region (shown by arrows in Figure 3.4) are stored for reconstructing the original excitation. The reconstructed excitation signals for six arbitrarily selected source cells are given in Figure 3.5, and each is compared with the actual sources. The sources are perfectly reconstructed.

3.4.2 A Two-Dimensional Thin Source Region Composed of 400 Source Cells

This testing source region is composed of two rows of source cells each with length of 200 grids as shown in Figure 3.6. It occupies the center of a computational domain with size 250×20 grids bounded by zero-reflection absorbing boundaries. The

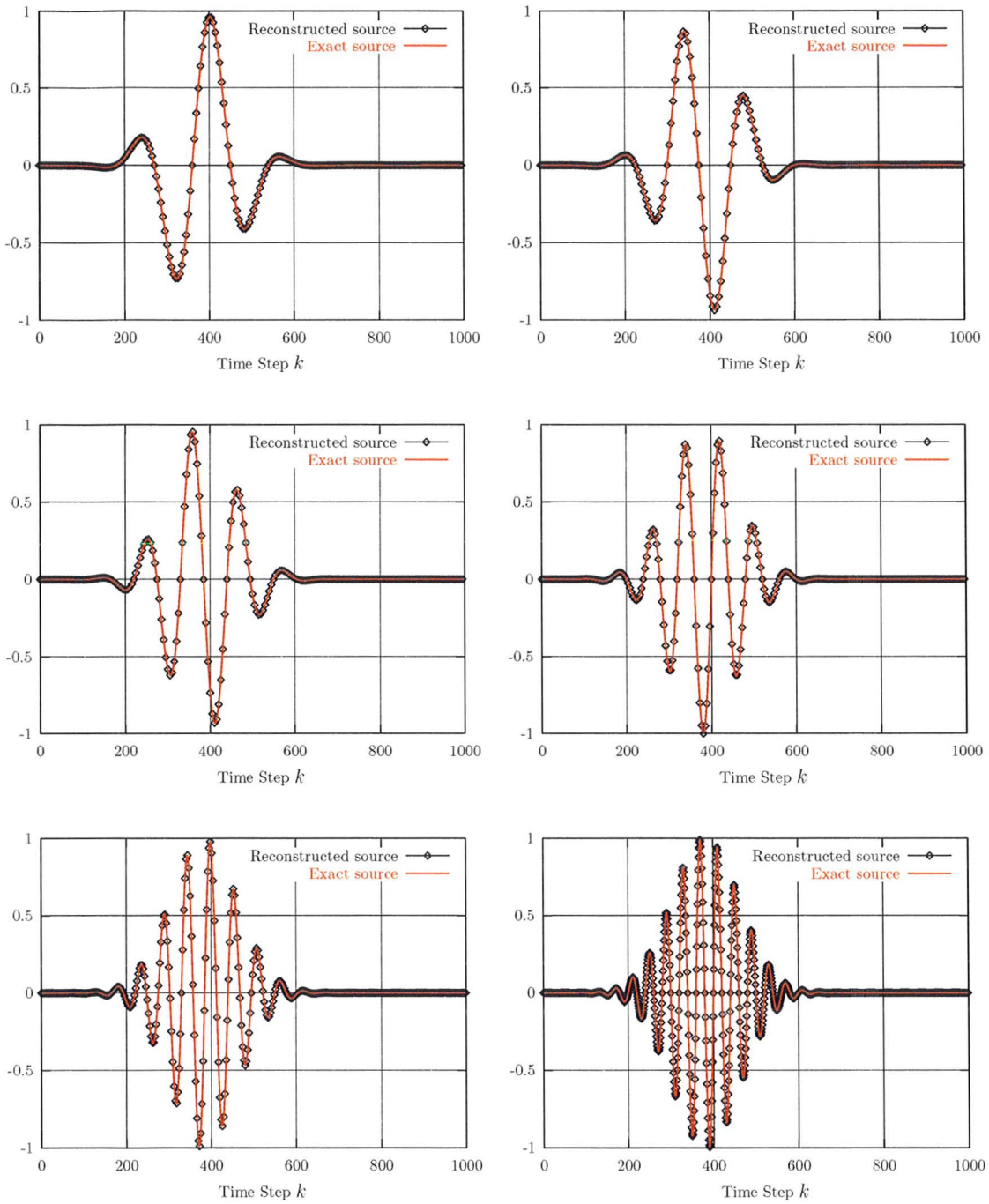

Figure 3.5 The reconstructed excitation sources on six arbitrarily selected source cells inside the thin source region with shape 2 by 4 grids.

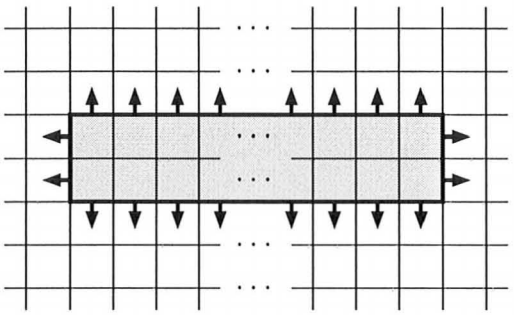

Figure 3.6 A discretized two-dimensional source region composed of 400 source cells with shape 2 by 200 grids. Observed link impulses are shown by arrows.

reconstructed excitation signals for six arbitrarily selected source cells are given in Figure 3.7, and each is compared with the actual sources.

3.4.3 A Two-Dimensional Thin Reentrant Source Region Composed of 12 Source Cells

This testing source region is composed of two rows of source cells each with length of 12 grids as shown in Figure 3.8. It occupies the center of a computational domain with size 50×50 grids bounded by zero-reflection absorbing boundaries. The reconstructed excitation signals for six arbitrarily selected source cells are given in Figure 3.9, and each is compared with the actual sources.

3.4.4 A Three-Dimensional Thin Source Region Composed of 288 Source Cells

This testing source region is composed of 288 source cells in cubic shape with size

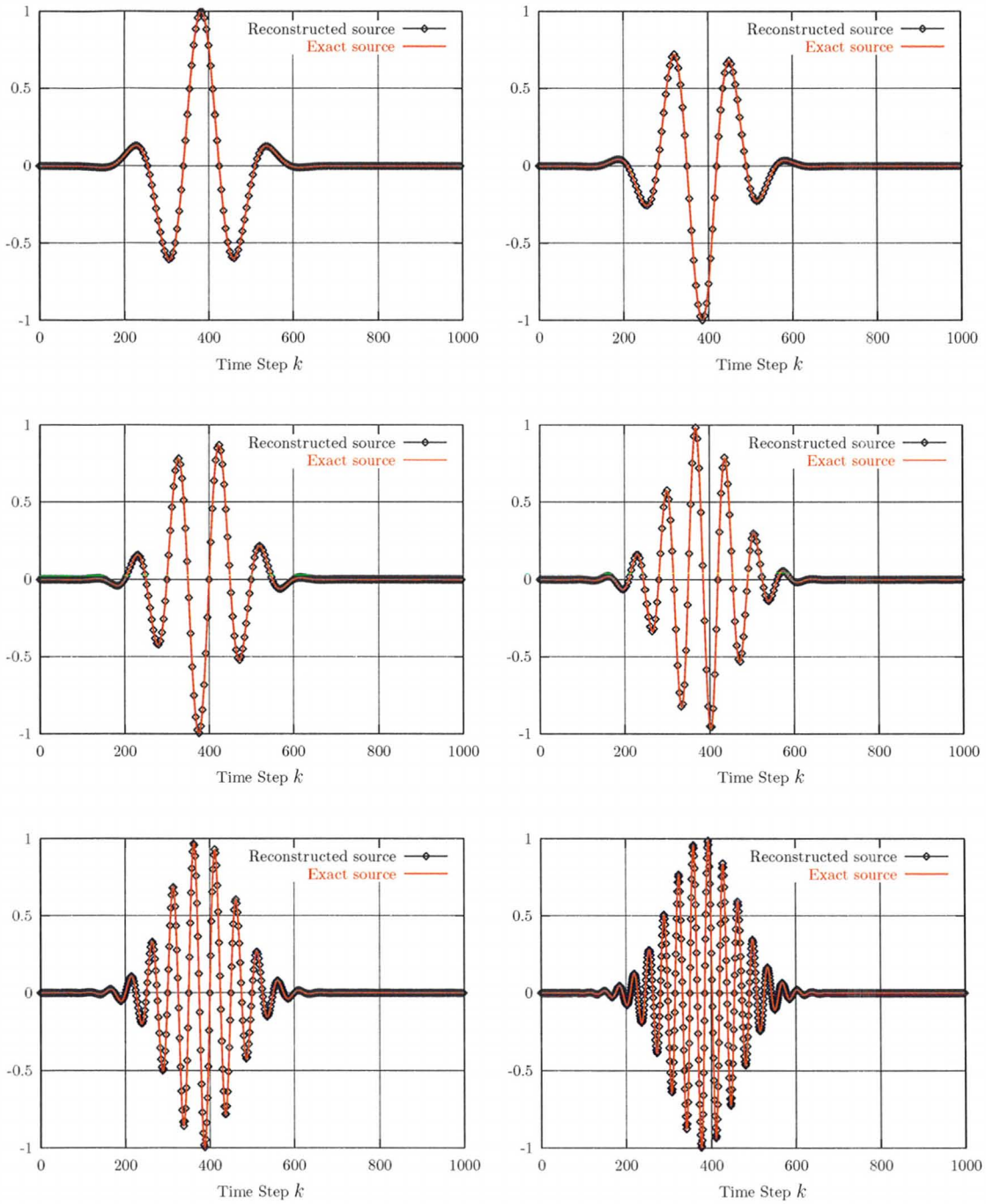

Figure 3.7 The reconstructed excitation sources on six arbitrarily selected source cells inside the thin source region with shape 2 by 200 grids.

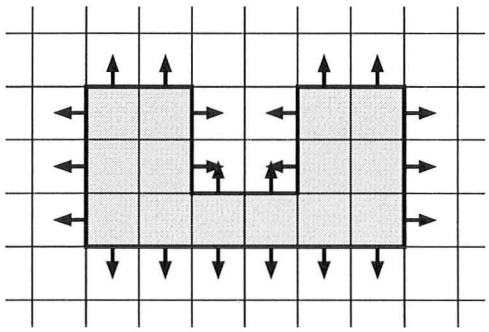

Figure 3.8 A discretized two-dimensional thin reentrant source region composed of 12 source cells. Observed link impulses are shown by arrows.

$12 \times 12 \times 2$ cubes as shown in Figure 3.10. It occupies the center of a computational domain with size $20 \times 20 \times 5$ cubes bounded by zero-reflection absorbing boundaries. In this example, we impose each source cells with vertical polarized isotropic excitation sources using modulated Gaussian pulses with different modulation frequencies. The reconstructed excitation signals for six arbitrarily selected source cells are given in Figure 3.11. Perfect match is obtained between the original and the reconstructed

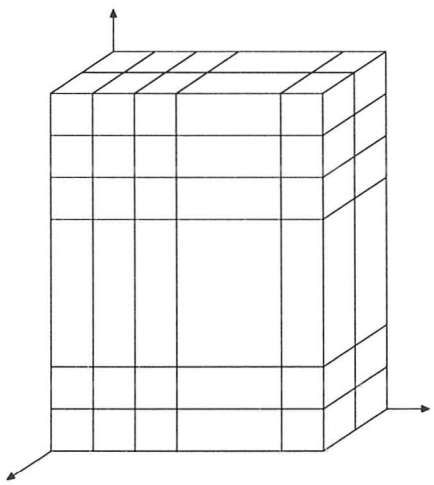

Figure 3.10 A three-dimensional source region with size $12 \times 12 \times 2$ cubes.

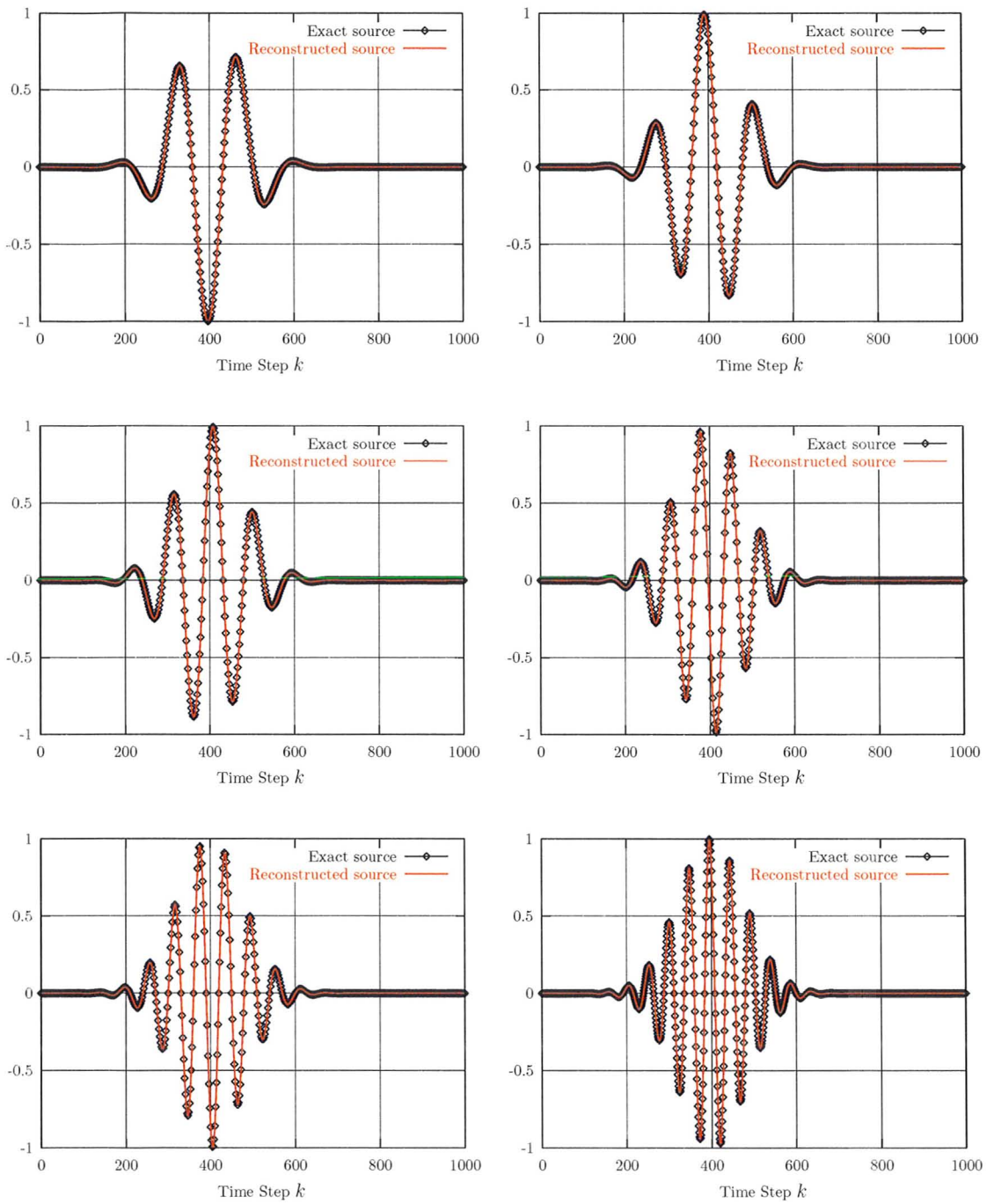

Figure 3.9 The reconstructed excitation sources on six arbitrarily selected source cells inside the thin reentrant source region.

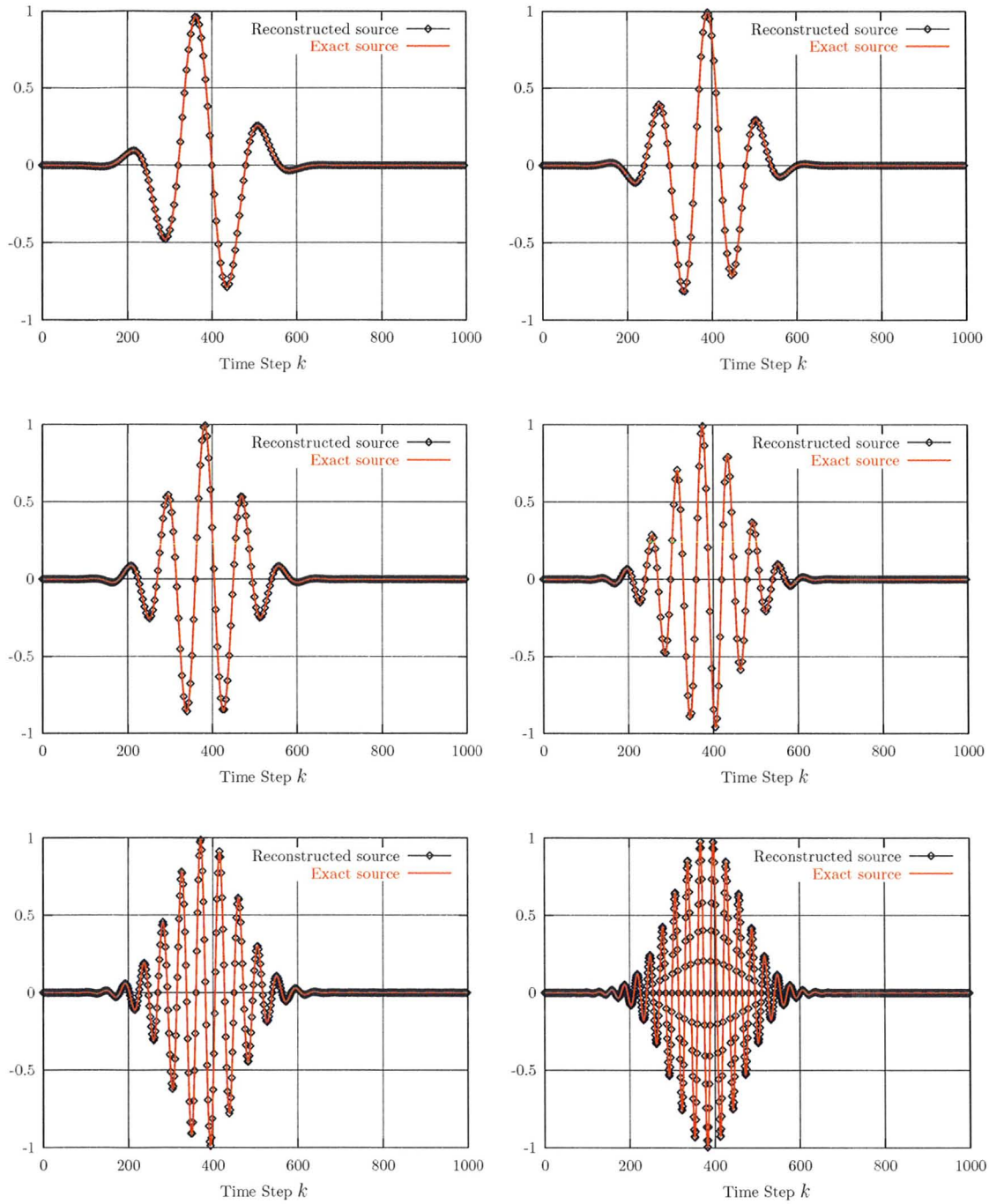

Figure 3.11 The reconstructed excitation sources on six arbitrarily selected source cells inside the three-dimensional thin source region with shape 12 by 12 by 2 cubes.

sources.

3.5 Effect of Noise

Noise is always unavoidable in physical world. In our case, $\mathbf{v}_k^b$ may be contaminated with noise, because it is practically impossible to obtain accurate field data on the boundary of the source region. The associated errors are mostly due to limitations of measurement devices.

For an ill-conditioned linear inverse problem, a small variation in the data, say due to noise, may result huge change in the obtained solution[1]. Thus it is important to evaluate our source reconstruction algorithm using noise. The numerical examples provided in the previous section assumes that the boundary field data $\mathbf{v}_k^b$ is noise-free. Here in this section, we consider the noisy case of $\mathbf{v}_k^b$.

To model the noisy field measurements, all elements in the vector $\mathbf{v}_k^b$ are perturbed by a random number given by:

$$\mathbf{v}_k^{b(e)} = (\boldsymbol{I} + \alpha \cdot \mathrm{diag}(\boldsymbol{e}_k))\, \mathbf{v}_k^b, \tag{3.13}$$

where $\boldsymbol{e}_k \in \mathbb{R}^M$ is a vector of Gaussian distributed random variables with zero mean and unity standard deviation (also known as standard normal distribution). The scalar α is a factor for adjusting the noise level, and $\boldsymbol{I} \in \mathbb{R}^{M \times M}$ is the identity matrix.

1 See section 2.1 and Figure 2.1 for detail.

At the kth time step $\mathbf{v}_k^{b(e)}$ is feed into our reconstruction algorithm instead of $\mathbf{v}_k^b$. The testing source region is composed of two rows of source cells each with length 200 grids. It occupies the center of a two-dimensional computational domain with size 250×20 grids bounded by zero-reflection absorbing boundaries. The numerical results are shown in Figure 3.12 for a noise level of -26 dB, Figure 3.13 for a noise level of -20 dB, and Figure 3.14 for a noise level of -16 dB.

Here, the noise level in $\mathbf{v}_k^{b(e)}$ for all k is defined using

$$n = \frac{\sum_{k=1}^{\tau} (\mathbf{v}_k^{b(e)} - \mathbf{v}_k^b)^T (\mathbf{v}_k^{b(e)} - \mathbf{v}_k^b)}{\sum_{k=1}^{\tau} \mathbf{v}_k^{bT} \mathbf{v}_k^b}, \tag{3.14}$$

where τ is the total number of time steps and operator T denotes the vector transpose. Similarly, for the reconstructed sources using noisy data $\mathbf{v}_k^{s(e)}$, the noise level is defined as

$$n = \frac{\sum_{k=1}^{\tau} (\mathbf{v}_k^{s(e)} - \mathbf{v}_k^s)^T (\mathbf{v}_k^{s(e)} - \mathbf{v}_k^s)}{\sum_{k=1}^{\tau} \mathbf{v}_k^{sT} \mathbf{v}_k^s}. \tag{3.15}$$

By inspection, the noise level in the reconstructed sources increases about 6 dB in average, and it does not grow with respect to the time step. Our algorithm is shown to be stable in the presence of the physical noise in the measured field.

3.6 Conclusions

Our proposed approach has been successfully demonstrated through the reconstruction of the sources inside various thin source regions. Our algorithm consistently

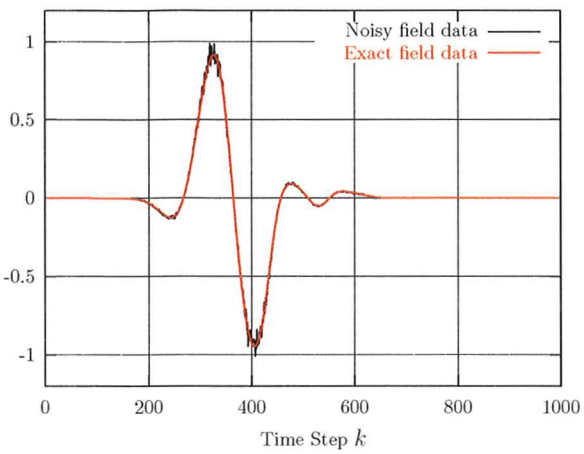

(a)

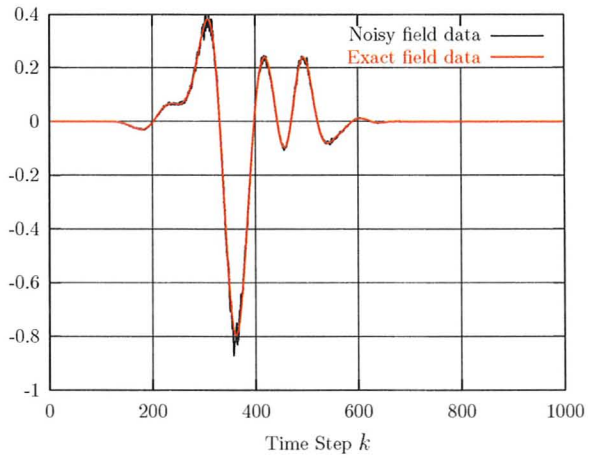

(b)

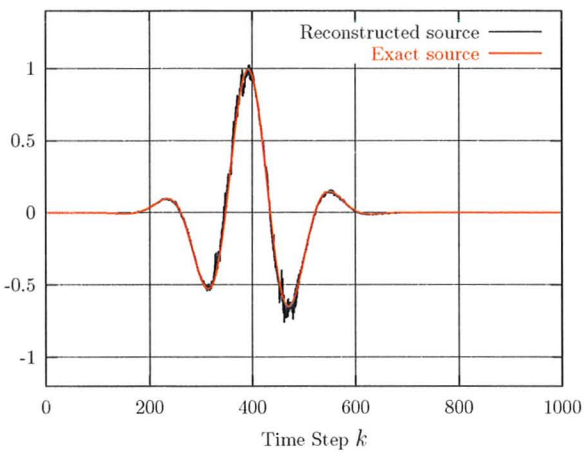

(c)

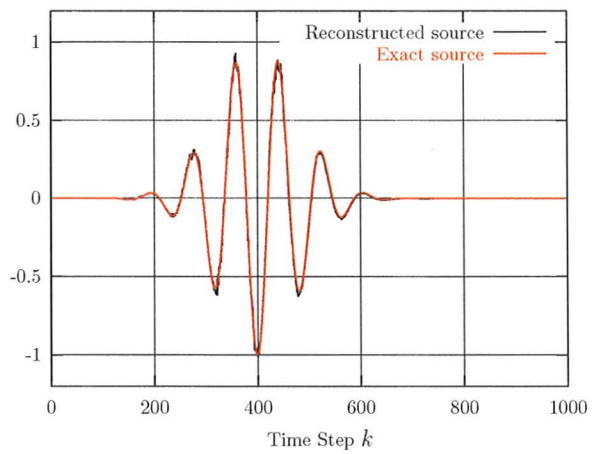

(d)

Figure 3.12 The reconstructed excitation sources under noisy condition with noise level -26 dB for the two-dimensional thin source region with shape 2 by 200 grids. The noise level for the reconstructed source is -20 dB. Figure (a) and (b) shows two arbitrarily selected noisy boundary link impulses. Figure (c) and (d) shows the reconstructed sources at two arbitrarily selected cell locations under noisy condition.

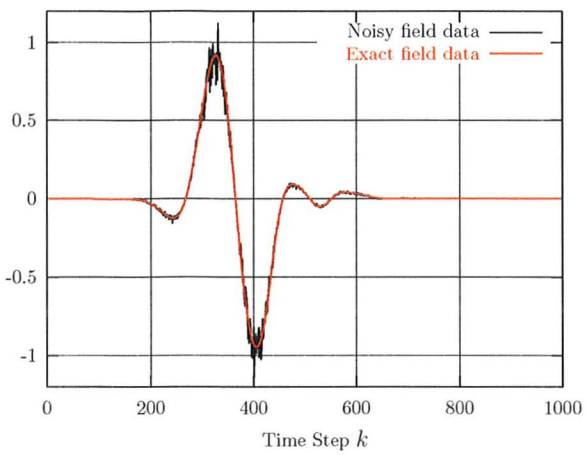

(a)

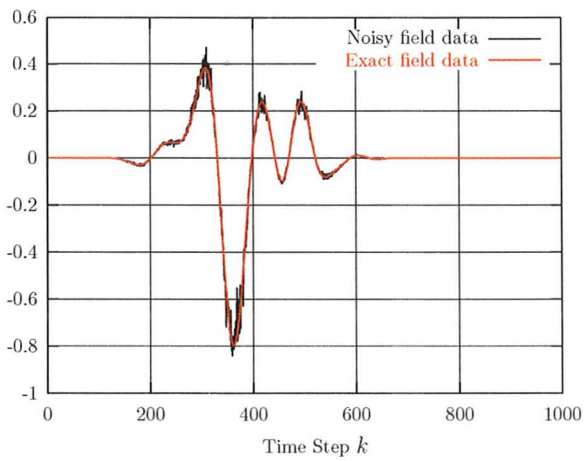

(b)

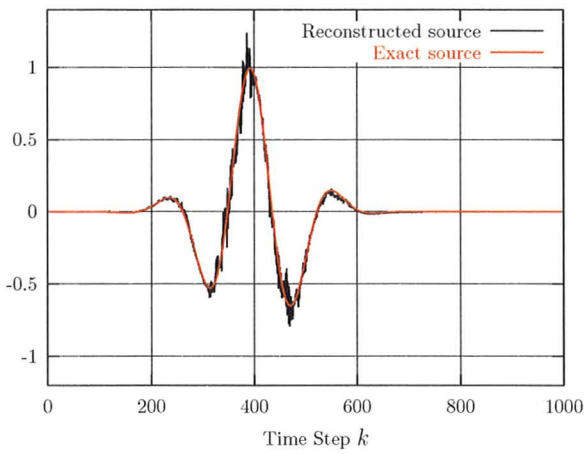

(c)

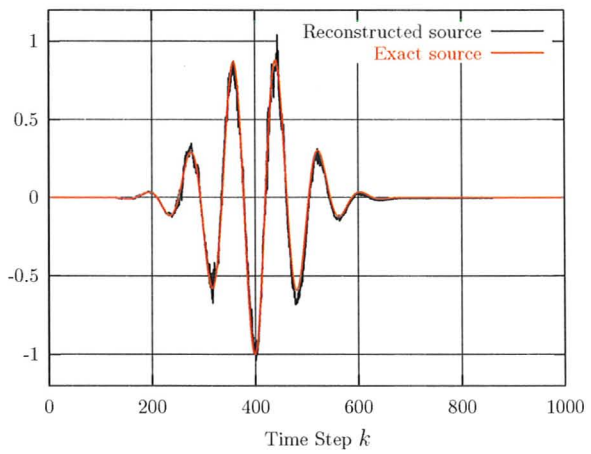

(d)

Figure 3.13 The reconstructed excitation sources under noisy condition with noise level −20 dB for the two-dimensional thin source region with shape 2 by 200 grids. The noise level for the reconstructed source is -20 dB. Figure (a) and (b) shows two arbitrarily selected noisy boundary link impulses. Figure (c) and (d) shows the reconstructed sources at two arbitrarily selected cell locations under noisy condition.

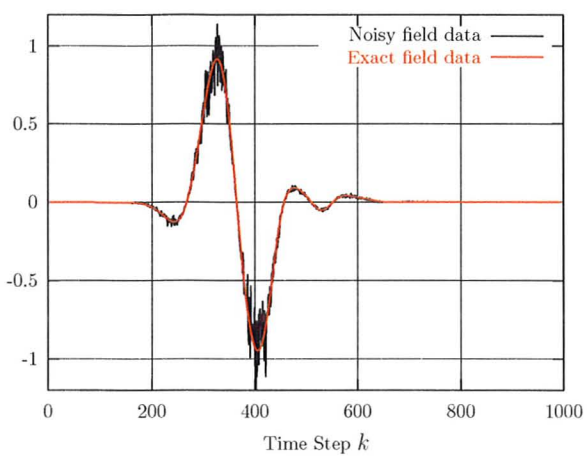

(a)

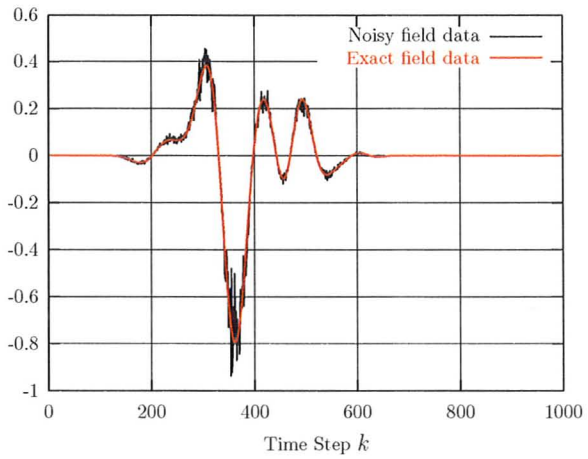

(b)

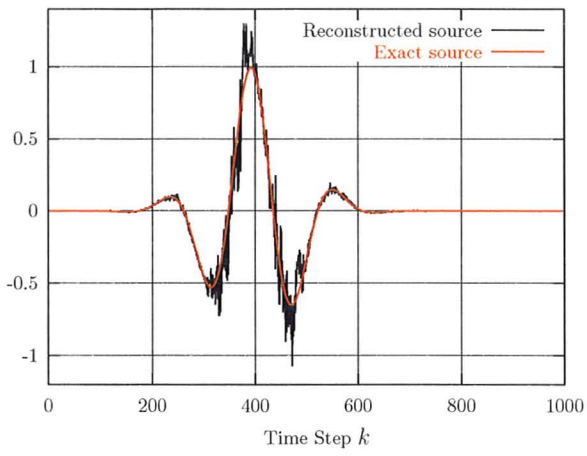

(c)

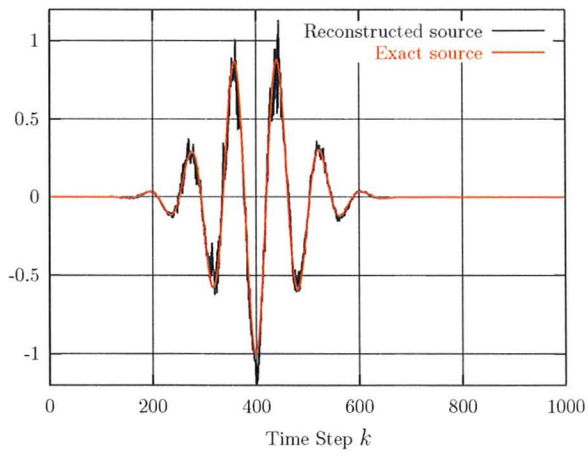

(d)

Figure 3.14 The reconstructed excitation sources under noisy condition with noise level −16 dB for the two-dimensional thin source region with shape 2 by 200 grids. The noise level for the reconstructed source is -10 dB. Figure (a) and (b) shows two arbitrarily selected noisy boundary link impulses. Figure (c) and (d) shows the reconstructed sources at two arbitrarily selected cell locations under noisy condition.

supplies a unique time-domain solution of sources in response to the given boundary link impulses. Our algorithm is efficient and requires three TLM iterations for reconstructing the source distribution at a single time step. If the boundary field data is noise-free, our reconstructed time-domain solution of the sources matches the exact solution.

Reference

[1] W. J. R. Hoefer, "The transmission-line matrix method–theory and applications," *IEEE Transactions on Microwave Theory and Techniques*, vol. 33, no. 10, pp. 882–893, 1985.

[2] M. H. Bakr, P. P. M. So, and W. J. R. Hoefer, "The generation of optimal microwave topologies using time-domain field synthesis," *IEEE Transactions on Microwave Theory and Techniques*, vol. 50, no. 11, pp. 2537–2544, 2002.

[3] M. H. Bakr and N. K. Nikolova, "An adjoint variable method for time-domain transmission-line modeling with fixed structured grids," *IEEE Transactions on Microwave Theory and Techniques*, vol. 52, no. 2, pp. 554–559, 2004.

Chapter 4

TLM Formulation of Inverse Source Problems with Smoothness Constraints

In this chapter, our TLM-based source reconstruction algorithm for thin source regions is generalized to source regions with arbitrary shapes inside a two-dimensional computational domain. For the case of thin source regions as discussed in Chapter 3, a unique time-domain solution can be obtained by solving a linear algebraic system using the time-domain field data radiated from the source region. However the uniqueness of the solution, as we shall see in this chapter, cannot be achieved for a source region with a generalized shape. This is due to the non-unique nature to the inverse source problem.

The inversion formalism developed in this chapter results in a discrete low-ranked linear algebraic system. To overcome the uniqueness, we additionally impose a

smoothness constraint (*a priori*) on the sources. Our solution is obtained by minimizing the first-order time and spatial derivatives of the reconstructed sources. Our algorithm is robust, and can accommodate arbitrary source geometries.

This section is organized as follows. In Section 4.1, we review the fundamental concept of the TLM method and derive the formulation for the direct problem. Then in Section 4.2 and Section 4.3, our inversion formulation of the problem and the regularization approach are each introduced respectively. Section 4.4 presents our source reconstruction algorithm using the TLM method. The numerical examples are given in Section 4.5. Finally, conclusions are drawn in Sectin 4.6.

4.1 TLM Formulation of the Direct Problem[1]

Before engaging to the new idea, we briefly guide through the essential ingredients of the TLM method in [1] to be employed in the following. The reader is referred to [1] for further details.

TLM method carries a sequence of scattering and connection procedure modelling the propagation of waves [1]. Considering a homogeneous (air filled) computational domain composed of Q number of mesh cells, it follows that a single TLM time step can be mathematically expressed as [2]:

$$\mathbf{v}_k = \boldsymbol{CS}\mathbf{v}_{k-1} + \mathbf{v}_k^s = \boldsymbol{A}\mathbf{v}_{k-1} + \mathbf{v}_k^s, \tag{4.1}$$

1 This section expands Section 3.1 by providing more detailed descriptions and graphic illustrations.

where $\mathbf{v}_k \in \mathbb{R}^{Q_L \times 1}$ is the vector of link impulses on all mesh links, which models the fields inside the computational domain at the kth time step. $Q_L = 4Q$ (for a two-dimensional computational domain) is the total number of mesh links associating with the Q number of mesh cells. $\boldsymbol{v}_k^s \in \mathbb{R}^{Q_L \times 1}$ is the vector of the excitation sources at the kth time step on all mesh links. In our case, the elements in $\boldsymbol{v}_k^s$ are non-zeros only for the mesh links inside the source region. Matrix $\boldsymbol{S} \in \mathbb{R}^{Q_L \times Q_L}$is the scattering matrix for all mesh cells and is assumed time invariant. Matrix $\boldsymbol{C} \in \mathbb{R}^{Q_L \times Q_L}$ is the connection matrix describing how reflected link impulses connect to neighboring mesh cells or boundaries. Matrix $\boldsymbol{A} \in \mathbb{R}^{Q_L \times Q_L}$ is the matrix product of $\boldsymbol{C}$ and $\boldsymbol{B}$, and its matrix-vector product refers to a complete TLM time iteration (see Figure 4.1).

By substituting $\mathbf{v}_{k-1}$ with $\mathbf{v}_{k-1} = \boldsymbol{A}\mathbf{v}_{k-2} + \mathbf{v}_{k-1}^s$, (4.1) can be written as

$$\begin{aligned} \mathbf{v}_k &= \boldsymbol{A}\left(\boldsymbol{A}\mathbf{v}_{k-2} + \mathbf{v}_{k-1}^s\right) + \mathbf{v}_k^s \\ &= \boldsymbol{A}^2\mathbf{v}_{k-2} + \boldsymbol{A}\mathbf{v}_{k-1}^s + \mathbf{v}_k^s. \end{aligned} \tag{4.2}$$

Following the same procedure, by substituting for $\mathbf{v}_{k-2}$ in (4.2) and then repeating for $\mathbf{v}_{k-3}$, $\mathbf{v}_{k-4}$, ..., and up to $\mathbf{v}_1$, the vector of incident impulses at the kth time step $\mathbf{v}_k$ can then be expressed as a linear combination of the excitations at all previous time steps. The resultant expression is given by

$$\mathbf{v}_k = \boldsymbol{A}^k\mathbf{v}_0^s + \boldsymbol{A}^{k-1}\mathbf{v}_1^s + \cdots + \mathbf{v}_k^s. \tag{4.3}$$

Equation (3.3) models the direct problem defining the mapping from the excitation sources to its produced fields. Consider only a two-dimensional problem with vector

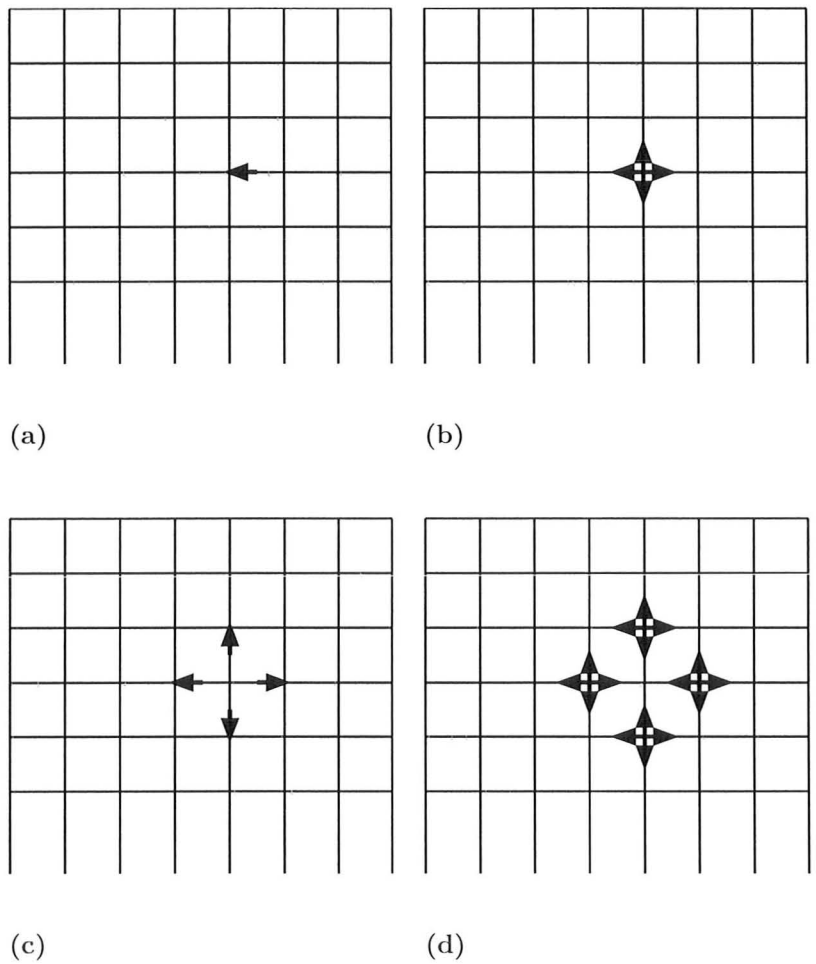

Figure 4.1 Illustration of the scattering and connection TLM procedures in a two-dimensional computational domain. (a) An impulse is incident on the center of the jth mesh cell at a given time step; (b) The incident impulse is scattered into four reflected impulses (scattering procedure); (c) The reflected impulses propagate to neighboring mesh cells (connection procedure); (d) the scattering procedure at the next time step.

fields $\boldsymbol{E}_y$, $\boldsymbol{H}_x$, $\boldsymbol{H}_z$, and a vector current density source $\boldsymbol{J}_y$ inside a computational domain on the xz-plane. At the kth time step the vector of excitation sources $\mathbf{v}_k^s$ can be obtained from the electric current density sources imposed on eahc mesh cells inside the source region by the following linear relation [3]:

$$\mathbf{v}_k^{s(cell)} = \frac{\Delta l Z_0}{\sqrt{2}} \cdot \boldsymbol{D}\mathbf{j}_k^{s(cell)}, \tag{4.4}$$

where at the kth time step the vector $\mathbf{j}_k^{s(cell)} \in \mathbb{R}^{Q\times 1}$ contains the current source densities imposed on each mesh cell. The vector $\mathbf{v}_k^{s(cell)} \in \mathbb{R}^{Q\times 1}$ contains the equivalent source values imposed on each mesh cells, which isotropically updates all link impulses inside each mesh cells. Δl is the distance between the centre of two adjacent mesh cells. Z_0 is the wave impedance of the free space. The matrix $\boldsymbol{D} \in \mathbb{R}^{Q\times Q}$ is given by

$$D_{ij} = \begin{cases} -\frac{1}{4}, & \text{if the } i\text{th and the } j\text{th elements in } \mathbf{v}_k^{s(cell)} \text{ are referring} \\ & \text{to a same mesh cell, } i = j; \\ -\frac{1}{16}, & \text{if the source cell corresponding to the } i\text{th element in} \\ & \mathbf{v}_k^{s(cell)} \text{ is adjacent to the source cell corresponding} \\ & \text{to the } j\text{th element in } \mathbf{v}_k^{s(cell)}; \\ 0, & \text{otherwise.} \end{cases} \tag{4.5}$$

The correspondent vector electric field $\boldsymbol{E}_y$ inside the computational domain at the kth time step can then be retrieved from $\mathbf{v}_k$ by using

$$\boldsymbol{E}_{y,j,k} = \frac{1}{2}\sum_{i=1}^{4} v_{j,k}^i \tag{4.6}$$

where at the kth time step $\boldsymbol{E}_{y,j,k}$ is the y-directed electric field at the jth mesh cell, and $v^i_{j,k}$ for $i = 1, 2, 3, 4$ are the four mesh links corresponding to the jth mesh cell.

4.2 The Linear Inverse Formulation

Now, we focus our attention to the source region, a sub-region inside the computational domain where all the excitation sources are localized. For a given source region as shown in Figure 4.2, we refer to its enclosed mesh cells as *source cells*. In particular, we call those source cells that are on the boundary as *boundary cells* (shown by dark squares in Figure 4.2), while the remaining cells are referred to as *interior cells* (shown by light squares in Figure 4.2). The arrows in Figure 4.2 are the link impulses radiated from the boundary cells due to the excitation sources inside the source region. In our inversion problem with unknown sources, these link impulses are obtained from the field measurements on its associated mesh cells by using (4.6).

We also group the source cells in terms of *layers* according to the following rule: all boundary cells are in the 1st layer; the source cells which are adjacent to source cells in the 1st layer are assigned to the 2nd layer; the remaining cells which are adjacent to cells in the 2nd layer are assigned to the 3rd layer, and same procedure are repeated until all source cells are assigned with a layer number.

For a source region composed of N source cells and M boundary cells ($N \leq M$), $v^s_{k,j}$ for $j = 1, 2, \ldots, N$ denotes the imposed source value on the jth source cell at the kth time step. ρ_j denotes the layer number of the jth source cell. $v^b_{k,i}$

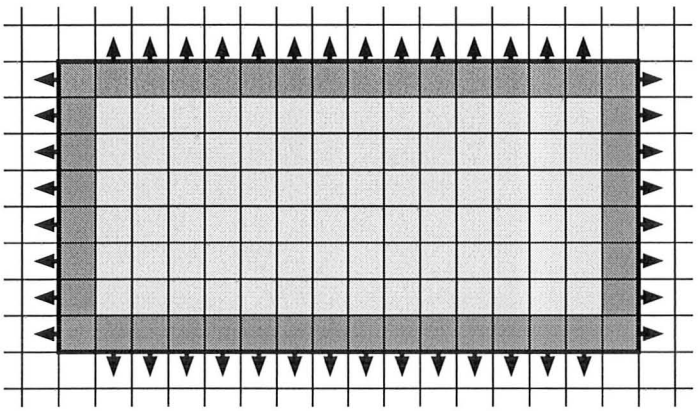

Figure 4.2 A discretized two-dimensional source region in a rectangular shape. Boundary cells are shown by dark squares, and boundary link impulses are shown by arrows.

for $i = 1, 2, \ldots, M$ denotes the radiated link impulse from the ith boundary cell at the kth time step. We refer these link impulses as *boundary link impulses* and $\boldsymbol{v}_k^b = [\, v_{k,1}^b \quad v_{k,2}^b \quad \ldots \quad v_{k,M}^b \,]^T$. Thereby, our inverse problem can thus be stated as being that of reconstructing $v_{k,j}^s$ (for all $j = 1, 2, \ldots, N$) for all time step k, from the knowledge of $v_{k,i}^b$ (for all $i = 1, 2, \ldots, M$) for all time step k. Once the $v_{k,j}^s$ is obtained for all j, the current density sources can then be retrieved by using (4.4).

Now, we restrict our attention to a single source cell, say the jth source cell, and investigate the field that it would produce. At the kth time step, by (3.3) the radiated link impulses on the entire computational domain due to only the source value imposed at the jth source cell, $\boldsymbol{v}_{k,j}$, is given by

$$\boldsymbol{v}_{k,j} = \boldsymbol{A}^k \boldsymbol{v}_{0,j}^s + \boldsymbol{A}^{k-1} \boldsymbol{v}_{1,j}^s + \cdots + \boldsymbol{v}_{k,j}^s, \tag{4.7}$$

where $\boldsymbol{v}_{k,j}^s \in \mathbb{R}^{Q_L \times 1}$ is the vector of excitations on all mesh links at the kth time step, and only the elements corresponding to the mesh links inside the jth source cell are nonzero and are equal to $v_{k,j}^s$.

Considering the layer number for the jth source cell, (4.7) can be further partitioned into three parts as

$$\boldsymbol{v}_{k,j} = \tilde{\boldsymbol{v}}_{k,j} + \boldsymbol{v}_{k,j}^{(b)} + \boldsymbol{v}_{k,j}^{(in)}, \tag{4.8}$$

where

$$\tilde{\boldsymbol{v}}_{k,j} = \boldsymbol{A}^k \boldsymbol{v}_{0,j}^s + \boldsymbol{A}^{k-1} \boldsymbol{v}_{1,j}^s + \cdots + \boldsymbol{A}^{\rho_j+1} \boldsymbol{v}_{k-\rho_j-1,j}^s, \tag{4.9}$$

$$\boldsymbol{v}_{k,j}^{(b)} = \boldsymbol{A}^{\rho_j} \boldsymbol{v}_{k-\rho_j,j}^s, \tag{4.10}$$

$$\boldsymbol{v}_{k,j}^{(in)} = \boldsymbol{A}^{\rho_j-1} \boldsymbol{v}_{k-\rho_j+1,j}^s + \boldsymbol{A}^{\rho_j-2} \boldsymbol{v}_{k-\rho_j+2,j}^s + \cdots + \boldsymbol{v}_{k,j}^s. \tag{4.11}$$

In (4.8), note that the first term $\tilde{\boldsymbol{v}}_{k,j}$ affects the link impulses on the entire computational domain. The second term $\boldsymbol{v}_{k,j}^{(b)}$ affects only the link impulses connecting to the source region and the link impulses inside the source region. The last term $\boldsymbol{v}_{k,j}^{(in)}$ affects only the mesh links inside the source region.

At the kth time step, the vector of boundary link impulses $\boldsymbol{v}_k^b$ is a subset of $\boldsymbol{v}_k$. We use the selection matrix $\boldsymbol{E} \in \mathbb{R}^{M \times Q_L}$ for selecting the vector elements corresponding to the boundary links from the mesh links on the entire computation domain, and $\boldsymbol{v}_k^b = \boldsymbol{E}\boldsymbol{v}_k$. Then by (4.8), it follows that the resultant boundary impulses due entirely to the excitation source at the jth source cell is given by

$$\begin{aligned} \mathbf{v}_{k,j}^{b} = \boldsymbol{E}\mathbf{v}_{k,j} &= \boldsymbol{E}\tilde{\mathbf{v}}_{k,j} + \boldsymbol{E}\mathbf{v}_{k,j}^{(b)} + \boldsymbol{E}\mathbf{v}_{k,j}^{(in)} \\ &= \boldsymbol{E}\tilde{\mathbf{v}}_{k,j} + \boldsymbol{E}\mathbf{v}_{k,j}^{(b)}. \end{aligned} \tag{4.12}$$

In (4.12), the term $\mathbf{v}_{k,j}^{(in)}$ does not radiate to the exterior of the source region. Therefore, it can be eliminated from the equation.

By summing up the field contributions from all sources cells, it follows that $\mathbf{v}_{k}^{b}$ is given by

$$\begin{aligned} \mathbf{v}_{k}^{b} &= \sum_{j=1}^{N} \boldsymbol{E}\tilde{\mathbf{v}}_{k,j} + \sum_{j=1}^{N} \boldsymbol{E}\mathbf{v}_{k,j}^{(b)} \\ &= \boldsymbol{E}\tilde{\mathbf{v}}_{k} + \sum_{j=1}^{N} \boldsymbol{E}\mathbf{v}_{k,j}^{(b)}, \end{aligned} \tag{4.13}$$

where

$$\tilde{\mathbf{v}}_{k} = \sum_{j=1}^{N} \tilde{\mathbf{v}}_{k,j}. \tag{4.14}$$

Considering the whole computational domain, we define $g(i, j, k')$ to be its discrete Green's function, which gives the value of the ith boundary link impulses at the kth time step due to the presence of the imposed unity source value at the jth source at the 0th time step. Using the discrete Green's function, the second term in (4.13) can be further expanded as

$$\sum_{j=1}^{N} \boldsymbol{E}\mathbf{v}_{k,j}^{(b)} = \sum_{j=1}^{N} \boldsymbol{E}\boldsymbol{A}^{\rho_j}\mathbf{v}_{k-\rho_j,j}^{s}$$

$$= \sum_{j=1}^{N} \begin{bmatrix} g(1,j,\rho_j)\cdot v_{k-\rho_j,j}^{s} \\ g(2,j,\rho_j)\cdot v_{k-\rho_j,j}^{s} \\ g(3,j,\rho_j)\cdot v_{k-\rho_j,j}^{s} \\ \vdots \\ g(M,j,\rho_j)\cdot v_{k-\rho_j,j}^{s} \end{bmatrix}$$

$$= \begin{bmatrix} g(1,1,\rho_1) & g(1,2,\rho_2) & \dots & g(1,N,\rho_N) \\ g(2,1,\rho_1) & g(2,2,\rho_2) & \dots & g(2,N,\rho_N) \\ \vdots & \vdots & \ddots & \vdots \\ g(M,1,\rho_1) & g(M,2,\rho_2) & \dots & g(M,N,\rho_N) \end{bmatrix} \cdot \begin{bmatrix} v_{k-\rho_1,1}^{s} \\ v_{k-\rho_2,2}^{s} \\ v_{k-\rho_3,3}^{s} \\ \vdots \\ v_{k-\rho_N,N}^{s} \end{bmatrix} \quad (4.15)$$

Substituting (4.15) into (4.13), we thus obtain the following linear system with size $M \times N$ describing our inversion formalism:

$$\boldsymbol{G}\tilde{\mathbf{v}}_k^{s} = \mathbf{v}_k^{b} - \boldsymbol{E}\tilde{\mathbf{v}}_k, \quad (4.16)$$

where

$$\boldsymbol{G} = \begin{bmatrix} g(1,1,\rho_1) & g(1,2,\rho_2) & \dots & g(1,N,\rho_N) \\ g(2,1,\rho_1) & g(2,2,\rho_2) & \dots & g(2,N,\rho_N) \\ \vdots & \vdots & \ddots & \vdots \\ g(M,1,\rho_1) & g(M,2,\rho_2) & \dots & g(M,N,\rho_N) \end{bmatrix}, \tilde{\mathbf{v}}_k^{s} = \begin{bmatrix} v_{k-\rho_1,1}^{s} \\ v_{k-\rho_2,2}^{s} \\ v_{k-\rho_3,3}^{s} \\ \vdots \\ v_{k-\rho_N,N}^{s} \end{bmatrix}. \quad (4.17)$$

For a special case—the thin source regions[1], whose enclosed source cells are all boundary cells, the number of source cells equals the number of observed boundary link impulses $N = M$. Then the system described in (4.16) is full-ranked. At the kth time step $\tilde{\mathbf{v}}_k^s$ can thus be uniquely determined by evaluating (4.16).

4.3 The Solution with the Smoothness Constraint

For a given source region, the number of source cells N is always greater or equal to the number of boundary cells M. For the most general case in which $N > M$, the linear system described in (4.16) is a low-ranked system. Therefore, a regularization procedure is required to overcome the non-uniqueness in the source solution.

Here, we apply the smoothness condition (*a priori*) to the sources by assuming that the imposed sources within the source region are smoothly distributed in both space and time for all time steps. For each source cells at each time steps, we additionally restrict its imposed source value with either the time-smoothness condition or the spatial-smoothness condition. The time-smoothness condition minimizes the first-order derivative with respect to time, while the spatial-smoothness condition minimizes the first-order spatial derivative with respect the sources imposed on its surrounding cells.

Our source solution with the smoothness constraint can then be obtained by solving a minimization problem with the optimizing variable $\tilde{\mathbf{v}}_k^s$:

1 The source reconstruction algorithm for thin source regions is discussed in Chapter 3.

$$\begin{aligned} \text{minimize} \quad & \mathcal{F} = \left\| \tilde{\mathbf{v}}^s_{k,(T)} - \tilde{\mathbf{v}}^s_{k-1,(T)} \right\|_2^2 + w^2 \left\| \boldsymbol{B}\tilde{\mathbf{v}}^s_k - \tilde{\mathbf{v}}^s_{k,(S)} \right\|_2^2, \\ \text{subject to} \quad & \boldsymbol{G}\tilde{\mathbf{v}}^s_k = \mathbf{v}^b_k - \boldsymbol{E}\tilde{\mathbf{v}}_k. \end{aligned} \tag{4.18}$$

In (4.18), the vector $\tilde{\mathbf{v}}^s_{k(T)} \in \mathbb{R}^{p\times 1}$ is a subset of $\tilde{\mathbf{v}}^s_k$ for source cells with the time-smoothness condition, where p is the total number of source cells constrained by the time-smoothness condition. The vector $\tilde{\mathbf{v}}^s_{k(S)} \in \mathbb{R}^{q\times 1}$ is another subset of $\tilde{\mathbf{v}}^s_k$ for source cells with the spatial-smoothness condition, where q is the total number of source cells constrained by the spatial-smoothness condition. The scalar w is the weighting factor between the two objective norms. The matrix $\boldsymbol{B} \in \mathbb{R}^{q\times N}$ gives the neighbouring relation for correspondent source cells in $\tilde{\mathbf{v}}^s_{k(S)}$, and is given by

$$B_{ij} = \begin{cases} \frac{1}{8}, & \text{if the source cell corresponding to the } i\text{th element in} \\ & \tilde{\mathbf{v}}^s_{k(S)} \text{ is an interior cell and is adjacent to or diagonally} \\ & \text{neighbouring to the source cells corresponding to the} \\ & j\text{th element in } \tilde{\mathbf{v}}^s_{k(S)}; \\ \frac{1}{5}, & \text{if the source cell corresponding to the } i\text{th element in } \tilde{\mathbf{v}}^s_{k(S)} \\ & \text{is an boundary cell and is adjacent to or diagonally} \\ & \text{neighbouring to the source cell corresponding to the} \\ & j\text{th element in } \tilde{\mathbf{v}}^s_{k(S)}; \\ 0, & \text{otherwise.} \end{cases} \tag{4.19}$$

Combining the two objective norms, (4.18) can be rewritten as

$$\begin{aligned}\mathcal{F} &= \left\| \begin{array}{l} \tilde{\mathbf{v}}^s_{k,(T)} - \tilde{\mathbf{v}}^s_{k-1,(T)} \\ w\boldsymbol{B}\tilde{\mathbf{v}}^s_k - w\tilde{\mathbf{v}}^s_{k,(S)} \end{array} \right\|_2^2 \\ &= \left\| \begin{array}{l} \boldsymbol{K}_{(T)}\tilde{\mathbf{v}}^s_k - \tilde{\mathbf{v}}^s_{k-1,(T)} \\ \boldsymbol{K}_{(S)}\tilde{\mathbf{v}}^s_k \end{array} \right\|_2^2 \\ &= \left\| \begin{bmatrix} \boldsymbol{K}_{(T)} \\ \boldsymbol{K}_{(S)} \end{bmatrix} \tilde{\mathbf{v}}^s_k - \begin{bmatrix} \tilde{\mathbf{v}}^s_{k-1,(T)} \\ \boldsymbol{0} \end{bmatrix} \right\|_2^2, \end{aligned} \tag{4.20}$$

where $\boldsymbol{K}_{(T)} \in \mathbb{R}^{p\times N}$ is given by

$$K_{ij,(T)} = \begin{cases} 1, & \text{if the } i\text{th element in } \tilde{\mathbf{v}}^s_{k(T)} \text{ and the } j\text{th element} \\ & \text{in } \tilde{\mathbf{v}}^s_k \text{ correspond to a same source cell;} \\ 0, & \text{otherwise.} \end{cases} \tag{4.21}$$

$\boldsymbol{K}_{(S)} \in \mathbb{R}^{q\times N}$ is given by

$$K_{ij,(S)} = \begin{cases} -w, & \text{if the } i\text{th element in } \tilde{\mathbf{v}}^s_{k(S)} \text{ and the } j\text{th element} \\ & \text{in } \tilde{\mathbf{v}}^s_k \text{ correspond to a same source cell;} \\ wB_{ij}, & \text{otherwise.} \end{cases} \tag{4.22}$$

Incorporating the equality constraints in (4.18) with the objective function using Lagrange multipliers $\lambda \in \mathbb{R}^M$, it follows that its correspondent Lagrange function $\mathcal{L}(\tilde{\mathbf{v}}^s_k,\ \lambda)$ is given by

$$\begin{aligned}\mathcal{L}(\mathbf{v}^s_k,\ \lambda) &= \left\|\tilde{\mathbf{v}}^s_{k,(T)} - \tilde{\mathbf{v}}^s_{k-1,(T)}\right\|_2^2 + w^2\left\|\boldsymbol{B}\tilde{\mathbf{v}}^s_k - \tilde{\mathbf{v}}^s_{k,(S)}\right\|_2^2 + \lambda^T\left(\boldsymbol{G}\tilde{\mathbf{v}}^s_k - \mathbf{v}^b_k + \boldsymbol{E}\tilde{\mathbf{v}}_k\right) \\ &= \left\| \begin{bmatrix} \boldsymbol{K}_{(T)} \\ \boldsymbol{K}_{(S)} \end{bmatrix} \tilde{\mathbf{v}}^s_k - \begin{bmatrix} \tilde{\mathbf{v}}^s_{k-1,(T)} \\ \boldsymbol{0} \end{bmatrix} \right\|_2^2 + \lambda^T\left(\boldsymbol{G}\tilde{\mathbf{v}}^s_k - \mathbf{v}^b_k + \boldsymbol{E}\tilde{\mathbf{v}}_k\right). \end{aligned} \tag{4.23}$$

Differentiating $\mathcal{L}(\tilde{\boldsymbol{v}}_k^s,\ \lambda)$ with respective to $\tilde{\boldsymbol{v}}_k^s$ and λ gives

$$\begin{aligned}\frac{\partial \mathcal{L}}{\partial \tilde{\boldsymbol{v}}_k^s} &= 2\left[\boldsymbol{K}_{(T)}^T \quad \boldsymbol{K}_{(S)}^T\right]\left(\begin{bmatrix}\boldsymbol{K}_{(T)}\\ \\ \boldsymbol{K}_{(S)}\end{bmatrix}\tilde{\boldsymbol{v}}_k^s - \begin{bmatrix}\tilde{\boldsymbol{v}}_{k-1,(T)}^s\\ \\ \boldsymbol{0}\end{bmatrix}\right) + \boldsymbol{G}^T\,\lambda \\ &= 2\left[\boldsymbol{K}_{(T)}^T \quad \boldsymbol{K}_{(S)}^T\right]\begin{bmatrix}\boldsymbol{K}_{(T)}\\ \\ \boldsymbol{K}_{(S)}\end{bmatrix}\tilde{\boldsymbol{v}}_k^s + \boldsymbol{G}^T\,\lambda - 2\left[\boldsymbol{K}_{(T)}^T \quad \boldsymbol{K}_{(S)}^T\right]\begin{bmatrix}\tilde{\boldsymbol{v}}_{k-1,(T)}^s\\ \\ \boldsymbol{0}\end{bmatrix}\end{aligned} \tag{4.24}$$

and

$$\frac{\partial \mathcal{L}}{\partial\ \lambda} = \boldsymbol{G}\tilde{\boldsymbol{v}}_k^s - \boldsymbol{v}_k^b + \boldsymbol{E}\tilde{\boldsymbol{v}}_k. \tag{4.25}$$

Equating (4.24) and (4.25) to zeros, we thus obtained the following extended linear system with size $N+M$ by $N+M$.

$$\begin{bmatrix} 2\left[\boldsymbol{K}_{(T)}^T \quad \boldsymbol{K}_{(S)}^T\right]\begin{bmatrix}\boldsymbol{K}_{(T)}\\ \\ \boldsymbol{K}_{(S)}\end{bmatrix} & \boldsymbol{G}^T \\ \\ \boldsymbol{G} & \boldsymbol{0}\end{bmatrix}\begin{bmatrix}\tilde{\boldsymbol{v}}_k^s\\ \\ \lambda\end{bmatrix} = \begin{bmatrix} 2\left[\boldsymbol{K}_{(T)}^T \quad \boldsymbol{K}_{(S)}^T\right]\begin{bmatrix}\tilde{\boldsymbol{v}}_{k-1,(T)}^s\\ \\ \boldsymbol{0}\end{bmatrix}\\ \\ \boldsymbol{v}_k^b - \boldsymbol{E}\tilde{\boldsymbol{v}}_k\end{bmatrix}. \tag{4.26}$$

The solution to (4.26) is unique and is our solution with smoothness constraint.

4.4 Practical Implementation

For the jth source cell, our algorithm finds $\tilde{\boldsymbol{v}}_k^s$ given by (4.17) using the radiated boundary link impulses at the kth time step.

Before the start of the reconstruction algorithm, we first initialize the homogeneous computational domain and the geometry of the source region. We then index each source cells and the radiated boundary link impulses. After that, we assign layer numbers to each source cells.

Once the initialization phase is over, we compute the matrix $\boldsymbol{G}$, the matrix $\boldsymbol{K}_{(T)}$ and the matrix $\boldsymbol{K}_{(S)}$ using (4.17), (4.21), and (4.22) respectively. We then construct the system matrix on the left hand side of the (4.26) using the previously computed $\boldsymbol{G}$, $\boldsymbol{K}_{(T)}$, and $\boldsymbol{K}_{(S)}$.

At the kth time step, our algorithm reconstructs $\tilde{\boldsymbol{v}}_k^s$ from the knowledge of $\boldsymbol{v}_k^b$ using the following two sequences:

I. Compute $\tilde{\boldsymbol{v}}_k$ using (4.14) and (4.9);

II. Solve for $\tilde{\boldsymbol{v}}_k^s$ by evaluating the linear system (4.26).

Considering only the first sequence (I), one may note that it is computationally impractical to obtain $\tilde{\boldsymbol{v}}_k$ by directly applying (4.14) and (4.9), which would require a great number of TLM iterations. As a much improved alternative, we rewrite (4.14) using the previous result of $\tilde{\boldsymbol{v}}_k$ (i.e. $\tilde{\boldsymbol{v}}_{k-1}$). The resultant expression for $\tilde{\boldsymbol{v}}_k$ at the kth time step is then given by

$$\tilde{\boldsymbol{v}}_k = \boldsymbol{A}\left(\tilde{\boldsymbol{v}}_{k-1} + \sum_{j=1}^{N} \boldsymbol{A}^{\rho_j}\tilde{\boldsymbol{v}}_{k-\rho_j-1,j}^s\right). \tag{4.27}$$

The summation term in (4.27) can be computed in a single TLM computational domain by carrying $\rho_{\max}$ number of TLM time iterations, and $\rho_{\max}$ is the total number of layers of the given source region. This forward TLM time iterations is done by imposing a source value given by $v^s_{k-\rho_j-1,j}$ on the jth source cell for $j = 1, 2, \ldots, N$ at the kth time step ($0 < k \leq \rho_{\max}$), only when the jth source cell and the time step k satisfies the relation $k = \rho_{\max} - \rho_i$.

The resultant summation term in (4.27) is added to the previous result of $\tilde{\boldsymbol{v}}_k$, $\tilde{\boldsymbol{v}}_{k-1}$. The source solution $\tilde{\boldsymbol{v}}_k$ is then obtained by performing a TLM time iteration in a new computational domain on this computed vector term $\tilde{\boldsymbol{v}}_{k-1} + \sum_{j=1}^{N} \boldsymbol{A}^{\rho_j} \tilde{\boldsymbol{v}}^s_{k-\rho_j-1,j}$.

The second sequence (II) is more straight forward. First, we computed the right hand side of the (4.26) using $\tilde{\boldsymbol{v}}^s_{k-1(T)}$, $\boldsymbol{v}^b_k$, and the computed vector $\tilde{\boldsymbol{v}}_k$ from sequence I. Then $\tilde{\boldsymbol{v}}^s_k$ can be evaluated by solving the linear system given by (4.26).

In summary, for the kth reconstruction time step, our algorithm requires total of $\rho_{\max} + 1$ number of TLM iterations for the computation of $\tilde{\boldsymbol{v}}_k$, and requires solving a linear system of size $N + M$ by $N + M$ to obtain $\tilde{\boldsymbol{v}}^s_k$.

4.5 Numerical Examples

Our algorithm is illustrated through the reconstruction of the excitation sources inside various two-dimensional source regions for both the noise-free and the noisy case. In this section, selected numerical examples are presented.

For our numerical examples, each source region is placed at the center of a computational domain with size 50 by 50 grids. The computational domain is bounded by zero-reflection boundaries.

Our testing procedure can be summarized using the following two phases:

I. *Forward computation* For the phase of the forward computation, we utilized the forward algorithm (described by (4.1)) to compute the field results of the direct problem. At the kth time step each source cells within the source region is excited by a known source. We then compute for the link impulses that is radiated from the boundary of the source region. These field results are then stored in the vector $\mathbf{v}_k^b$. This step emulates the actual measurements.

II. *Reverse computation* For the phase of the reverse computation, we utilize our algorithm (see Section 4.4) to reconstruct the excitation sources imposed on each source cells using the knowledge of $\mathbf{v}_k^b$ from the forward computation. At the kth time step, our results of the reconstructed sources are then compared with their exact imposed sources.

For each tested source region, its enclosed source cells are imposed with modulated Gaussian pulses as the testing signal. The imposed Gaussian pulses differ in the amplitude and phase among the source cells, and follow a smooth spacial distribution over the source region for all time steps. The source signal at the source cell with indices (x, z) is given by

$$v^s_{x,z}[k\Delta t] = A(x,z) \cdot \exp\left(-\frac{(k\Delta t - \mu - P(x,z)\Delta t)^2}{2\sigma^2}\right) \sin\left(\frac{2\pi\,(k - P(x,z))\,\Delta t}{150\Delta t}\right). \tag{4.28}$$

For our testing purpose, in (4.28) we set μ to be $600\Delta t$ and σ to be $100\Delta t$, where Δt is the time increment. $A(x,z)$ is the amplitude profile of the sources over the whole source region, and is given by

$$A(x,z) = -0.002(x - 5.0)^2 - 0.003(z - 8.0)^2 + 0.9. \tag{4.29}$$

$P(x,z)$ is the phase profile of the sources over the whole source region, and is given by

$$P(x,z) = 6z. \tag{4.30}$$

In (4.28), (4.29), and (4.30), x and z are the cell indices, and are each with respect to the vertical direction and the horizontal direction. The lower left corner of a given source region is indexed as $(x = 0, z = 0)$.

4.5.1 A Rectangular Source Region

We first consider the example of reconstructing the sources inside a source region with size 12 by 16 as shown in Figure 4.3. This source region is composed of 192 source cells and 42 boundary cells. The spatial distributions of the reconstructed sources at some selected time steps are shown in Figure 4.4. The reconstructed source signals

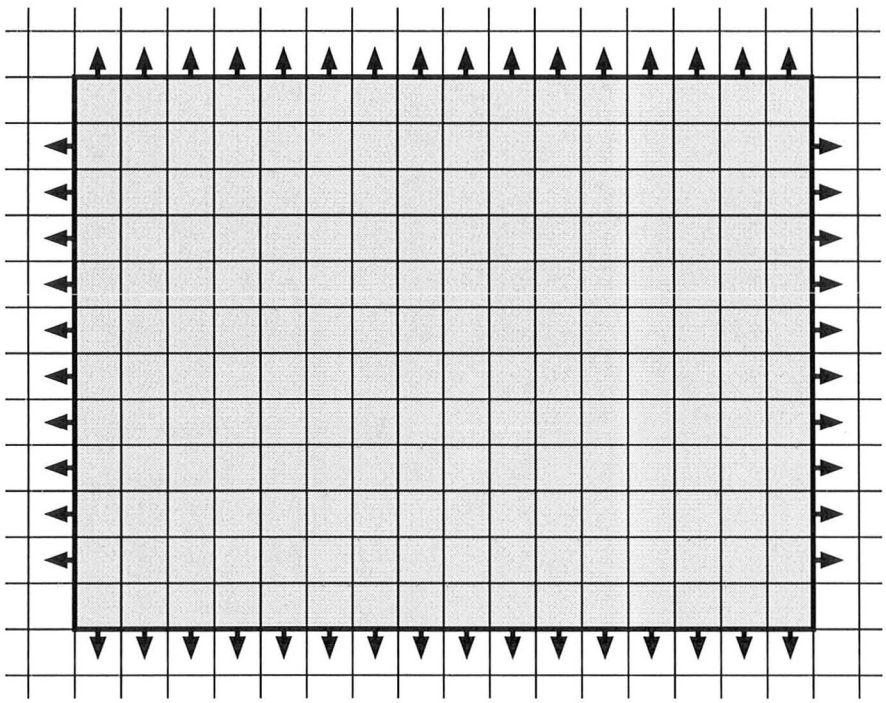

Figure 4.3 A six-layer source region with size 12 by 16 grids. Total of 42 radiated link impulses (shown by arrows) are observed.

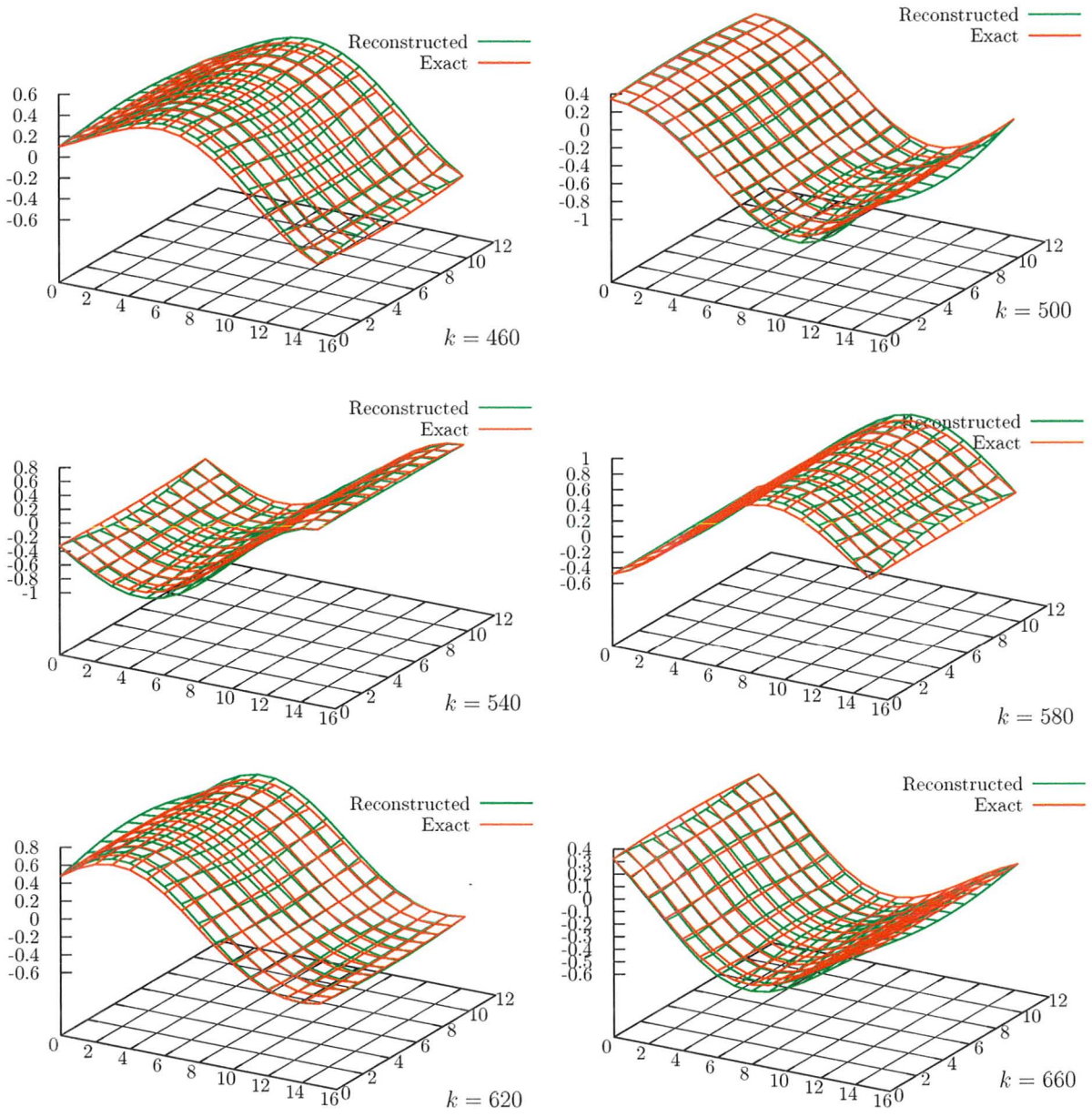

Figure 4.4 The spatial distribution of the exact sources and the reconstructed sources at selected time steps for the rectangular source region of size 12 by 16 grids.

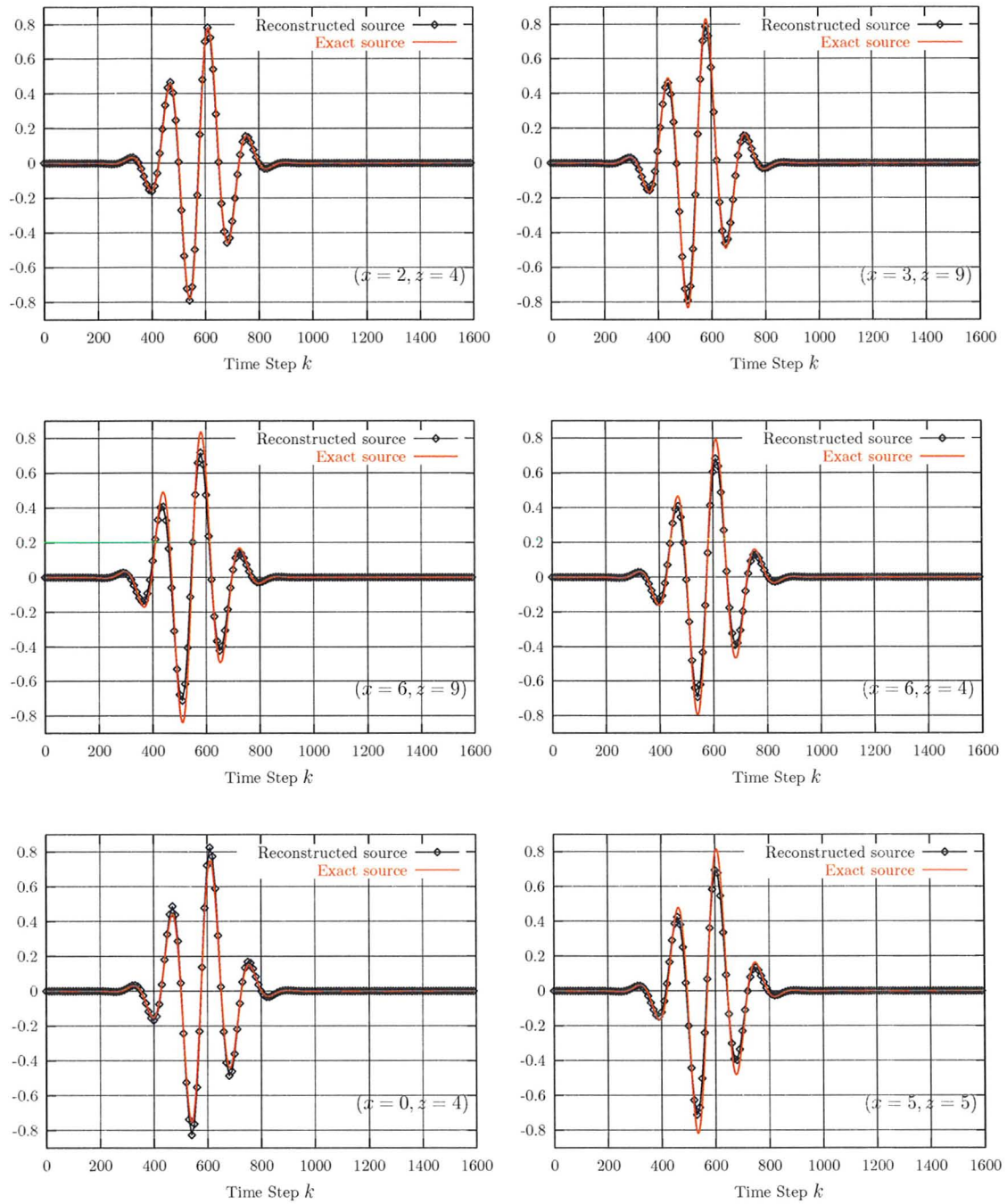

Figure 4.5 The reconstructed sources with respect to time at selected cell locations inside the rectangular source region of size 12 by 16 grids.

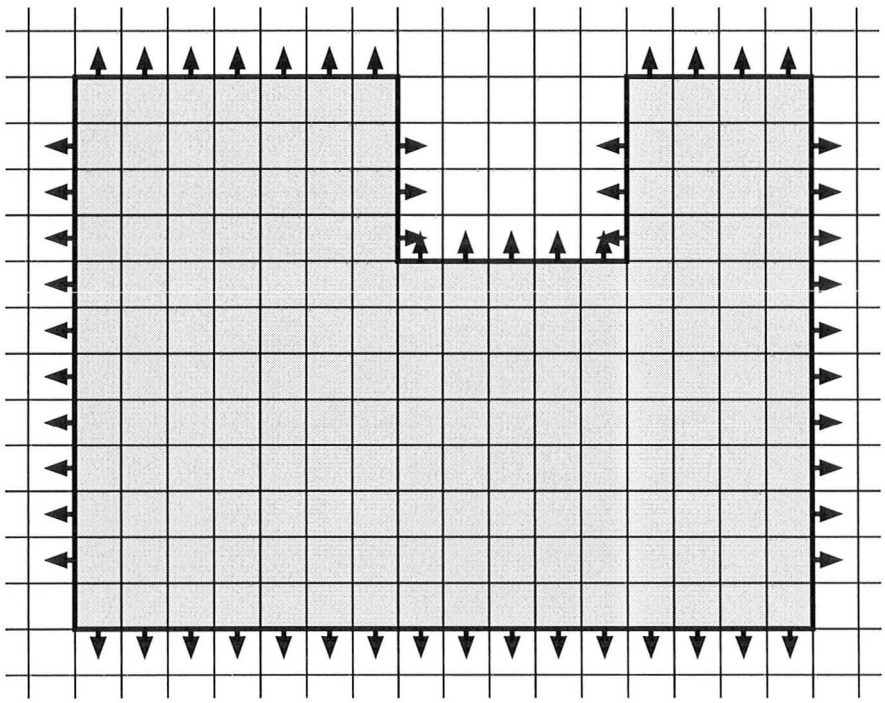

Figure 4.6 A four-layer reentrant source region composed of 172 source cells. Total of 48 radiated link impulses (shown by arrows) are observed.

with respect to time at selected source cells are shown in Figure 4.5. The comparison shows that our results agree with the exact results within a good accuracy.

4.5.2 A Re-entrant Source Region

The second illustrated example is a reentrant source region as shown in Figure 4.6. This source region is composed of 172 source cells and 48 boundary cells. The spatial distributions of the reconstructed source at some selected time steps are shown in Figure 4.7. The reconstructed source signals with respect to time at selected source cells are shown in Figure 4.8. The comparison shows that our results agree with the exact results within a good accuracy.

4.5.3 Effect of Noise

Noise is always unavoidable in physical world. In our case the boundary link impulses $\boldsymbol{v}_k^b$ may be contaminated with noise, because it is practically impossible to obtain accurate field data on the boundary of the source region. The associated errors are mostly due to limitations of measurement devices.

To model noisy field measurements, all elements in vector $\boldsymbol{v}_k^b$ are perturbed by a random number given by

$$\boldsymbol{v}_k^{b(e)} = \boldsymbol{v}_k^b + \alpha \boldsymbol{e}_k, \tag{4.31}$$

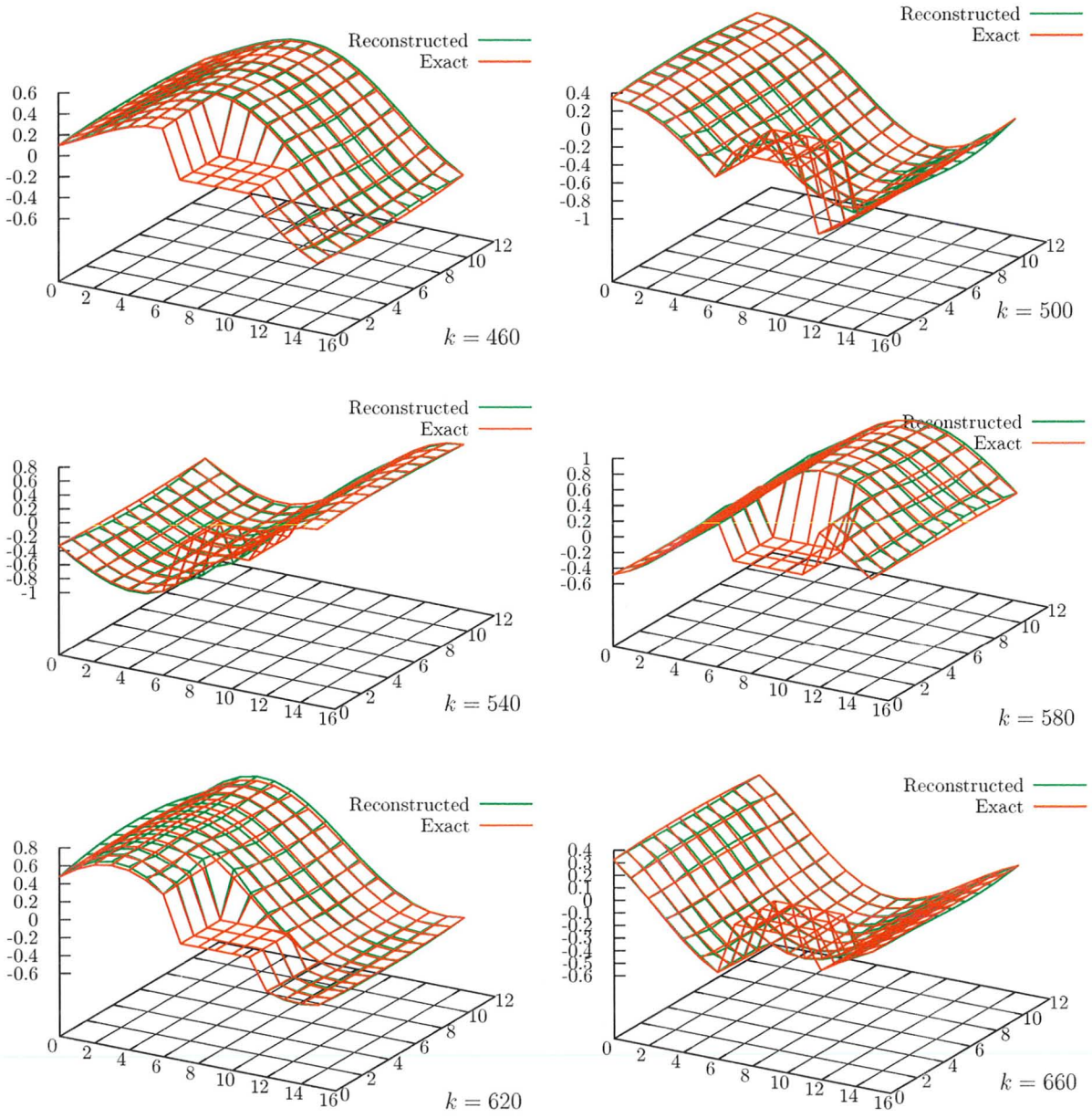

Figure 4.7 The spatial distribution of the exact sources and the reconstructed sources at selected time steps for the reentrant source region composed of 172 source cells.

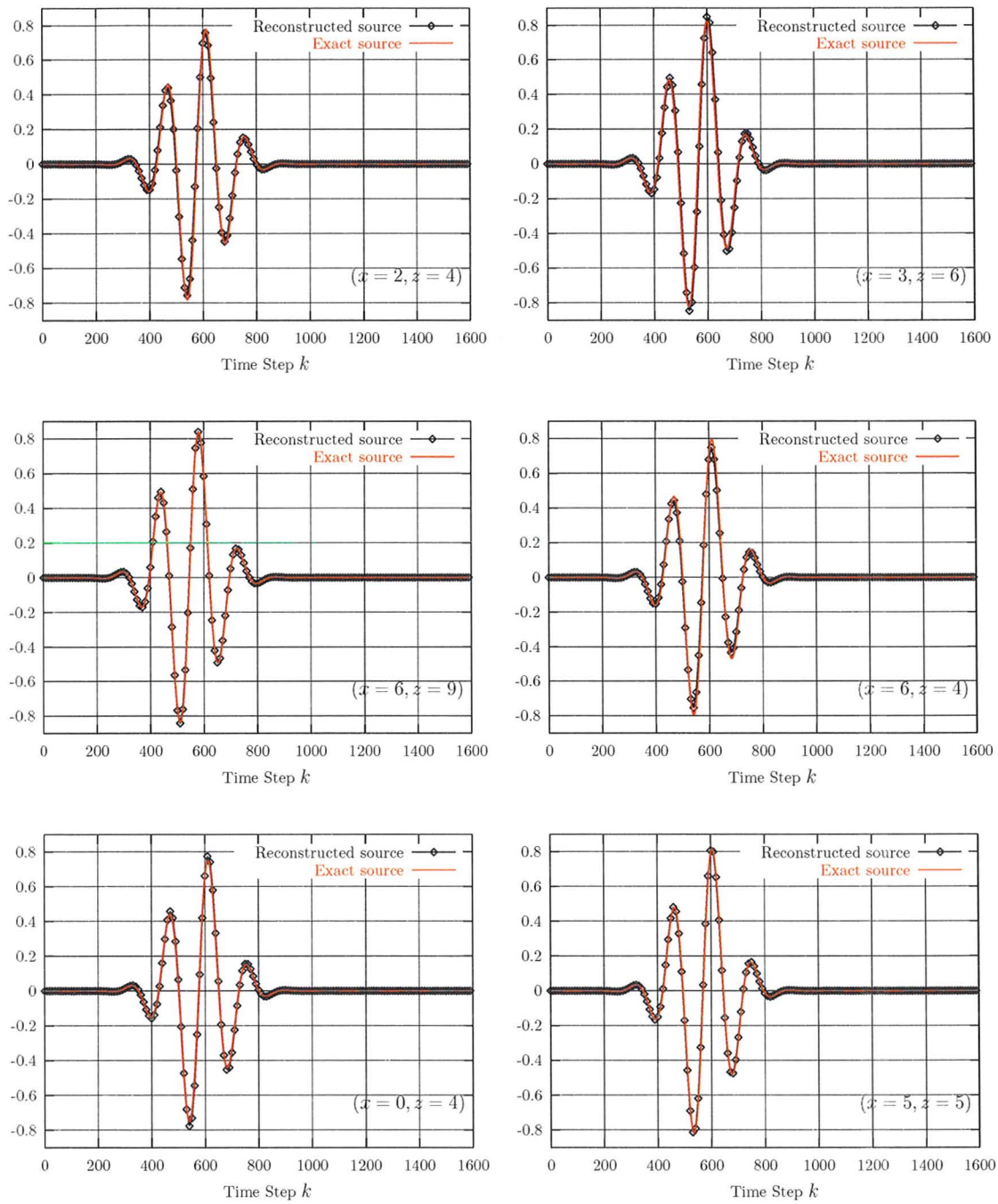

Figure 4.8 The reconstructed sources with respect to time at selected cell locations inside the reentrant source region composed of 172 source cells.

where $\boldsymbol{e} \in \mathbb{R}^{M\times 1}$ is a vector of Gaussian distributed random variables with zero mean and unit standard deviation. The scalar α is a factor for adjusting the noise level. At the kth time step, $\boldsymbol{v}_k^{b(e)}$ is fed into our reconstruction algorithm instead of $\boldsymbol{v}_k^b$.

We use the same testing source region as shown in Figure 4.3. The numerical results of constructed sources are shown in Figure 4.9 for a perturbed noise level of -28 dB, Figure 4.10 for a noise level of -22 dB, and Figure 4.11 for a noise level of -7.8 dB.

By inspection, the noise level in the reconstructed sources increase for about 15 dB in average. Our algorithm is shown to be stable in the presence of noise in the measured field data.

4.6 Conclusions

This chapter presents a numerical algorithm for solving the inverse source problem in electromagnetics using the knowledge of near field data. Our results converges to the exact results for higher ratio of M/N, where N is the number of source cells for a given source region, and M is the number of boundary cells. In particular, for thin source regions (discussed in Chapter 3) in which N is equal to M, the resultant linear system described in (4.16) is full-ranked. In this case, a unique solution can be obtained even without the regularization procedures, and the produced results are identical to the exact solutions.

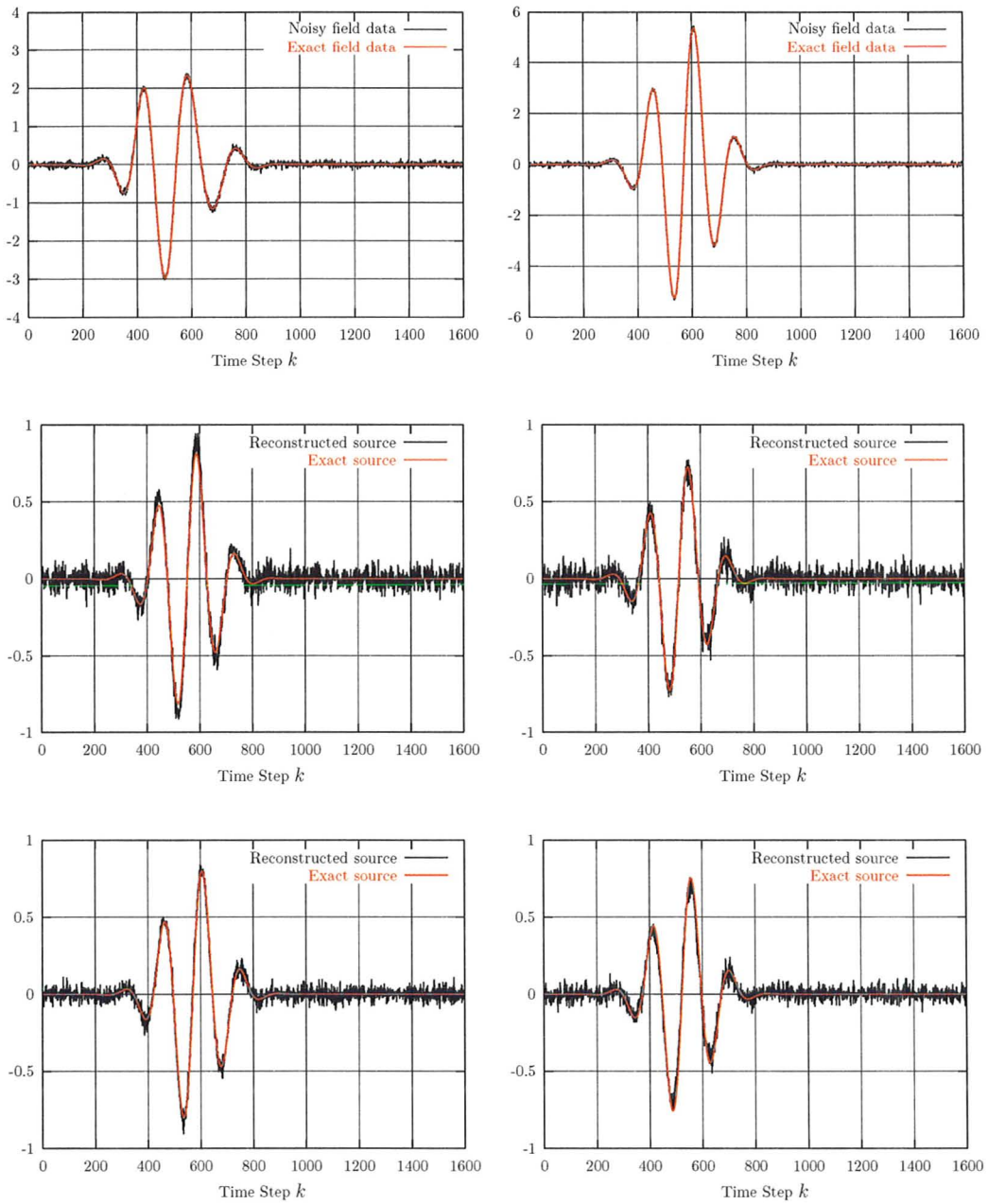

Figure 4.9 The reconstructed excitation sources using the noisy field data with noise level -28 dB. Top two figures shows two arbitrarily selected noisy boundary link impulses. The remaining four figures show the reconstructed sources at selected source cells.

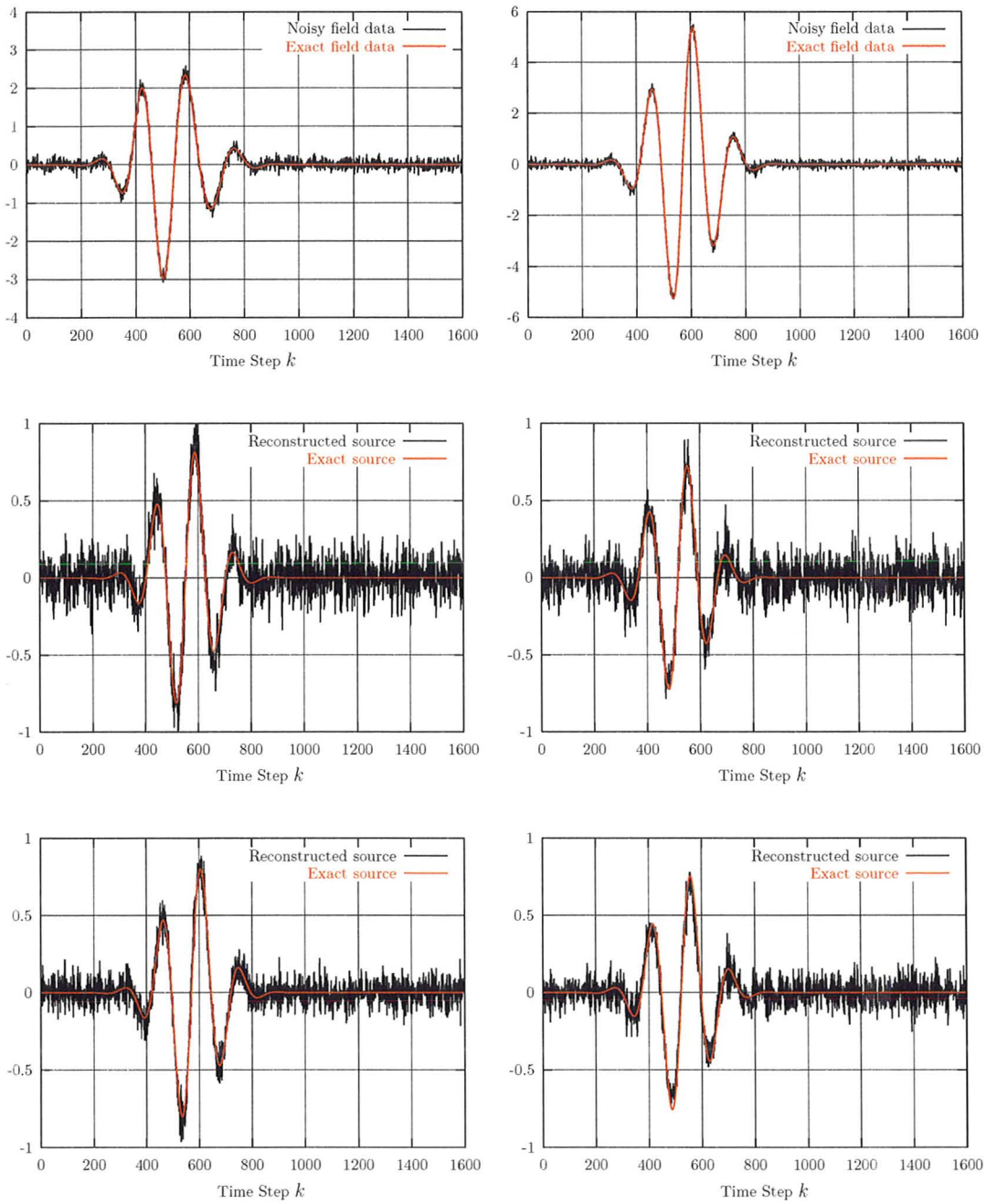

Figure 4.10 The reconstructed excitation sources using the noisy field data with noise level -5.6 dB. Top two figures shows two arbitrarily selected noisy boundary link impulses. The remaining four figures show the reconstructed sources at selected source cells.

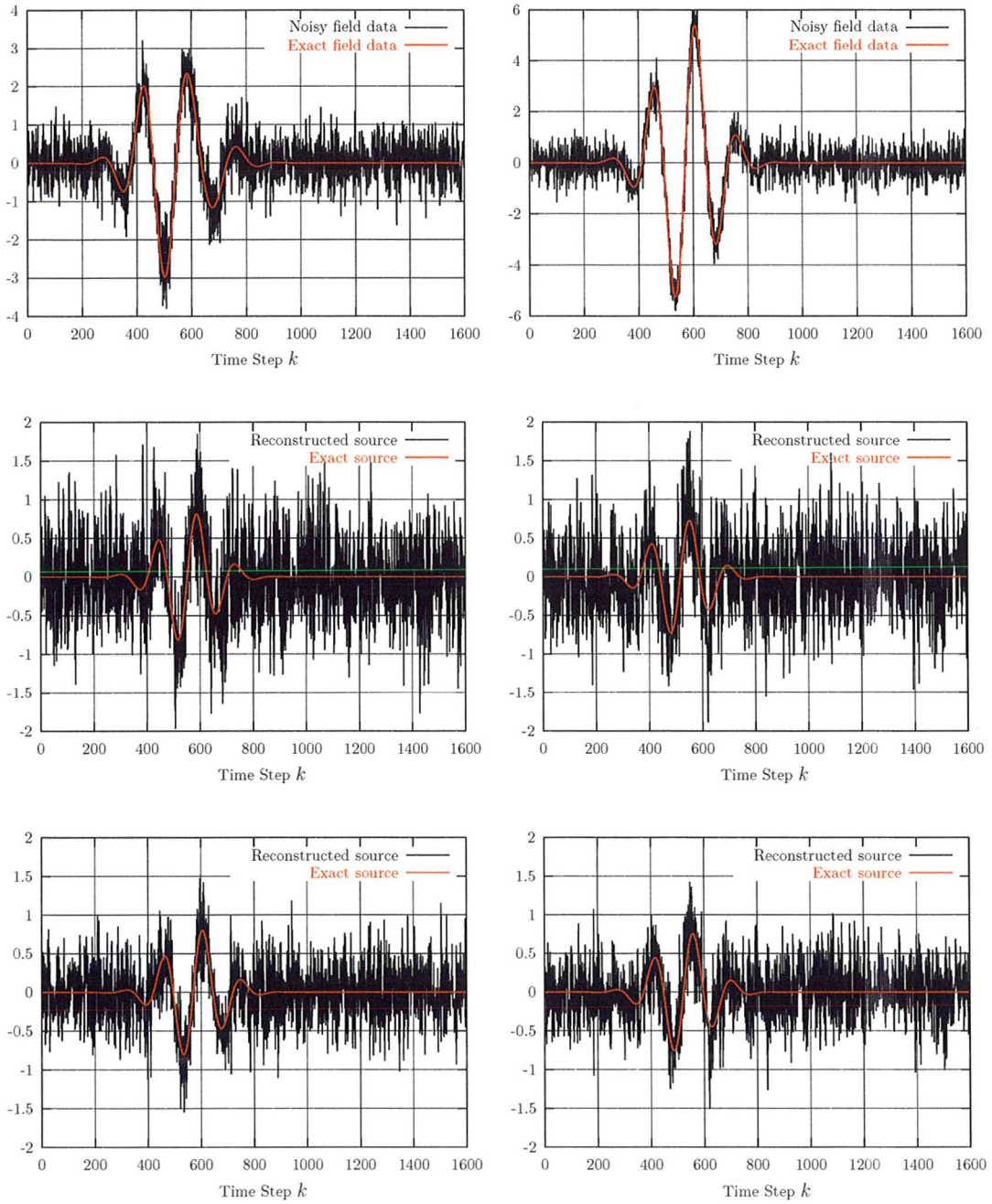

Figure 4.11 The reconstructed excitation sources using the noisy field data with noise level 8.2 dB. Top two figures shows two arbitrarily selected noisy boundary link impulses. The remaining four figures show the reconstructed sources at selected source cells.

Our algorithm, however, also exhibits one limitation. For a given source region, the number of boundary cells M always depends on the geometry of the discretization. If more discrete field data is available at the boundary of the source region, only M of which can be used for source reconstruction. Therefore, the accuracy of our solution produced by our algorithm cannot be improved in the presence of more boundary field data. This issue shall be addressed in the future work.

Reference

[1] W. J. R. Hoefer, "The transmission-line matrix method–theory and applications," *IEEE Transactions on Microwave Theory and Techniques*, vol. 33, no. 10, pp. 882–893, 1985.

[2] M. H. Bakr and N. K. Nikolova, "An adjoint variable method for time-domain transmission-line modeling with fixed structured grids," *IEEE Transactions on Microwave Theory and Techniques*, vol. 52, no. 2, pp. 554–559, 2004.

[3] B. Bader, M. Krumpholz, and P. Russer, "Current sources in TLM," in *Antennas and Propagation Society International Symposium*, vol. 2, 1994, pp. 1110–1115.

Chapter 5

Conclusion

This thesis presents a novel numerical approach for solving the inverse source problem in electromagnetics. Our source solution is obtained in the time domain using the knowledge of boundary field data at discrete locations. A smoothness condition (*a priori*) is imposed to the solution space, which overcomes the non-uniqueness of the reconstructed source. Our work, to the authors' knowledge, is the first numerical approach of solving inverse source problems in the time domain using near field measurements.

In chapter 2, the concept and theory of inverse source problems are reviewed. The non-unique nature in inverse source problems are discussed with emphasis on the so-called non-radiating (NR) sources. The regularization techniques and the use of *priori* conditions are also discussed. Past approaches of solving inverse source problems are reviewed.

In chapter 3, we present our TLM-based inversion approach for solving the inverse source problem in the time domain. Our algorithm supplies a unique source solution for the case of thin source regions. Our approach is demonstrated thought reconstructing the sources inside various source regions. Our algorithm is efficient and requires three TLM iterations for a single reconstruction time step. If the boundary field data is noise-free, our obtained time-domain solution of the sources matches the exact solution.

In chapter 4, our approach is generalized to accommodate a source region with arbitrary shape. By utilizing the Green matrix of the TLM computational domain, we formulated our discrete inversion problem as a low-ranked linear algebraic system. A unique source solution is then obtained by additionally imposing the smoothness *prior* constraint. Our numerical results show that for small source regions our source reconstruction algorithm can accurately reconstruct the excitation sources using the field data on the boundary. Our results converges to the exact results for smoother excitation distribution, and for higher ratio of M/N, where N is the total number of the source cells inside the given source region, and M is the total number of source cells on the boundary (i.e. boundary cells).

From the experience gained during the course of this work, the author suggests the following research topics to be addressed in future developments:

(1) Extend our source reconstruction algorithm discussed in Chapter 4 to accommodate three-dimensional source regions using Symmetrical Condensed TLM

Node (SCN).

(2) Address the issue of instability for the source reconstruction algorithm introduced in Chapter 4. For our present work, the instability usually happens after a sufficient long reconstruction time steps, if the total number source cells is greater than 400.

(3) Improve the accuracy of the source solution by accepting more boundary field data. For our present work, the number of discrete boundary field data that can be directly used for computation equals the number of boundary cells on the source region.

Bibliography

A. Abubakar and P. M. Berg, *The contrast source inversion method for location and shape reconstructions*, Inverse Problems **18** (2002), 495

R. Albanese and P. B. Monk, *The inverse source problem for Maxwell's equations*, Inverse Problems **22** (2006), no. 3, 1023–1035

H. Ammari, G. Bao, and J. L. Fleming, *An inverse source problem for Maxwell's equations in magnetoencephalography*, SIAM Journal on Applied Mathematics **62** (2002), no. 4, 1369–1382

B. Bader, M. Krumpholz, and P. Russer, "Current sources in TLM," in *Antennas and Propagation Society International Symposium*, vol. 2, 1994, pp. 1110–1115.

M. H. Bakr and N. K. Nikolova, *An adjoint variable method for time-domain transmission-line modeling with fixed structured grids*, IEEE Transactions on Microwave Theory and Techniques **52** (2004), no. 2, 554–559

M. H. Bakr, P. P. M. So, and W. J. R. Hoefer, *The generation of optimal microwave topologies using time-domain field synthesis*, IEEE Transactions on Microwave Theory and Techniques **50** (2002), no. 11, 2537–2544

M. Bertero, *Linear inverse and ill-posed problems*, Advances in electronics and electron physics **75** (1989), no. 1, 1–120

M. Bertero and P. Boccacci, *Introduction to Inverse Problems in Imaging.* (Institute of Physics Publishing, Philadelphia, PA, 1998).

N. Bleistein and J. K. Cohen, *Nonuniqueness in the inverse source problem in acoustics and electromagnetics*, Journal of Mathematical Physics **18** (1977), no. 2, 194–201

A. E. Bulyshev *et al.*, *Three-dimensional vector microwave tomography: theory and computational experiments*, Inverse Problems **20** (2004), 1239–1259

J. H. Bungey, *Sub-surface radar testing of concrete: a review*, Construction and Building Materials **18** (2004), no. 1, 1–8

S. Caorsi, G. L. Gragnani, and M. Pastorino, *Two-dimensional microwave imaging by a numerical inverse scattering solution*, IEEE Transactions on Microwave Theory and Techniques **38** (1990), no. 8

W. H. Carter and E. Wolf, *Inverse problem with quasi-homogeneous sources*, Journal of the Optical Society of America A **2** (1985), no. 11, 1994–2000

H. M. Chen *et al.*, *Imaging for concealed weapon detection: a tutorial overview of development in imaging sensors and processing*, IEEE signal processing Magazine **22** (2005), no. 2, 52–61

W. C. Chew *et al.*, *On the inverse source method of solving inverse scattering problems*, Inverse Problems **10** (1994), 547

R. E. Collin, *Field Theory of Guided Waves.* (McGraw-Hill New York, 1960).

A. J. Devaney, *Nonuniqueness in the inverse scattering problem*, Journal of Mathematical Physics **19** (1978), 1526–1535

A. J. Devaney, *The inverse problem for random sources*, Journal of Mathematical Physics **20** (1979), no. 8, 1687–1691

A. J. Devaney, *Inverse source and scattering problems in ultrasonics*, IEEE Transactions on Sonics and Ultrasonics **30** (1983), no. 6, 355–363

A. J. Devaney *et al.*, *The inverse source problem for wavelet fields*, IEEE Transactions on Antennas and Propagation **56** (2008), no. 10, 3179–3187

A. J. Devaney and E. A. Marengo, *A method for specifying non-radiating, monochromatic, scalar sources and their fields*, Pure and Applied Optics: Journal of the European Optical Society Part A **7** (1998), 1213–1220

A. J. Devaney, E. A. Marengo, and M. Li, *Inverse source problem in nonhomogeneous background media*, SIAM Journal on Applied Mathematics **67** (2007), no. 5, 1353–1378

A. J. Devaney and R. P. Porter, *Holography and the inverse source problem. Part II: Inhomogeneous media*, Journal of the Optical Society of America A **2** (1985), no. 11, 2006–2011

A. J. Devaney, G. Sherman, S. D. Res, and C. T. Ridgefield, *Nonuniqueness in inverse source and scattering problems*, IEEE Transactions on Antennas and Propagation **30** (1982), no. 5, 1034–1037

A. J. Devaney and E. Wolf, *Radiating and nonradiating classical current distributions and the fields they generate*, Physical Review D **8** (1973), no. 4, 1044–1047

A. J. Devaney and E. Wolf, *Multipole expansions and plane wave representations of the electromagnetic field*, Journal of Mathematical Physics **15** (1974), 234

A. Formisano, *Regularization of inverse magnetostatic problems: possibilities and pitfalls*, COMPEL: The International Journal for Computation and Mathematics in Electrical and Electronic Engineering **24** (2005)

A. Gamliel, K. Kim, A. Nachman, and E. Wolf, *A new method for specifying nonradiating, monochromatic, scalar sources and their fields*, Journal of the Optical Society of America A **6** (1989), no. 9, 1388–1393

G. Gbur and E. Wolf, *Nonradiating sources and other 'invisible' objects*, Progress in Optics **45** (2003), 273–316

T. M. Habashy, R. W. Groom, and B. R. Spies, *Beyond the Born and Rytov approximations: a nonlinear approach to electromagnetic scattering*, Journal of Geophysical Research **98** (1993), no. B2, 1759–1775

J. Hadamard, *Lectures on Cauchy's Problem in Linear Partial Differential Equations.* (Dover Pubns, Mineola, NY, 2003).

D. M. Hailu, N. K. Nikolova, and M. H. Bakr, "Sub-wavelength microwave radar imaging for detection of breast cancer tumors," in *International Symposium on Signals, Systems and Electronics*, 2007, pp. 107–110.

S. He and V. G. Romanov, *Identification of dipole sources in a bounded domain for Maxwell's equations*, Wave Motion **28** (1998), no. 1, 25–40

E. Heyman and A. J. Devaney, *Time-dependent multipoles and their application for radiation from volume source distributions*, Journal of Mathematical Physics **37** (1996), no. 2, 682–692

W. J. R. Hoefer, *The transmission-line matrix method–theory and applications*, IEEE Transactions on Microwave Theory and Techniques **33** (1985), no. 10, 882–893

B. Hoenders and H. Ferwerda, *The non-radiating component of the field generated by a finite monochromatic scalar source distribution*, Pure and Applied Optics: Journal of the European Optical Society Part A **7** (1998), 1201–1211

M. Ikehata, *An inverse source problem for the heat equation and the enclosure method*, Inverse Problems **23** (2007), 183–202

V. Isakov, *Some inverse problems for the diffusion equation*, Inverse Problems **15** (1999), 3–10

J. D. Jackson and R. F. Fox, *Classical electrodynamics*, American Journal of Physics **67** (1999), 841

C. E. S. Johan and E. A. Marengo, *Inverse source problem in the spheroidal geometry: Vector formulation*, IEEE Transactions on Antennas and Propagation **56** (2008), no. 4, 961–969

P. B. Johns, *A symmetrical condensed node for the TLM method*, IEEE Transactions on Microwave Theory and Techniques **35** (1987), no. 4, 370–377

Y. Kagawa and M. Analoui, *Application of TLM model to an inverse problem (identification of source and scatterer in time domain)*, Compel-International Journal for Computation and Math in Electrical and Electronic Engineering **13** (1994), 271–276

M. R. Khodja and E. A. Marengo, *Radiation enhancement due to metamaterial substrates from an inverse source theory*, Physical Review E **77** (2008), no. 4, 46605

K. Kim and E. Wolf, *Non-radiating monochromatic sources and their fields*, Optics Communications **59** (1986), no. 1, 1–6

R. Kress, L. K "uhn, and R. Potthast, *Reconstruction of a current distribution from its magnetic field*, Inverse Problems **18** (2002), 1127–1146

I. J. LaHaie, *Inverse source problem for three-dimensional partially coherent sources and fields*, Journal of the Optical Society of America A **2** (1985), no. 1, 35–45

I. J. LaHaie, *Uniqueness of the inverse source problem for quasi-homogeneous partially coherent sources*, Journal of the Optical Society of America A **3** (1986), no. 7, 1073–1079

A. K. Louis and A. Rieder, *Incomplete data problems in X-ray computerized tomography*, Numerische Mathematik **56** (1989), no. 4, 371–383

M. Malmivuori, "An inverse problem for time-harmonic electromagnetic currents in a smoothly layered medium," in *Annales Academiae scientarum Fennicae. Mathematica*, vol. 30, no. 2, 2005, pp. 437–458.

E. A. Marengo, *Observations on "Nonradiating surface sources": comment*, Journal of the Optical Society of America A **23** (2006), no. 1, 142–145

E. A. Marengo and A. J. Devaney, *The inverse source problem of electromagnetics: linear inversion formulation and minimum energy solution*, IEEE Transactions on Antennas and Propagation **47** (1999), no. 2, 410–412

E. A. Marengo and A. J. Devaney, *Nonradiating sources with connections to the adjoint problem*, Physical Review E **70** (2004), no. 3, 37601

E. A. Marengo, A. J. Devaney, and F. K. Gruber, *Inverse source problem with reactive power constraint*, IEEE Transactions on Antennas and Propagation **52** (2004), no. 6, 1586–1595

E. A. Marengo, A. J. Devaney, and R. W. Ziolkowski, *New aspects of the inverse source problem with far-field data*, Journal of the Optical Society of America A **16** (1999), no. 7, 1612–1622

E. A. Marengo, A. J. Devaney, and R. W. Ziolkowski, *Inverse source problem and minimum-energy sources*, Journal of the Optical Society of America A **17** (2000), no. 1, 34–45

E. A. Marengo, M. R. Khodja, and A. Boucherif, *Inverse source problem in non-homogeneous background media. Part II: Vector formulation and antenna substrate performance characterization*, SIAM Journal on Applied Mathematics **69** (2008), no. 1, 81–110

E. A. Marengo and R. W. Ziolkowski, *On the radiating and nonradiating components of scalar, electromagnetic, and weak gravitational sources*, Physical review letters **83** (1999), no. 17, 3345–3349

E. A. Marengo and R. W. Ziolkowski, *Inverse source problem with regularity constraints: normal solution and nonradiating source components*, Journal of Optics A: Pure and Applied Optics **2** (2000a), 179–187

E. A. Marengo and R. W. Ziolkowski, *Nonradiating and minimum energy sources and their fields: Generalized source inversion theory and applications*, IEEE Transactions on Antennas and Propagation **48** (2000b), no. 10, 1553–1562

H. E. Moses, *Solution of Maxwell's equations in terms of a spinor notation: the direct and inverse problem*, Physical Review **113** (1959), no. 6, 1670–1679

H. E. Moses, *Eigenfunctions of the curl operator, rotationally invariant Helmholtz theorem, and applications to electromagnetic theory and fluid mechanics*, SIAM Journal on Applied Mathematics **21** (1971), no. 1, 114–144

H. E. Moses, *The time-dependent inverse source problem for the acoustic and electromagnetic equations in the one-and three-dimensional cases*, Journal of Mathematical Physics **25** (1984), no. 6, 1905–1923

C. Müller, *Electromagnetic radiation patterns and sources*, IEEE Transactions on Antennas and Propagation **4** (1956), no. 3, 224–232

M. M. Ney, A. M. Smith, and S. S. Stuchly, *A solution of electromagnetic imaging using pseudoinverse transformation*, IEEE Transactions on Medical Imaging **3** (1984), 155–162

R. P. Porter, *Diffraction-limited, scalar image formation with holograms of arbitrary shape*, Journal of the Optical Society of America **60** (1970), no. 8, 1051–1059

R. P. Porter and A. J. Devaney, *Generalized holography and computational solutions to inverse source problems*, Journal of the Optical Society of America **72** (1982b), no. 12, 1707–1713

R. P. Porter and A. J. Devaney, *Holography and the inverse source problem*, Journal of the Optical Society of America **72** (1982a), no. 3, 327–330

F. Sabath, D. V. Giri, F. Rachidi, and A. Kaelin, editors, *Proceedings of the Ninth International Conference on Ultrawideband Short Pulse Electromagnetics* (Lausanne, Swizerland, 1998).

B. W. Schilling and G. C. Templeton, *Three-dimensional remote sensing by optical scanning holography*, Applied Optics **40** (2001), no. 30, 5474–5481

P. R. Smith, T. M. Peters, and R. H. T. Bates, *Image reconstruction from finite numbers of projections*, Journal of Physics A: Mathematical, Nuclear and General **6** (1973), 361–382

J. C. E. Sten and E. A. Marengo, *Inverse source problem in an oblate spheroidal geometry*, IEEE Transactions on Antennas and Propagation **54** (2006), no. 11, 3418–3428

L. Tsang, A. Ishimaru, R. P. Porter, and D. Rouseff, *Holography and the inverse source problem. III. Inhomogeneous attenuative media*, Journal of the Optical Society of America A **4** (1987), no. 9, 1783–1787

W. Weiyan and Z. Shourong, *Unrelated illumination method for electromagnetic inverse scattering of inhomogeneous lossy dielectric bodies*, IEEE Transactions on Antennas and Propagation **40** (1992), no. 11, 1292–1296